UNIVERSITÀ
DEGLI STUDI
DI PADOVA

Sede Amministrativa: Università degli Studi di Padova
Dipartimento di Biologia

SCUOLA DI DOTTORATO DI RICERCA IN:
BIOSCIENZE E BIOTECNOLOGIE
INDIRIZZO: BIOCHIMICA E BIOFISICA
CICLO XXVIII

YAP/TAZ and somatic stem cells

Direttore della Scuola: Ch.mo Prof. Paolo Bernardi
Coordinatore d'indirizzo: Ch.mo Prof. Fabio Di Lisa
Supervisore: Ch.mo Prof. Michelangelo Cordenonsi

Dottorando: Dr. Tito Panciera

INDEX

PUBLICATIONS

Mariaceleste Aragona, Tito Panciera, Andrea Manfrin, Stefano Giulitti, Federica Michielin, Nicola Elvassore, Sirio Dupont, Stefano Piccolo. **A mechanical checkpoint controls multicellular growth through YAP/TAZ regulation by actin-processing factors**. Cell 154: 1047–1059, 2013.

Luca Azzolin, Tito Panciera, Sandra Soligo, Elena Enzo, Silvio Bicciato, Sirio Dupont, Silvia Bresolin, Chiara Frasson, Giuseppe Basso, Vincenza Guzzardo, Ambrogio Fassina, Michelangelo Cordenonsi, Stefano Piccolo. **YAP/TAZ incorporation in the beta-catenin destruction complex orchestrates the Wnt response**. Cell 158: 157– 170, 2014.

This work was realized in the laboratory of Prof. Stefano Piccolo and in close collaboration with Dr. Mariaceleste Aragona and Dr. Luca Azzolin.

ABSTRACT

(ENGLISH VERSION)

The co-transcription factors YAP/TAZ are potent inducers of tissue and organ growth during development and tissue regeneration after damage. In this work we have expanded on the repertoire of YAP/TAZ regulations and on their biological properties. We found that these are regulated by the mechanical properties of the microenvironement and by the Wnt signaling cascade. The latter is induced by mutations in the tumor suppressor APC, a hallmark of intestinal cancer, and here we show that this is accompanied by YAP/TAZ stabilization and is functional for transformation of intestinal cells. Both the mechanical and Wnt regulations have been published (Azzolin et al., 2014; Aragona et al., 2013). Aberrant YAP/TAZ activation is known to be associated to tissue overgrowth, tumorigenesis and acquisition of cancer stem cell traits. Here we explore the role of YAP/TAZ as key factors in somatic stem cell self-renewal and somatic cell plasticity (unpublished).

ABSTRACT

(ITALIAN VERSION)

I co-fattori di trascrizione YAP/TAZ sono potenti induttori di espansione tissutale durante lo sviluppo embrionale e la rigenerazione dei tessuti. In questo lavoro abbiamo ampliato lo studio del repertorio di regolazioni di YAP/TAZ e il loro ruolo biologico. Abbiamo scoperto che YAP/TAZ sono regolati dalle proprietà meccaniche del microambiente cellulare e dalla cascata di segnale di Wnt. Quest'ultima è indotta da mutazioni a carico dell'oncosoppressore APC, un elemento caratteristico dei tumori intestinali. In questo studio, dimostriamo che la mutazione di APC è accompagnata dalla stabilizzazione di YAP/TAZ e che questo evento è funzionale alla trasformazione delle cellule intestinali. Le regolazioni di YAP/TAZ, da parte di stimoli meccanici e tramite la via di trasduzione di Wnt, sono trattate in lavori pubblicati (Aragona et al., 2013; Azzolin et al., 2014). L'attivazione anomala di YAP/TAZ è associata a iperplasia, tumorigenesi e acquisizione di caratteristiche tipiche di cellule staminali tumorali. In questo lavoro esploriamo il ruolo di YAP/TAZ come fattori essenziali per l'auto-rinnovamento di cellule staminali somatiche e per la plasticità cellulare (non pubblicato).

EXTENDED ABSTRACT

The co-transcription factors YAP/TAZ are potent inducers of tissue and organ growth during development and tissue regeneration after damage. In this work we have expanded on the repertoire of YAP/TAZ regulations and on their biological properties. We found that these are regulated by the mechanical properties of the microenvironement and by the Wnt signaling cascade. The latter is induced by mutations in the tumor suppressor APC, a hallmark of intestinal cancer, and here we show that this is accompanied by YAP/TAZ stabilization and is functional for transformation of intestinal cells. Aberrant YAP/TAZ activation is associated to tissue overgrowth, tumorigenesis and acquisition of cancer stem cell traits. It is tempting to speculate that YAP/TAZ might be key factors involved in the maintenance or the acquisition of the somatic SC state whenever natural, pathological or *ex vivo* conditions demand de novo generation and expansion of resident or facultative SCs. Indeed, we found that YAP/TAZ are pivotal factors genetically required for the expansion of somatic stem cells *ex vivo*, at least for three different paradigmatic cases: the intestinal epithelium, the exocrine pancreas and the central nervous system. The prospect to induce autologous, tissue-specific somatic stem cells *in vitro* is an important goal for regenerative medicine and disease modeling. Here we show that expression of a single factor, YAP, into terminally differentiated cells explanted from different tissues efficiently creates cells with functional and molecular attributes of their corresponding tissue-specific SCs, that can be expanded *ex vivo* as organoid cultures (ySCs). The ySC state can be transmitted through cell generations without need of continuous expression of ectopic YAP/TAZ, indicating that a transient activation of YAP is sufficient to induce a heritable self-renewing state. In particular, this treatment stably converts murine terminally differentiated pancreatic exocrine cells into pancreatic duct-like progenitors and brain neurons into neural SCs. Thus the same factor induces distinct tissue-specific SCs through cell reprogramming. If extended to human cells, the present findings would represent a generally applicable procedure to generate *in vitro* a variety of normal, tissue-reconstituting autologous SCs at will.

INTRODUCTION

Stem cells (SCs) display the capacity to renew themselves when they divide, and to generate a differentiated progeny. Somatic SCs operate in multiple adult organs for continuous tissue renewal or repair after injury. Yet, these cells are still mainly defined by operational definitions and cell surface markers rather than the molecular traits that govern their special status (Fuchs and Chen, 2013). Unlimited availability of normal, somatic SCs will be critical for effective organ repopulation in regenerative medicine applications, to understand SC biology and for disease modeling in the Petri dish. These efforts are frustrated by the fact that SCs are rare and difficult to purify from native tissues or to expand *ex vivo*. A recent groundbreaking step forward in this direction has been the description of culture systems allowing adult epithelial SCs of endodermal origin to expand and self-organize into "organoids" (Sato et al., 2009). Yet, these protocols still require the isolation of native SCs as starting material.

Direct conversion of terminally differentiated cells back into their corresponding tissue-specific SCs may represent an attractive alternative to obtain somatic SCs. Stemness and differentiation are not hierarchically fixed states defined only by intrinsic cellular properties, but rather inherently plastic and interchangeable states, greatly influenced by extrinsic cues operating at the tissue level. Indeed, several reports have recently highlighted a surprising plasticity in somatic cell fates, as differentiated cells can return to a SC status under special conditions, such as tissue damage (Blanpain and Fuchs, 2014).

However, the identity of the factors able to control the somatic SC status remains poorly understood, limiting the exploitation of such plasticity. YAP/TAZ have been portrayed as stemness factors (reviewed in Ramos and Camargo, 2012) and indeed these factors are strictly required whenever somatic stem cells need to be amplified for tissue regeneration after damage or in the case of aberrant growth triggered by oncogenic transformation. It is thus tempting to speculate that YAP/TAZ might be key factors involved in the maintenance or the acquisition of the somatic SC state whenever natural, pathological or ex-vivo conditions demand de novo generation and expansion of resident or facultative SCs.

YAP/TAZ regulations

Hippo signaling

Recently, the Hippo signaling cascade has emerged at the center of mechanisms that control tissue growth and organ size (Pan, 2010) providing an entry point to tackle the long-standing issue of how organs can control their size and shape during development or regeneration.

The core elements in Hippo signaling, which constitute an intracellular signal transduction kinase cascade, were first discovered in *Drosophila* genetic screenings for tumor suppressor genes, identifying four key components (Pan, 2010; Ramos and Camargo, 2012): the protein kinase Hippo -after which the signaling pathway is named - and its partner Salvador, the NDR family protein kinase Warts, and its adaptor protein Mob-as-tumor-suppressor (Mats).

These discoveries in *Drosophila* led to the investigation of Hippo signaling also in mammals, revealing several conserved aspects of the pathway. The mammalian genome harbors two Hippo homologs, MST1 and MST2, one Salvador homolog, known as SAV1, two Warts homologs, LATS1 and LATS2, and two Mats homologs, collectively referred to as MOB1 (see scheme in Figure 1A). Importantly, several loss-of-function mutant phenotypes in *Drosophila* can be rescued by the re-expression of their respective human homologs.

The Hippo intracellular kinase cascade leads to inactivation of the transcriptional co-factors YAP and TAZ

At the core of the mammalian Hippo signaling cascade are the kinases MST1/2 and LATS1/2 (Figure 1A) (reviewed in Pan, 2010; Ramos and Camargo, 2012): activated MST1/2 directly phosphorylate the large tumor suppressor kinases LATS1 and LATS2, as well as MOB1, allowing the formation of a stable LATS1/2-MOB1 complex. Hippo signaling-dependent transcriptional responses are mediated by two transcriptional co-factors: YAP (Yes-associated protein) and TAZ (transcriptional co-activator with PDZ-binding motif), also known as WWTR1. Activated LATS1/2 phosphorylate YAP at Ser127 and TAZ at Ser89,

promoting binding to 14-3-3 proteins. This leads to cytoplasmic retention and reduced nuclear accumulation of these factors. In addition, phosphorylation can also inhibit YAP and TAZ by promoting their degradation through ubiquitination and proteasomal pathway (see scheme in Figure 1A). Phosphorylation of a specific HXRXXS motif at S381 by LATS1/2 primes YAP for subsequent phosphorylation by CK1δ/ε, followed by the recognition by the E3 ubiquitin ligase $SCF^{\beta\text{-}TrCP}$ and ubiquitin-mediated degradation of YAP. Both S381 and S127 are critical for YAP inactivation by the hippo pathway, because only a YAP isoform carrying mutations at both sites, but not YAP wild-type or YAP carrying single mutations is able to transform NIH 3T3 cells (Zhao et al., 2010). The S381 phosphodegron of YAP is conserved in TAZ; phosphorylation of TAZ S311 by LATS primes the protein for subsequent phosphorylation on S314 by CK1ε and recruitment of the $SCF^{\beta\text{-}TrCP}$ E3 ubiquitin ligase, thus leading to TAZ ubiquitylation and degradation (Liu et al., 2010). Collectively, phosphorylation clearly inactivates YAP and TAZ-dependent transcriptional responses.

When YAP/TAZ escape this control (i.e., when LATS is inhibited), they localize to the nucleus where they serve as co-activators of different DNA-binding factors, such as p73, Runx2, PPAR-γ, thyroid transcription factor1, Pax3 and the TEA-domain family members TEAD1/2/3/4. YAP and TAZ are transcriptional activators devoid of a DNA binding domain and thus require the association with a DNA-binding partner to activate the transcription of their target genes. Among DNA-binding co-factors, the TEAD family of transcription factors, which are homologs of *Drosophila* Scalloped, are the most relevant mediators of YAP and TAZ function (Zanconato et al., 2015; Zhang et al., 2009; Zhao et al., 2008). Together, the YAP/TAZ-TEAD complex promotes proliferative and survival programs by inducing the expression of a genetic program that is just beginning to be explored.

Upstream elements in Hippo signaling

Although the signal transduction within the core kinase cascade is well defined, the mechanisms and proteins involved in upstream regulation of the Hippo pathway are not as well established (reviewed in Pan, 2010; Piccolo et al., 2014;

Ramos and Camargo, 2012). The mammalian genome contains homologs of a number of *Drosophila* upstream regulators of the Hippo pathway, including two homologs of the cytoskeleton binding proteins Expanded (FRMD6 and FRMD1) and Merlin (NF2/Mer), and two homologs of their interacting partner Kibra (KIBRA/WWC1 and WWC2).

Merlin/NF2 is localized at the cell membrane of confluent monolayers of epithelial cells, where it is suggested to exert its tumor-suppressive function by promoting the correct protein assembly for LATS activation by phosphorylation (Yin et al., 2013; Yu et al., 2010) (see Scheme in Figure 1A). Indeed, reconstitution of Merlin in the NF2-deficient MDA-MB-231 cell line leads to a strong, LATS-dependent inhibition of YAP/TAZ activity (Aragona et al., 2013). Epithelial architecture has been shown to be a relevant regulator of YAP/TAZ activity; the baso-lateral polarity protein Scribble promotes the assembly of a MST-LATS-TAZ complex at the membrane, required for LATS activation and TAZ inhibition (see scheme in Figure 1A). The disruption of epithelial architecture and epithelial-to-mesenchymal transition is a hallmark of cancer and leads to delocalization of Scribble and TAZ activation (Cordenonsi et al., 2011).

Recently, YAP/TAZ and angiomotin (AMOT) family proteins were shown to interact, resulting in YAP/TAZ localization to tight junctions and inhibition through phosphorylation-dependent and independent mechanisms (Chan et al., 2011; Mana-Capelli et al., 2014). Other evidence, however, showed that at least in some conditions, as in the context of NF2 deficiency, AMOTs can function also as YAP activators (Kim et al., 2011; Schlegelmilch et al., 2011; Yi et al., 2013). In addition, α-catenin loss was shown to induce a potent activation of YAP activity in keratinocytes, by a mechanism that entails a decrease in YAP-phosphorylation, possibly through the modulation of a kinase different from LATS (Kim et al., 2011). The diverse modalities of Hippo pathway activation argue for the notion that the adhesive properties of the cell are of central importance for the modulation of YAP/TAZ activity through the Hippo pathway.

The biological roles of Hippo signaling

Overexpression of YAP/TAZ or mutation of diverse components of the Hippo pathway leads to the development of hugely overgrown organs, due to the increase in mitosis and to decreased susceptibility to cell death (reviewed in Halder and Johnson, 2011; Piccolo et al., 2014; Zhao et al., 2010) portraying Hippo signaling as a fundamental regulator of organ size. For instance, overexpression of the YAP/TAZ orthologue Yorkie in *Drosophila* results in a massive enlargement of the eye and of the wing imaginal discs (Figures 1B-C) (Dong et al., 2007; Huang et al., 2005). Strikingly similar phenotypic effects are observed in mammals; conditional knockout of the Hippo pathway component Salvador leads to cardiomegaly (Figure 1D) (Heallen et al., 2011) and YAP overexpression results in massive liver overgrowth in transgenic mice (Figure 1E) (Dong et al., 2007). Different studies show that two general physiological roles of Hippo signaling are the promotion of cellular quiescence and of cellular differentiation (reviewed in Piccolo et al., 2014; Ramos and Camargo, 2012). As will be detailed below, conditional mutants for Hippo pathway components result in expansion of the progenitor cell compartment of diverse organs and tissues. This is consistent with *in vitro* evidence, whereby YAP hyperactivation leads to failure of cell cycle exit and terminal differentiation.

The Hippo nuclear transducers also play a prominent role in the phenomenon of cell contact inhibition. When scratch wounds are generated in confluent cell cultures to relieve contact inhibition, YAP nuclear localization is significantly elevated in cells at the border of the wound, while cells further away show cytoplasmic localization of YAP (Zhao et al., 2007). Importantly, cells experiencing YAP nuclear localization are also positive for Ki67, a marker of cell proliferation, indicating that these cells have re-entered the cell division cycle. It must however be noted, as will be discussed below, that more recent evidence has shown that for overt growth arrest and quantitative YAP/TAZ nuclear exclusion to occur, a mechanical inhibitory step must take place, whereby cells undergo contact inhibition of proliferation when cell projected area drops below a defined size, due to progressive cell crowding (Aragona et al., 2013).

All these sets of evidence indicate a role for Hippo signaling in balancing cell proliferation and differentiation in different contexts.

YAP and TAZ in mechanotransduction

In addition to the aforementioned regulations, YAP and TAZ can respond to a variety of stimuli, as hinted by the recent discovery that they are regulated by extra-cellular matrix (ECM) stiffness, cell shape and cytoskeletal tension (Dupont et al., 2011; reviewed in Halder et al., 2012). When cells are cultured on stiff substrates TAZ and YAP are nuclear and can induce the expression of their target genes; conversely, if cells are grown on soft substrates, YAP and TAZ are re-localized to the cytoplasm and thus inactivated. Intriguingly, one set of data suggests that mechanical signals regulate YAP and TAZ through a pathway that acts in parallel to the classic kinase cascade of the Hippo pathway, as knockdown of LATS1 and LATS2 was not sufficient to restore YAP and TAZ activity in cells cultured on soft extra-cellular matrix (Dupont et al., 2011). Crucially, YAP and TAZ are the key mediators of the biological effects of ECM stiffness and cell shape. For example, endothelial cells die when forced to remain small, whereas they proliferate when allowed to spread, and the levels of YAP and TAZ dictate these opposite behaviors: if YAP and TAZ are artificially increased in small cells, these start to proliferate; in contrast, attenuation of YAP and TAZ in spread cells causes them to die (Dupont et al., 2011).

Regulation by Rho GTPases

YAP/TAZ activity can also be influenced by Rho-GTPases. The first evidence in this direction came from the observation that YAP/TAZ are potently inhibited by treatment with the *Clostridium botulinum* toxin C3 (Dupont et al., 2011), a known Rho-GTPase inhibitor. In addition, a number of G-protein coupled receptors (GPCRs) have been shown to signal through YAP/TAZ (Yu et al., 2012). Recent studies found that the metabolic pathway triggered by the mevalonate/HMG-CoA reductase is instrumental in supporting YAP/TAZ activity, as some byproducts of the mevalonate cascade are essential to sustain the activity of Rho-GTPases at cell membranes (Sorrentino et al., 2014; Wang et al., 2014).

Some results suggest that the Rho and cytoskeletal pathway are formally distinct, as Rho regulates YAP through phosphorylation, while the mechanotransduction pathway impinges on YAP/TAZ activity in a phosphorylation-independent manner. Thus, the relationship between Rho GTPases and the actin cytoskeleton remains an open question in the field of YAP/TAZ regulations.

YAP/TAZ role in tissue and organ growth

Germ line knockouts

In *Drosophila* the loss of Hippo pathway components or of F-actin inhibitors results in tissue overgrowth, and the YAP/TAZ orthologue Yorkie is required for cell proliferation in several embryonic tissues (Fernandez et al., 2011; Hamaratoglu et al., 2006; Harvey and Tapon, 2007; Justice et al., 1995; Maitra et al., 2006; Sansores-Garcia et al., 2011; Tapon et al., 2002). This function is conserved in mammals; indeed YAP transgenic mice display extensive cell proliferation and tissue overgrowth (Camargo et al., 2007; Dong et al., 2007). Germ line knockouts of the Hippo pathway components NF2, MST1/2, and LATS2 are lethal at relatively early embryonic stages*: Nf2*$^{-/-}$ and *Mst1/2*$^{-/-}$ caused impaired development of the extraembryonic tissues (McClatchey et al., 1997; McPherson et al., 2004; Zhou et al., 2009).

Yap/Taz double null mutants die before embryo implantation (Nishioka et al., 2009). *Yap*$^{-/-}$ embryos die shortly after gastrulation, at stage E8.5 (Morin-Kensicki et al., 2006). These embryos show some similarities to the phenotype observed in double *Tead1/2* knockout embryos, where the axial mesoderm is not maintained (Sawada et al., 2008). *Taz* knockouts display high rates of embryonic lethality, but a fraction of *Taz* mutants develop to term and die of polycystic kidney disease and pulmonary emphysema (Hossain et al., 2007; Makita et al., 2008).

Immunofluorescence at the morula stage shows that YAP and TAZ are localized in the nucleus of trophoectoderm (TE) cells, while inner cell mass (ICM) cells display cytoplasmic YAP/TAZ. Overexpression of activated forms of YAP or TEAD, or inactivation of LATS1/2, is sufficient to induce expression of the TE master gene *Cdx2* in ICM; conversely, LATS2 overexpression suppresses Cdx2

expression in TE (Nishioka et al., 2009). These findings suggest a role for YAP/TAZ activity as inhibitors of embryonic pluripotency and crucial regulators of the development of TE.

Conditional knockouts

Conditional knockout alleles and inducible transgenic mice suggested some key functions of YAP/TAZ and Hippo signaling in organ growth, cell proliferation, stem cell amplification, and cell fate decision in organs and tissues as diverse as liver (Camargo et al., 2007; Yimlamai et al., 2014; Zhou et al., 2009), kidney (Hossain et al., 2007; Reginensi et al., 2013), heart (Heallen et al., 2011; Xin et al., 2013), pancreas (Gao et al., 2013; George et al., 2012), intestinal epithelium (Cai et al., 2010; Lee et al., 2008; Zhou et al., 2011), epidermis (Schlegelmilch et al., 2011; Zhang et al., 2011) and the nervous system (Lavado et al., 2013).

Nuclear YAP is endogenously restricted to intestinal progenitor cells at the bottom of intestinal crypts, as shown by immunohistochemical stainings (Barry et al., 2013). YAP overexpression in transgenic mice enhances intestinal cell proliferation and impairs differentiation (Camargo et al., 2007). YAP/TAZ are required for intestinal epithelium regeneration after inflammatory damage, but are dispensable form normal intestinal homeostasis (Cai et al., 2010; Azzolin et al., 2014).

In contrast to what is observed for other organs, such as in the case of the liver (Camargo et al., 2007; Yimlamai et al., 2014; Zhou et al., 2009), conditional deletion of the Hippo pathway components MST1/2 in the pancreas does not result in organ overgrowth, but rather in a reduction of organ size. (Gao et al., 2013; George et al., 2012). Ductal cells of *Mst1/2* knockout pancreata were shown to maintain a proliferative status throughout adult life, in accordance with increased YAP activity. Importantly, deletion of one single allele of *Yap* in *Mst1/2* double knockout tissue was sufficient to rescue these phenotypes. In line with this evidence, overexpression of a constitutively active YAP mutant caused the expansion of ductal cells with the loss of acinar structures. Notably, again arguing in favor of the notion that YAP/TAZ are dispensable for normal tissue

homeostasis, pancreatic tissue remains histologically normal after homozygous deletion of YAP in the adult pancreas (Zhang et al., 2014).

YAP has been implicated also in the regulation of brain development. Loss of the Hippo pathway upstream regulator NF2 in the dorsal telencephalon of transgenic mice leads to brain malformations characterized by aberrant expansion of neural progenitor cells in the hippocampus, neocortex and cortical hem. In line, the overexpression of transgenic YAP leads to alterations of the hippocampus similar to those observed in NF2 mutant brains, while the NF2-loss phenotype is rescued by concomitant YAP depletion, arguing in favor of a prominent role of YAP in this context (Lavado et al., 2013). Again, similarly to what described above for other organs, YAP inactivation per se has no detectable phenotypic consequences (Lavado et al., 2013).

YAP/TAZ and Stem cells

Emerging evidence suggests that the determination of organ size by YAP/TAZ could involve the regulation of stem cells and progenitor cells self-renewal and expansion reviewed in (Ramos and Camargo, 2012; Zhao et al., 2010). For instance, YAP and TAZ were reported to regulate human and mouse embryonic stem cells self-renewal in response to TGFβ/BMP (transforming growth factor beta/bone morphogenetic protein) signaling (Varelas et al., 2008). Additionally, as mentioned above, the Hippo pathway also regulates tissue-specific progenitor cells. YAP is specifically expressed in the intestinal crypt stem cell compartment (Barry et al., 2013), where overexpression of a LATS1/2-insensitive YAP mutant results in reversible expansion of undifferentiated cells (Camargo et al., 2007). Moreover, YAP/TAZ have been implicated in the control of the expansion of progenitor cells in the epidermis and in the liver in transgenic mouse models and of neural progenitors in mouse, frog and chick neural tubes (Schlegelmilch et al., 2011; Silvis et al., 2011; Zhang et al., 2011; Benhamouche et al., 2010; Lee et al., 2010; Song et al., 2009; Zhang et al., 2010; Zhou et al., 2009; Lavado et al., 2013; Cao et al., 2008; Gee et al., 2011). Of note, the fact that YAP/TAZ are stabilized and act in stem and progenitor cells, typically lodged in specific tissue niches (Ramos and Camargo, 2012), suggests that the ECM, the cell's cytoskeletal

organization, and ensuing tensional forces may impart physical instructions that regulate stem cells behavior through a mechanotransduction-YAP/TAZ pathway.

Recently YAP and TAZ have also been indicated as inductors of cancer stem cells in malignant glioma and in breast cancer (Bhat et al., 2011; Cordenonsi et al., 2011). It was demonstrated that TAZ is required for the tumor-initiation capacities of breast cancer cells, as assayed by the capacity of cells to grow as mammospheres and to form tumors once injected at limiting dilutions in immuno-compromised mice. Gain of TAZ endows tumor-initiating capacity to non-cancer-stem-cells populations and loss of TAZ impairs this capacity in cancer-stem-cell-enriched populations (Cordenonsi et al., 2011). In parallel with this, TAZ protein levels are found elevated in poorly differentiated human primary breast cancer, as assayed by immunohistochemistry analysis. Significantly, loss of TAZ impairs invasiveness, self-renewal and tumorigenic potential also in primary glioblastoma stem cells (Bhat et al., 2011).

However, the emerging perception of YAP/TAZ as "stemness factors" (reviewed in Ramos and Camargo, 2012) is mainly based on two distinct pieces of evidence that remain so far poorly connected, as interpretations are hampered by the paucity of double YAP/TAZ knockout studies. This notion is in fact mainly supported by the organ overgrowth phenotypes induced by Hippo mutants or YAP transgenic overexpression in the embryo and the preferential localization of YAP/TAZ proteins in cells belonging to the stem cell compartment of adult organs.

The mechanism of action of YAP/TAZ during embryonic growth is still unexplored and, at the same time, the possible connection between somatic, tissue-specific stem cells and embryonic progenitors remains elusive and debated.

As detailed above data based on conditional genetic inactivation of YAP in adult organs, such as pancreas and liver, and double knockout of YAP and TAZ in the intestine, show that YAP/TAZ activity is largely dispensable for normal tissue homeostasis. Still, YAP and TAZ are essential in any condition in which stem cells need to be amplified for tissue regeneration or after oncogenic transformation (Azzolin et al., 2014; Zhang et al., 2010; Zhang et al., 2014). This evidence argues in favor of the notion that YAP/TAZ might regulate stem cells

only when these are stimulated by specific intrinsic or extrinsic cues that drive their expansion.

AIMS AND WORKING HYPOTHESES

Here we aimed to get deeper insights on the regulation and biology of YAP/TAZ. Part of this work is published and relates to the regulation by secreted factors and mechanical signals. We started by the observation that inactivation of the β-catenin destruction complex stabilizes YAP/TAZ, and our own prior work (Azzolin et al., 2012) and continued to demonstrate the role of YAP/TAZ downstream of APC inactivation and in cultured intestinal organoids. We also took advantage of prior work (Dupont et al., 2011) to demonstrate that increasing intracellular biomechanical tension and changing the cell's cytoskeletal organization are very potent regulators of YAP/TAZ. As for the so far unpublished part of this thesis, we were attracted by the fact that dysregulation of the Hippo signaling pathway has been recently associated with cellular dedifferentiation in some contexts. In tumors, the activation of the Hippo pathway transcriptional effectors YAP/TAZ can reprogram non-stem cancer cells into less-differentiated cancer SCs (Cordenonsi et al., 2011). Genetic inactivation of the Hippo cascade in the liver induces the formation of a massive organ, in part through transient lineage conversion of hepatocytes into biliary cells (Yimlamai et al., 2014). Irrespectively of their complex roles in normal and aberrant tissues (as detailed in Introduction), this scenario raises the distinct possibility that ectopic expression of YAP or TAZ may be sufficient to turn any cell, even a normal differentiated cell, into a somatic SC.

Here we first tested the relevance of YAP/TAZ to maintain the somatic stem cell status, employing *ex vivo* cultures of somatic progenitor cells derived from different organs as a model reminiscent of *in vivo* conditions in which stem cell expansion is called into action. Secondly, we tested the hypothesis, based on their capacity to reprogram non-stem cancer cells into cancer SCs (Cordenonsi et al., 2011), that the transcriptional regulators YAP/TAZ may bestow stemness characteristics to normal differentiated cells, turning the latter into their corresponding, tissue-specifc somatic stem cells. We tested this hypothesis in two paradigm cell types of terminal differentiation, pancreatic exocrine acinar cells and neurons.

RESULTS

YAP/TAZ regulation by cell density and tissue architecture

YAP and TAZ inactivation underlies contact inhibition of proliferation (CIP), a classic paradigm of epithelial biology, defined by an arrest of cell divisions when cells become confluent and occupy the entire available space for their growth. This phenomenon recapitulates the growth-arrested condition of most epithelia when these reach their appropriate size and loss of this control mechanism is considered one of the hallmarks of cancer. Hippo pathway has been reported to be activated during the process of contact inhibition, as phosphorylation of YAP at S127 increases at the onset of CIP (Zhao et al., 2007). However, some evidence suggests that this regulation might be more complex, as combined MST1/2 knockouts in mouse embryonic fibroblasts showed that regulation by the Hippo pathway is dispensable for CIP in that system (Schlegelmilch et al., 2011).

In our recent work, we proposed a two-step model of YAP/TAZ regulation for CIP (Aragona et al., 2013). When cells engage in cell-cell contacts, the E-cadherin/catenin system leads to LATS activation and YAP/TAZ phosphorylation. This, however, contributes for only 30% of growth inhibition and YAP/TAZ cytoplasmic re-localization. For overt growth arrest and quantitative YAP/TAZ nuclear exclusion to occur, a mechanical inhibitory step must take place: as cells proliferate, cell crowding in a monolayer progressively forces individual cells into smaller areas; in turn this impairs the YAP/TAZ mechanical pathway in a way reminiscent of YAP/TAZ inhibition in isolated single cells plated on small ECM islands or soft ECM. Indeed, by plating epithelial cells at different densities we found that overt growth arrest and YAP/TAZ inhibition occurs only in densely packed cells, as compared to confluent or sparse conditions (Figures 2A-C). YAP/TAZ inhibition by cell crowding and ensuing growth arrest closely resemble that observed in cells forced to acquire a small projected area by seeding on confined adhesive areas, as

compared to cells allowed to spread on un-patterned substrate (Figures 2D-E). We could in fact show that contact inhibition of proliferation occurs through mechanical cues impinging on YAP/TAZ activity; by employing a monolayer stretching device we found that stretching of a densely packed monolayer, which results in an increase of cell projected area, is sufficient to rapidly reactivate YAP/TAZ, as monitored by nuclear localization, and cause cells to re-enter S-phase (Figures 2F-G).

By a loss-of-function screening for known F-actin inhibitors we found that YAP/TAZ inhibition entails the remodeling of the F-actin cytoskeleton mediated by the F-actin capping and severing proteins Cofilin, CapZ, and Gelsolin (Figures 2H-I). These proteins thus give rise to a mechanotransduction pathway that, through YAP/TAZ regulation, represents a tissue-level checkpoint for mammalian epithelial sheets. This also provides a means by which cells perceive the architectural topology of a tissue as patterns of local mechanical stresses, translating into different levels of YAP/TAZ activity that in turn pattern cell proliferation (Figure 2J). Of note, we could also show that the regulation of YAP/TAZ by cell mechanics is not only distinct from Hippo pathway-induced YAP/TAZ inhibition but, in fact, dominates over it. Remarkably, LATS1/2 inactivation is per se inconsequential in cells experiencing a low mechanical stress (Figure 2J) (Aragona et al., 2013). Moreover, depletion of F-actin-capping/severing proteins sustains YAP/TAZ activity without affecting their phosphorylation. In fact, LATS-mediated inhibition of YAP/TAZ requires a mechanically competent cytoskeleton, as the effect of LATS knockdown becomes manifest only in the absence of F-actin-capping/severing proteins (Figure 2J). In addition to the Hippo pathway, we found that mechanical cues also dominate the cellular response to soluble cues positively affecting YAP and TAZ activity. YAP/TAZ activation by WNT (see below) or GPCR signaling requires a mechanically stressed cytoskeleton or, in cells experiencing a soft ECM or contact-inhibited, inactivation of F-actin capping and severing proteins (Figure 2J) (Aragona et al., 2013).

Crosstalk between YAP/TAZ and WNT signaling

YAP/TAZ can also respond to ligands of the Wnt family, a class of soluble growth factors implicated in the regulation of cell proliferation, stem cell expansion and tumorigenesis (Clevers, 2006; Niehrs and Acebron, 2012).

Recently a body of work, carried on by us and other groups, revealed a deep integration of YAP/TAZ in the canonical Wnt pathway (Azzolin et al., 2014; Azzolin et al., 2012; Imajo et al., 2012). In particular, we found that stimulation by ligands of the canonical Wnt pathway, such as Wnt3A, results in nuclear accumulation of YAP/TAZ and triggers YAP/TAZ transcriptional activity (Figures 3A-C). Mechanistically, in absence of Wnt signaling, YAP/TAZ are components of the cytoplasmic β-catenin destruction complex, as revealed by co-immunoprecipitation assays for the central scaffold component of complex Axin1 (Figure 3D) (Azzolin et al., 2014). The β-catenin destruction complex is the core component of the canonical Wnt pathway, composed by a central scaffold protein, Axin, that coordinates other factors, such as adenomatous polyposis coli (APC), CK1, and glycogen synthase kinase-3 (GSK3). Inside the β-catenin destruction complex β-catenin is phosphorylated by GSK3 and ubiquitinated by β-TrCP, leading to its subsequent proteasomal degradation. Wnt ligand stimulation causes the inactivation of the destruction complex by recruitment to the LRP6 co-receptor, allowing β-catenin accumulation and activation of β-catenin-TCF/Lef transcriptional functions (Clevers, 2006). We found that Wnt stimulation also causes concomitant release of YAP/TAZ from the complex, allowing for their nuclear accumulation (Figure 3D). In line, depletion of destruction complex components, such as APC or Axin1/2, induces YAP and TAZ nuclear accumulation and is sufficient to trigger YAP/TAZ transcriptional activity in absence of Wnt stimulation (Figures 3E-G). By exploring the composition of the β-catenin destruction complex using co-immunoprecipitation assays we also uncovered an essential role of YAP/TAZ for the inhibition of β-catenin in Wnt-off state. The presence of YAP/TAZ in the complex is essential for recruitment of β-TrCP, and thus for β-catenin inhibition in absence of Wnt signaling, as siRNA mediated depletion of YAP/TAZ impaired association of β-TrCP to the

destruction complex and resulted in the activation of β-catenin transcriptional activity (Figures 3H-I) (Azzolin et al., 2014). By freeing YAP/TAZ from the destruction complex, Wnt stimulation also releases β-catenin from ubiquitination, leading to its nuclear accumulation. By this mechanism, Wnt stimulation can concomitantly trigger activation of both β-catenin and YAP/TAZ in a coordinated fashion (see scheme in Figure 3J).

We could illustrate a remarkable example of the biological roles of YAP/TAZ as transducers of the Wnt pathway in the intestinal epithelium. The homeostasis of this tissue depends on stem cells located at the bottom of the intestinal crypts, whose maintenance depends on Wnt signaling. YAP/TAZ activity is dispensable for Wnt-dependent intestinal homeostasis, as intestinal specific double knockout of YAP and TAZ is apparently inconsequential for normal intestinal physiology (Figure 3K) (Azzolin et al., 2014). Still, we found that YAP/TAZ are genetically required for intestinal crypts overgrowth triggered by aberrant Wnt signaling upon inactivation of the tumor suppressor APC (Figure 3K) (Azzolin et al., 2014). This result is also in line with the requirement of YAP/TAZ for regeneration of the intestinal epithelium after inflammatory damage (Cai et al., 2010). These results hint to the possibility that β-catenin and YAP/TAZ transcriptional programs may mediate distinct outcomes of Wnt signaling, with β-catenin/TCF being responsible for the control of normal homeostasis and YAP/TAZ being activated in conditions in which intense intestinal proliferation is required, such as tumorigenesis and regeneration.

YAP/TAZ are required for self-renewal of somatic stem cells *ex vivo*

Intestinal crypt cultures

We first assessed the role of YAP/TAZ in the most established *ex vivo* culture system for somatic stem cells of endodermal origin: intestinal crypt cells. For this we first monitored the expression of endogenous YAP and TAZ by western blotting in dissected crypts and villi from the small intestine of adult mice. As

shown in Figure 4A, both YAP and TAZ are specifically expressed in the crypt compartment. These results are consistent with a recent report on YAP immunolocalization in the stem cells located at the crypt base (Barry et al., 2013).
Inactivation of both YAP and TAZ in the intestinal epithelium has no effects on normal tissue homeostasis (Figure 3K) (Azzolin et al., 2014). However, YAP/TAZ are required for regeneration of the intestinal epithelium, as lack of YAP impairs crypt repopulation after injury (Cai et al., 2010). Moreover, combined deletion of YAP and TAZ rescues intestinal crypt hyperplasia caused by aberrant activation of the Wnt pathway after APC depletion (Figure 3K) (Azzolin et al., 2014).
We thus sought to assess the combined relevance of YAP and TAZ for crypt regeneration *ex vivo*. For this, we focused on the growth of explanted intestinal crypts into budding organoids, as this represents a well-defined experimental system reminiscent of *in vivo* regeneration (de Lau et al., 2011). We cultured *ex vivo* intestinal crypts explanted from the small intestine (Sato et al., 2009) from control *Villin-CreERT2* mice or from mice carrying double YAP/TAZ conditional alleles (*Villin-CreERT2*; $Yap^{fl/fl}$; $Taz^{fl/fl}$) and then seeded in Matrigel with a cocktail of supplements, including the Wnt-agonist R-Spondin, which is essential for crypt maintenance and growth. Control explants formed organoids irrespective of the presence or absence of tamoxifen. Remarkably, tamoxifen-induced deletion of YAP/TAZ blocked crypt growth and led to the demise of the mutant crypts (Figures 4B, C and D), revealing the essential role of YAP/TAZ in this process.

Pancreatic progenitor cultures

As a second paradigm of somatic progenitor cells, we focused on pancreatic progenitors purified from the pancreatic duct, that have been recently shown to be expandable *in vitro* (Huch et al., 2013).
We explanted primary pancreatic duct fragments from pancreata of adult mice and cultured them as progenitor cultures in three-dimensional organoid culture conditions (Figure 5A).
We found that, in contrast to primary acinar cells, pancreatic progenitors display nuclear YAP/TAZ, as shown by immunofluorescence (Figure 5B). In line with

this evidence, pancreatic progenitors display elevated YAP/TAZ activity compared to primary acinar cells, as measured by qRT-PCR for a number of endogenous YAP/TAZ targets, as *Ctgf*, *AnkrD1*, *AmotL2* and *Axl* (Figure 5C). We thus asked whether, similarly to intestinal crypt organoids, pancreatic progenitor cultures genetically required YAP/TAZ for their propagation as organoids. For this, we derived pancreatic progenitor cultures from wild-type (*wt*) or from double conditional $Yap^{fl/fl};Taz^{fl/fl}$ mice and then excised the conditional alleles by transduction of Cre recombinase (or GFP as control) using adenoviral vectors (Adeno-Cre or Adeno-GFP) on these cultures upon passaging. Control progenitor cells (*wt*) formed organoids in the presence or absence of Adeno-Cre. Remarkably, combined deletion of YAP/TAZ severely inhibited organoid formation and led to the demise of all the mutant cells, revealing the essential role of YAP/TAZ for the self-renewal of pancreatic progenitors (Figures 3D and E).

Neural stem cells

As third paradigm of somatic stem cells we studied neural stem cells. We started by comparing YAP/TAZ activity in neural stem cells and in terminally differentiated neurons. For this, we prepared neurons by dissociating the hippocampus or cortex of late mouse embryos (E19), and selected for post-mitotic neurons by culturing primary cells in neuronal-differentiation medium containing AraC for 7 days (Han et al., 2008). This procedure eliminates proliferating cells, resulting in a population of mature post-mitotic neurons (>95%) displaying multiple neurites and expressing βIII-Tubulin (TuJ1), NeuN and other typical neuronal markers (see below and Figures 10B and 13C). In parallel, we also derived primary neural SCs (NSCs) from dissociated cerebral hemispheres; as previously reported (Palmer et al., 1997), NSCs formed floating neurospheres that could be passaged multiple times.

By immunofluorescence, endogenous YAP and TAZ proteins were highly expressed and localized in the nucleus of Nestin-positive NSCs, but absent in TuJ1-positve neurons (Figure 6A). Consistently, YAP/TAZ target genes were specifically upregulated in NSCs, as measured by qRT-PCR on YAP/TAZ endogenous target genes *Axl*, *Cyr61* and *AmotL2* (Figure 6B). In light of the

results obtained with intestinal crypts and pancreatic progenitors, we thus asked if YAP/TAZ activity was instrumental for the propagation of NSCs in *ex vivo* cultures. For this, we derived neural stem cells from the brain of *wt* or $Yap^{fl/fl};Taz^{fl/fl}$ mice and transduced these cells with Adeno-Cre to excise YAP/TAZ conditional alleles. Remarkably, combined deletion of YAP/TAZ blocked neurosphere formation, while control (*wt*) NSCs formed neurospheres also in the presence of Adeno-Cre (Figure 6C). We thus conclude that YAP/TAZ are the essential endogenous factors that are required for the self-renewal/expansion *ex vivo* of somatic progenitor cells from a number of different tissues, namely the epithelia of the intestine and of the pancreas, and the nervous tissue of the brain.

Ex vivo generation of pancreatic progenitors from exocrine cells

Starting from the observed requirement of YAP/TAZ for the maintenance of progenitor cells in *ex vivo* conditions, we next asked whether these factors might also be sufficient to endow stem properties to more differentiated cells. More in detail, we asked whether a transient pulse of YAP expression could be sufficient to convert explanted differentiated pancreatic acinar cells into normal ductal progenitors. To this end, we dissociated the pancreas of *R26-rtTA; tetOYAP*^{S127A} adult mice to obtain a highly pure preparation of exocrine acini (see Figure 9A for validation of differentiation markers expression in these explants). We embedded whole pancreatic acini explanted from *R26-rtTA; tetOYAP*^{S127A} pancreata in collagen and cultured them in low serum, that is, under conditions known to preserve acinar cell identity *ex-vivo* (Means et al., 2005) (see experimental outline in Figure 7A). When treated with doxycycline to induce YAP expression, pancreatic acini converted within few days to ductal organoid structures, and with high efficiency (> 70%) (Figures 7B and D). As control, acini lacking YAP expression (e.g., left without doxycycline, see Figure 7 D), remained as such for over 2 weeks and never converted to ducts. After transferring to 100% Matrigel/pancreatic organoid medium, the YAP-induced ducts, but not control acini, regrew into organoids. After initial derivation, YAP-induced organoids (or

"yDucts") could be passaged for several months even in absence of doxycycline and thus in absence of exogenous YAP/TAZ (for at least 10 passages, i.e. 6 months) (Figure 7C). By morphology, size and growth pattern, organoids derived from converted acinar cells were comparable to those obtained from handpicked pancreatic duct fragments after whole pancreas dissociation (Huch et al., 2013) (compare Figure 5A, rightmost panel, with Figure 7C).

Validation of acinar cell reprogramming by genetic lineage tracing

To validate that yDucts were indeed derived from differentiated exocrine acinar cells, we carried out genetic lineage tracing experiments using *Ptf1a-CreERTM; R26-LSL-rtTA-IRES-EGFP; tetO-YAP*^{S127A} mice. In the *Ptf1a-CreERTM; R26-LSL-rtTA-IRES-EGFP* background, tamoxifen treatment of adult mice causes irreversible genetic tracing exclusively of pancreatic acinar cells (Pan et al., 2013). After treatment, mice were kept without tamoxifen for 1 week and then pancreata were explanted to prepare whole acini, that were cultured as above (see experimental outline in Figure 8A). As expected, with this genetic lineage tracing setup organoids derived from endogenous ductal progenitors explanted from *Ptf1a-CreERTM; R26-LSL-rtTA-IRES-EGFP; tetO-YAP*^{S127A} pancreata were not labeled (Figure 8B), while pancreatic acinar cells were irreversibly labeled by EGFP (Figure 8C). These EGFP-positive cells never formed any organoid in absence of doxycycline (Figure 8C). Instead, doxycycline-induced YAP expression caused formation of expandable yDucts that retained EGFP positivity over passaging, formally demonstrating their derivation from terminally differentiated exocrine cells (Figures 8D,E).

Characterization of the early steps of YAP-induced conversion of exocrine cells

In order to have a deeper understanding of the YAP-induced conversion process, we also performed a time-course analysis of gene-expression dynamics occurring at the single cell level during reprogramming induced by tetO-Yap. As shown in Figure 8F, at the beginning of the experiment explanted cells expressed exocrine

markers (*Amy* and *Ptf1a*) but not markers of pancreatic progenitors (*Pdx1*, *Sox9*, *K19*, *Car2*), cell proliferation (*CyclinD1*) or the YAP targets *Ctgf* and c*Myc* (Zanconato et al., 2015). After 2 days of doxycycline treatment, pancreatic progenitor markers were turned on in most cells, and did so more robustly at day 4 and very homogeneously in yDuct cells. At day 2 and day 4, but not in yDucts, most acinar cells retained concomitant expression of acinar markers, and could be thus considered as cells caught in transition. Interestingly, *Nestin*, an embryonic pancreatic progenitor marker (Delacour et al., 2004; Esni et al., 2004), is also turned on only in these reprogramming intermediates, being absent in both differentiated cells and yDucts. We further noticed that progenitor markers are already present at day 2, before cells acquire expression of the proliferation marker *CyclinD1*.

Characterization of yDucts

yDuct-derived organoids are composed by an epithelial monolayer surrounding a central cavity (Figure 9B), a structure closely reminiscent of that one of organoids formed by endogenous pancreatic progenitors in culture (Huch et al., 2013). We then sought to characterize yDucts more deeply at the molecular level, in order to evaluate to what extent they are endowed of features associated to bona-fide pancreatic progenitors. For this, we compared the expression of exocrine differentiation versus ductal progenitor markers in primary pancreatic acini, yDucts and pancreatic progenitor cultures (Ducts). By qRT-PCR and immunofluorescence, YAP-induced organoids lost markers of exocrine differentiation (*Ptf1a*, *α-amylase, Elastase, and CPA1*) and acquired expression of ductal markers (*K19, Sox9, Hes1, Cd44*) and proliferative markers (*cMyc* and *CyclinD1*), all to levels comparable to those of native ductal organoids (Figures 9A and B). To determine the extent of YAP-induced conversion of acinar cells, and their molecular overlap with native ductal progenitors, we carried out transcriptomic analyses. As shown in Figure 9C, yDucts diverged profoundly from parental acinar cells to become overtly similar to bona-fide pancreatic progenitors.

Moreover, when placed in differentiating conditions, yDuct-derived cells could be induced to re-express the differentiated exocrine marker CPA1 and to

downregulate K19 (Figure 9D). When transplanted into the pancreas of NOD-SCID mice, yDucts remained as such, and never formed any tumor (n=6, data not shown) indicating that yDucts are indeed non-transformed and non tumorigenic. Together, the results indicate that exocrine cells with a history of exposure to YAP acquired key molecular and biological features of ductal pancreatic progenitors

YAP expression turns neurons into NSC-like cells

As a second model of YAP-induced reprograming of differentiated cells we focused on neurons. Neurons are post-mitotic cells that have long been considered refractory to any cell fate change. The evidence above described, showing that YAP/TAZ are nuclearly localized and active in NSCs, but not in neurons, and that YAP/TAZ are genetically required for the expansion of NSCs in culture (see Figure 6), prompted us to verify whether ectopic expression of YAP in neurons was sufficient to convert them into NSCs.

For this we prepared neurons by dissociating the hippocampus or cortex of late mouse embryos (E19) or newborns, and selected for post-mitotic neurons by culturing primary cells in neuronal-differentiation medium containing AraC for 7 days in order to eliminate proliferating cells. These primary cultures were the starting cells of our reprogramming efforts and were validated as post-mitotic neurons as follows: i) our primary neurons displayed multiple neurites marked by bIII-Tubulin (TuJ1) and Tau and were extensively decorated by the synaptic marker Synaptophysin (Figure 6A and Figure 10A); ii) neurons also expressed NeuN and were negative for NSC/progenitor markers, such as Nestin, Sox2, Vimentin (Figure 13A); iii) by qRT-PCR and transcriptomic analyses, neurons expressed a number of late differentiation genes but lacked of NSC-associated markers (Figures 13B and C) (see expression of *Syn1, Snap25, a-synuclein, CamK2a, Synaptotagmin, Synaptophysin* and many others (see a full list in Table 1).

In order to test whether YAP could revert post-mitotic neurons to a NSC-like state, primary cells were infected with lentiviral vectors encoding for rtTA and

inducible wild-type YAP (see Experimental procedures). After AraC treatment, neurons were shifted to NSC medium in the presence of doxycycline (see experimental outline in Figure 10B). Remarkably, after 2 weeks, neurosphere-like structures emerged from YAP-expressing neurons (P0-spheres), but never from neurons transduced with rtTA alone, or rtTA combined with EGFP, empty vectors or transcriptionally inactive YAPS94A (Figure 10C). P0-spheres were then transferred to new plates for further growth, and could be then propagated for several passages as clonal outgrowths after single cell dissociation, indistinguishably from and at comparable frequency of native NSCs (Figure 10D). Of note, the propagation of YAP-induced NSCs (hereafter called yNSCs) as neurospheres did not require addition of doxycycline, indicating that transient exposure to exogenous YAP is sufficient to induce self-renewal properties that are autonomously maintained.

Validation of neuronal reprogramming by genetic lineage tracing

To validate that yNSCs derived from terminally differentiated neurons, we repeated YAP-induced reprograming starting from genetically lineage-traced neurons (see scheme in Figure 11A).

For this, we employed the most established transgenic mouse strain used to genetically label exclusively post-mitotic neurons starting from late embryogenesis (Zhu et al., 2001), that is *Syn1-Cre* mice. These mice express the Cre recombinase under the control of the neuronal-specific Synapsin1 promoter; we crossed this strain with the conditional reporter line *R26-CAG-LSL-tdTomato*. We derived neurons form the brain of *Syn1-Cre; R26-CAG-LSL-tdTomato* transgenic mice and confirmed by immunofluorescence analyses that in our primary neuronal cultures expression of the lineage tracer (tdTomato) is indeed restricted to post-mitotic neurons, all displaying unambiguous neuronal morphology and expressing TuJ1 (in 100% of tdTomato-positive cells, n=635), Tau (100%, n=140) and NeuN (90%, n=252). None of these genetically-traced cells was ever positive for the neural stem cell markers Nestin, Vimentin, Mash1, or for proliferation markers (EdU; Ki67) (0%, n>4000 cells) (see figures 11B and

C). All labeled cells were also characterized by extensive dendritic processes, punctuated by the synaptic markers Synaptophysin and SV2A (Figure 11D).
Moreover, in order to exclude the possibility that *Syn1-Cre* and might be expressed in rare or quiescent NSC contaminating our neuronal cultures, we also derived NSCs from *Syn1-Cre; R26-CAG-LSL-tdTomato* brains and found that, oppositely to neurons of the same genotypes, in no case we could detect lineage labeled neurospheres (0% over n>160 spheres obtained) (Figure 12A, bottom panels).
Importantly, upon YAP-induced reprogramming, lineage-traced neurons from the brain of *Syn1-Cre; R26-CAG-LSL-tdTomato* transgenic mice gave rise to tdTomato-positive neurospheres (Figure 12A). In contrast, as mentioned above, NSCs derived from the same strain were invariably unlabeled (Figure 12A, bottom left panel), confirming that these drivers are not active in natural NSCs and thus that yNSCs originated from differentiated neurons rather than through amplification of pre-existing, contaminating progenitors. All lineage-traced yNSCs could be passaged for several generations (Figure 12A, bottom panels). This lineage-tracing setup also allowed us to follow YAP reprogramming of neurons explanted from *Syn1-Cre; R26-CAG-LSL-tdTomato* mice over several days with continuous imaging. YAP expression was specifically associated to a discrete set of sequential events (Figure 12A, top panels): after 24/48 hours of doxycycline addition and switch to NSC medium, lineage-traced neurons started to lose neurites and flattened, acquiring an irregular, polygonal shape with rough borders. In the following days (96 hours) cells turned to a more elongated shape and proliferated. Cells compacted in discrete foci, each leading to dome-like outgrowths from which a floating spheroid detached (either spontaneously or after plate tipping) that got collected as P0 cultures.

Characterization of the early steps of neuronal reprograming

In order to follow the early stages of YAP-induced reprogramming, YAP expression was induced by addition of doxycycline 24 hours before switching to NSC medium. By using immunofluorescence, this approach allowed following more closely the dynamic of individual genetically-labeled neurons expressing YAP. As in previous experiments, tdTomato-traced/YAP-expressing cells entered reprogramming as NeuN-positive and invariably Nestin-negative neurons. Just 48

hours after switching to NSC medium, all tdTomato-positive/YAP-expressing neurons lost expression of NeuN and wholesale turned on Nestin expression. Importantly, this transition occurred with similar efficiency even in presence of the anti-mitotic drug AraC (Figures 12B and C). By day 5, all the non-infected neurons had died and the culture consisted exclusively of YAP-expressing cells. Taken together, the validation of the starting cell population, the fact that yNSCs are genetically labeled by a bona-fide transgenic tracer specific for neurons and not NSCs, the rapid dynamic and essentially quantitative conversion of YAP-expressing neurons to yNSCs, and the fact that this occurs even independently of proliferation, all indicate that yNSCs originate from mature neurons and argue against the possibility that acquisition of NSC-traits could be secondary to survival and expansion of rare, preexistent, contaminant endogenous NSCs.

Characterization of yNSCs

Next, we characterized yNSCs by marker gene expression, using immunofluorescence, qRT-PCR and gene expression profiling. As shown in Figures 13A and C, yNSCs completely lost expression of the terminal differentiation markers present in the original neurons (such as TuJ1, Tau and NeuN), and instead expressed high levels of NSC markers (Nestin, Sox2, Vimentin), and to levels comparable to native NSCs. Note also that in 2D cultures yNSCs and native NSCs are morphologically indistinguishable (Figure 13A).
In order to characterize to what extent YAP triggers conversion of neurons into a bona-fide NSC-status, we compared the transcriptome of parental neurons, yNSCs and native NSCs. As shown in Figure 13B, yNSCs completely lost their neuronal identity and acquired a gene expression profile closely similar to native NSCs. By Gene Ontology (GO), genes upregulated in both yNSCs and NSCs were specifically enriched of gene categories associated to positive regulation of the cell cycle and development/maintenance of the neural progenitor state. Genes downregulated in both yNSCs and NSCs were specifically enriched for GO terms related to terminal differentiation of neurons, transmission of nerve impulse, and nerve cell function.

yNSCs display tripotent differentiation potential

Neural SCs are defined as tripotent, as attested by their ability to differentiate in astrocytes, neurons and oligodendrocytes. We thus examined the differentiation potential of yNSCs. Once plated on fibronectin and treated with BMP4 and LIF (Bonaguidi et al., 2005), yNSCs completely switched to typical astrocyte morphology, expressing high levels of GFAP (Figure 14A, left panels). For neuronal differentiation, we implemented a recently reported culture system involving plating of NSCs on Matrigel (Choi et al., 2014) (see Experimental procedures). In these conditions, yNSCs underwent widespread differentiation in neurons, characterized by an extensive neurite outgrowth, that were TuJ1- and Tau-positive but Nestin-negative (Figure 14A, middle panels and Figure 14B). Moreover, upon treatment with IGF and T3 (Hsieh et al., 2004), yNSCs could also differentiate into oligodendrocytes, displaying the typical branching morphology and CNPase positivity (Figure 14A, right panels).

To investigate the *in vivo* differentiation potential of yNSCs, we transduced yNSCs with lentiviral vectors encoding for constitutively expressed EGFP and transplanted EGFP-labeled yNSCs in the brain of newborn mice (n=5). Four weeks after transplantation, grafted yNSCs invariably lost Nestin positivity (Figure 14C) and mainly remained close to the injection site, where they primarily acquired expression of GFAP, indicative of astrocyte-differentiation (Figures 14D,E). However, some cells migrated away from the graft (Figure 14F) and differentiated in NeuN- and TuJ1-positive neurons or CNPase-positive oligodendrocytes (Figure 14G). Importantly, no tumor formation was ever observed after histological examination of the yNSCs-injected brain parenchyma. Thus, YAP induces conversion of neurons into cells that are functionally corresponding to normal NSCs.

DISCUSSION

A dysregulated Hippo pathway has been shown to induce cell fate changes in transgenic livers and mammary cells (Cordenonsi et al., 2011; Fitamant et al., 2015; Skibinski et al., 2014; Yimlamai et al., 2014). Yet, the possibility that YAP/TAZ activity could be used to generate normal somatic SCs de novo remained so far unexplored. Here we report that expression of a single factor, YAP, into terminally differentiated cells explanted from different tissues efficiently creates cells with functional and molecular attributes of their corresponding tissue-specific SCs, that can be expanded *ex-vivo* as organoid cultures. The ySC state can be transmitted through cell generations without need of continuous expression of ectopic YAP/TAZ, indicating that a transient activation of YAP or TAZ is sufficient to induce a heritable self-renewing state.

YAP turns terminally differentiated cells into SC-like cells.

We used several approaches to validate the notion that ySCs originate from conversion of fully differentiated cells, rather than from amplification of contaminant, rare, pre-existing, tissue SCs. This notion is supported primarily by tracing of differentiated cells with established lineage-specific Cre-drivers. Pancreatic acinar cells were labeled with *Ptf1a-CreERTM*: upon tamoxifen treatment of adult mice, this driver has been previously shown to exclusively label pancreatic acinar cells (Pan et al., 2013), and indeed, this transgenic line has been previously employed to demonstrate that KRas-induced tumors in fact originated from acinar cells (Kopp et al., 2012). As for neurons, we adopted a well-established neuronal specific driver, *Syn1-Cre* that has been used, as confirmed here, to mark post-mitotic neurons already in embryos (Zhu et al., 2001). Endogenous pancreatic progenitors or NSCs derived from the same mice employed to derive differentiated exocrine acini or neurons, respectively, were never labeled, collectively supporting the view that differentiated cells are the cellular targets of YAP. Most importantly, in no case we could detect dedifferentiation or emergence of spheroids in control cultures infected with the sole rtTA, empty vectors or a point-mutant of YAP unable to interact with

TEAD, the YAP/TAZ DNA binding platform. Collectively, these data do not favor the notion that rare stem cells may be the origin of YAP-induced SCs.

YAP-induced reprograming generates cells with normal SC traits, as: i) ySCs are non transformed and non tumorigenic; ii) ySCs are endowed with differentiation potential and can generate a multilineage progeny, in a manner indistinguishable from their corresponding native SCs; iii) at the transcriptomic level, ySCs display massive overlaps with native SCs; iv) in the case of yNSCs, we could also show as proof-of-principle that these cells display multilineage differentiation capacity also when transplanted *in vivo*.

YAP/TAZ as the centerpiece of somatic cell plasticity

Lineage infidelity and reversion to a SC-like status rarely occur during homeostasis of normal tissues, but are associated to tissue repair or oncogenic activation (Blanpain and Fuchs, 2014; Lim et al., 2009; Robel et al., 2011; Skibinski et al., 2014; Tetteh et al., 2015; Yimlamai et al., 2014). Of note, genetic depletion of YAP and/or TAZ in several adult epithelia is inconsequential for normal homeostasis, but in fact absolutely essential for regeneration, tumor growth (Azzolin et al., 2014; Bailleul et al., 1990; Cai et al., 2010; Mani et al., 2008), and, as shown here, for expansion of somatic SCs *in vitro*. It is thus tempting to propose YAP/TAZ as "master-genes" required and sufficient for somatic cell plasticity and SC maintenance whenever natural, pathological or *ex-vivo* conditions demand de novo generation and expansion of resident or facultative SCs.

It is intriguing to note that previous work on YAP/TAZ and its ability to convert non-stem tumor cells into cancer-SCs (Cordenonsi et al., 2011) may be re-interpreted as a role of YAP/TAZ in controlling cell plasticity even within established tumors.

Further work is required to dissect the means by which expression of YAP overcomes the differentiated cell state and triggers a stable, de novo SC status in distinct cell types. At the molecular level, this is clearly linked to YAP-regulated gene transcription, relying on YAP binding to its transcriptional partner TEAD, as we show that ySC generation is impaired after YAP is mutated at a residue critical for the association to TEAD (YAP S94A). Gene-expression studies provided some intriguing mechanistic insights, as we found that YAP induces several genes known to be instrumental for SC self-renewal and/or functionally implicated in SC biology

for the various tissues here analyzed. This includes transcription factors, such as Sox2 and Sox9 that are essential for maintenance/regeneration of NSCs and pancreatic progenitors, respectively (Favaro et al., 2009; Seymour et al., 2007). Of note, it has been recently shown that, in the embryonic pancreas, Sox9 is directly induced by YAP through a TEAD-bound enhancer (Cebola et al., 2015), at least suggesting that some of the factors involved in somatic SC biology may be direct YAP/TAZ targets. Moreover, although the activation of cell proliferation is clearly a hallmark of ySC generation, our work at least suggests that the early stages of reprogramming are independent of induction of cell proliferation.

We further note that YAP/TAZ are not just "exogenous" triggers of a *de novo* SC state but also the endogenous factors enriched in the corresponding native SCs, required to maintain their organoid-forming potential *ex-vivo*, as validated for all the cell types here investigated. These results at least suggest the existence of a YAP/TAZ-centered stemness network in various types of somatic SCs, whose components remain to be identified. We can only speculate at this stage that YAP/TAZ must intersect with lineage- and cell-specific transcription factors, possibly at composite enhancer elements (Zanconato et al., 2015), to turn off transcription of terminally differentiated traits and concomitantly sustain expression of progenitor-specific genes while respecting tissue-barriers.

ySCs represent a novel reprograming paradigm

Immortalized or transformed cell lines are the workhorses of cell biology; however, it is still unclear to what extent the biology of normal cells may be recapitulated by these models. Moreover, for each histotype, the number of available cell lines is restricted, and each line diverges from the others and their tissue of origin for a number of genetic and epigenetic abnormalities. This complicates interpretation and modeling of diseases, as each patient carries a specific subset of genetic alterations and a unique genetic milieu. Thus, a potential application of the reprograming procedure here presented is the possibility to generate, expand and functionally interrogate *in vitro* patient-specific cells of various tissue sources starting from abundant differentiated cells, even in conditions in which resident SCs are not available because naturally rare, old, not extractable from a living body or exhausted

by damage or disease. Differently from iPSCs, the reprogramming to ySCs preserves the epigenetic memories of the tissue of origin, eliminating the need to differentiate pluripotent cells along with the risks associated to their intrinsic tumorigenicity (Ben-David and Benvenisty, 2011).

Another paradigm for changing cell fate and for *in vitro* generation of patient-specific cell types is directed differentiation, aiming to convert one somatic cell into another mature cell type. Reprogramming to ySCs may overcome the fundamental limitation of this approach, as mature cells are typically postmitotic or lack significant proliferative potential; this limits the number of cells that can be generated and thus compromises long-term expandability, self-organization and organ repopulation potentials, all features that appear essential for most present and future applications. YAP-induced SCs may thus expand the current reprogramming paradigms by focusing on somatic stem cell generation, a state that has been so far challenging to capture.

EXPERIMENTAL PROCEDURES

Reagents, plasmids and transfections

Doxycycline hyclate, fibronectin, collagen I, insulin, dexamethasone, SBTI (Soybean Trypsin Inhibitor), gastrin, N-acethylcysteine, nicotinamide, T3 (Triiodo-L-Thyronine), tamoxifen and 4-OH-tamoxifen were from Sigma. Murine EGF, murine bFGF, human FGF10, human Noggin, human IGF, murine BMP4 were from Peprotech. N2, B27, BPE and ITS-X (Insulin-Transferrin-Selenium-Ethanolamine) supplements were from Life Technologies. R-Spondin1 was from Sino Biological. Matrigel was from BD Biosciences (Corning). Rat tail collagen type I was from Cultrex.

GFP- and Cre-expressing adenoviruses were from University of Iowa, Gene Transfer Vector Core. For inducible expression of YAP and TAZ, cDNA for siRNA-insensitive Flag-hYAP1 wt, S94A (TEAD-binding mutant; (Zhao et al., 2008)) were subcloned in FUW-tetO-MCS, obtained by substituting the Oct4 sequence in FUW-tetO-hOct4 (Addgene #20726; (Hockemeyer et al., 2008)) with a new multiple cloning site (MCS). This generated the FUW-tetO-wtYAP, FUW-tetO-YAPS94A used throughout this study. FUW-tetO-MCS (empty vector) or FUW-tetO-EGFP plasmids were used as controls, as previously indicated (Cordenonsi et al., 2011).

For stable expression of GFP, pRRLSIN.cPPT.PGK-GFP.WPRE (gift of L. Naldini) lentiviral vector was used. All constructs were confirmed by sequencing.

DNA transfections were done with TransitLT1 (Mirus Bio) according to manufacturer instructions.

Lentivirus preparation

HEK293T cells (checked routinely for absence of mycoplasma contaminations) were kept in DMEM supplemented with 10% FBS (Life Technologies), Glutamine and Antibiotics (HEK medium). Lentiviral particles were prepared by transiently transfecting HEK293T with lentiviral vectors (10 micrograms/10 cm dishes) together with packaging vectors pMD2-VSVG (2.5 micrograms) and pPAX2 (7.5 micrograms)

by using TransIT-LT1 (Mirus Bio) according to manufacturer instructions. Specifically, 60 µl of TransIT-LT1 reagent was diluted in 1.5 ml of Opti-MEM (Life Technologies) for each 10 cm dish, incubated with the vector DNA 15 min at RT and gently distributed over to the cell medium (dish contained about 10 ml of HEK medium). After 8 hr, HEK medium was changed. 48 hr post-transfection supernatant was collected, filtered through 0.45 micrometers and directly stored at -20°C; we did not concentrate viral supernatants. For a typical infection of a 3 cm dish containing primary cells, we used 500 µl of each unconcentrated viral supernatant diluted to 1x cell-specific medium (see below) in 2 ml final volume. We also seldom measured the lentiviral titer of various supernatants used in our experiments using the QuickTiter Lentivirus Titer kit (lentivirus-associated HIV p24; Cell Biolabs) according to the manufacturer's protocol. As reference, viral supernatants were in the range 16 - 20 ng of p24/ml. This titer corresponds to a viral particle concentration of about $2x10^8$ particles/ml. As determined by PCR of integrated lentiviral DNA of HEK293T transduced with pRRL-EGFP, this roughly corresponds to $2x10^6$ transduction units (TU)/ml in the unconcentrated viral supernatant stock.

Pancreatic acinar cells isolation and induction of yDucts

Primary pancreatic acini were isolated from the pancreas of 6- to 9-week-old mice, according to standard procedures (Means et al., 2005). Digested tissue was filtered through a 100 µm nylon cell strainer. The quality of isolated acinar tissue was checked under the microscope. For culture of entire acini, explants were seeded in neutralized rat tail collagen type I (Cultrex)/acinar culture medium (1:1) (Means et al., 2005), overlaid with acinar culture medium (Waymouth's medium (Life Technologies) supplemented with 0.1% FBS (Life Technologies), 0.1% BSA, 0.2 mg/ml SBTI, 1x ITS-X (Life Technologies), 50 µg/ml BPE (Life Technologies), 1µg/ml dexamethasone (Sigma), and antibiotics) once collagen formed a gel. For induction of pancreatic organoids, entire acini of the indicated genotypes were seeded in medium supplemented with 2 µg/ml doxycycline. Negative control cells were cultured in the same conditions in absence of doxycycline. Cells were treated with 2 µg/ml doxycycline for 7 days and organoid formation was morphologically followed. Organoids were then passaged or processed for further analyses. To assess enrichment

of acinar cells in our preparation, we compared RNA extracts from whole pancreas and our fresh acinar cell preparation for expression of exocrine cell markers, such as *α-amylase*, *elastase* and *CPA1*, normalized to *18-S rRNA* and found a >400 fold enrichment of these markers in acinar preparations.

For the experiment depicted in Figures 8B-D (see also scheme in Figure 8A), we obtained acinar explants from 6 week-old *Ptf1a-CreERTM; R26-LSL-rtTA-IRES-EGFP/+; tetO-YAP*^{S127A} mice (Pan et al., 2013). Mice with this genotype were given tamoxifen by three daily i.p. injections of a 10 mg/ml solution in corn oil. 1 week after the last tamoxifen injection, mice were sacrificed and pancreas was dissociated to obtain *rtTA-IRES-EGFP*$^{+}$-labeled exocrine acinar cells. Primary pancreatic acinar cells were isolated and cultured as above. For induction of pancreatic organoids, acinar explants were treated with 2 μg/ml doxycycline as above.

Matrigel culture of yDucts organoids

To show the self-renewal capacity of pancreatic organoids independently of exogenous YAP supply (i.e, independently of doxycycline administration), organoids were recovered from collagen cultures, trypsinized to obtain a single cell suspension and re-seeded in 100% Matrigel. Once Matrigel formed a gel, cells were supplemented with pancreatic organoid medium (Advanced DMEM/F12 supplemented with 1x B27, 1.25mM N-Acetylcysteine, 10 nM gastrin, 50 ng/ml murine EGF, 100 ng/ml human Noggin, 100 ng/ml human FGF10, 10 mM Nicotinamide, 1 μg/ml R-Spondin1 and antibiotics) supplemented with 0.2 mg/ml SBTI. For analysis, organoids were recovered from Matrigel and processed for immunofluorescence or for protein or RNA extraction.

For the differentiation experiments shown in Figure 9D, yDucts were removed from Matrigel, trypsin-dissociated and seeded as single cells in Matrigel- coated (1:50) chamber slides. Cells were expanded in DMEM supplemented with 0.5% BSA, 1% ITS-X and 1x N2 and 50 ng/ml EGF and antibiotics for 5 days. For differentiation, cells were switched to DMEM/F12 supplemented with 1% ITS-X, 10 ng/ml bFGF, 10 mM nicotinamide, 50 ng/ml Exendin-4 and 10 ng/ml BMP4 and antibiotics for further 8 days. Cells were fixed in 4% PFA at Day 0 or Day 8 of differentiation and processed for immunofluorescence.

Culture of pancreatic ductal organoids (Ducts)

For culture of pancreatic duct-derived organoids, pancreatic ducts were isolated from the bulk of the pancreas as previously described (Huch et al., 2013) with minor modifications. The whole pancreas of 6- to 9-week-old mice of the indicated genotypes was grossly minced and digested by collagenase/dispase dissociation: DMEM medium (Life Technologies) supplemented with collagenase type XI 0.012% (w/v) (Sigma), dispase 0.012% (w/v) (Life Technologies), 1% FBS (Life Technologies) and antibiotics at 37°C for 1 hour. Isolated pancreatic duct fragments were hand-picked under a dissecting microscope, carefully washed in DMEM medium and embedded in 100% Matrigel. After Matrigel formed a gel, pancreatic organoid medium (Advanced DMEM/F12 supplemented with 1x B27, 1.25mM N-Acetylcysteine, 10 nM gastrin, 50 ng/ml murine EGF, 100 ng/ml human Noggin, 100 ng/ml human FGF10, 10 mM Nicotinamide, 1 μg/ml R-Spondin1 and antibiotics) was added. Ductal fragments rapidly expanded to form cyst-like organoids within 5 days. Organoids were removed from Matrigel by incubation in ice cold HBSS, dissociated with trypsin 0.05% for 30 min to obtain a single cells suspension and reseeded in 100% fresh Matrigel. Organoid cultures were maintained for at least 9 months passaging every 10 days. For analysis, organoids were recovered from Matrigel as above and processed for immunofluorescence or for protein or RNA extraction.

For the experiments depicted in Figure 5D, pancreatic duct fragments were isolated from 9 weeks old $Yap^{fl/fl}$; $Taz^{fl/fl}$ mice, embedded in 100% Matrigel and cultured as above. Organoids were passaged once every 10 days. After at least 3 months of culture, organoids were removed from Matrigel by incubation in ice cold HBSS, trypsin-dissociated and transduced with adenovirus encoding for CRE recombinase to induce *Yap/Taz* knockout (or with GFP-encoding adenovirus as control). Single cells were resuspended in 2 ml Advanced DMEM/F12, transduced for 2 hours at 37°C with adenovirus, washed in Advanced DMEM/F12 and seeded in 100% Matrigel. After Matrigel formed a gel, cells were maintained in pancreatic organoid medium and organoid formation capacity was morphologically monitored over a period of 10 days. Pancreatic ductal organoids obtained from *wt* mice were used as additional controls and treated as above.

Single-cell gene expression analysis during the conversion of pancreatic acinar cells to yDucts

For the experiment depicted in Figure 8F, we dissociated and harvested single cells from pancreatic cultures of the *R26-rtTA; tetO-YAP S127A* genotype during the YAP-induced conversion from acinar cells to yDucts, that is at: day 0 = starting acini (without doxycycline); day 2 = cultures that have experienced 48 hours of doxycycline; day 4 = cultures that have experienced 96 hours of doxycycline; yDucts = yDucts obtained as above (n= 12/13 each time point). Single cells were collected by pipetting into 200 μl- conical tubes and processed for total RNA extraction, retro-transcription and pre-amplification with Single Cell-to-CT kit (Ambion), according to manufacturer's protocol. Specific target amplification products were then processed for qRT-PCR analysis on QuantStudio 6 Flex Real-time PCR System, 384-well (Applied Biosystems) with the following Taqman Gene Expression Assays: *18S* (Hs99999901_s1), *Amy2a5* (Mm02342486_mH), *Ptf1a* (Mm00479622_m1), *Nestin* (Mm00450205_m1), *Krt19* (Mm00492980_m1), *Sox9* (Mm00448840_m1), *Car2* (Mm00501576_m1), *Pdx1* (Mm00435565_m1), *Ctgf* (Mm01192933_g1), *Myc* (Mm00487804_m1), *Ccnd1* (Mm00432359_m1). Expression levels were normalized to *18S-rRNA* for each sample.

Primary neuron isolation and induction of yNSCs

Neurons were prepared from hippocampi or cortices of E18-19 embryos or newborn mice as previously described (Han et al., 2008). Briefly, hippocampi and cortices were dissected under the microscope in ice cold HBSS as quickly as possible, incubated with 0.05% trypsin (Life Technologies) 15 min at 37°C and, after trypsin blocking, resuspended in DMEM/10% FBS supplemented with 0.1 mg/ml DNase I (Roche), and mechanically dissociated by extensive pipetting. Cells were then plated on poly-L-lysine-coated wells in DMEM supplemented with 10% FBS, glutamine and antibiotics for hippocampal neurons, or in DMEM/Neurobasal (1:1) supplemented with 5% FBS, 1x B27, glutamine and antibiotics for cortical neurons (day 1). After 24 hours (day 2), the medium of both hippocampal and cortical preparation was changed to fresh DMEM/Neurobasal (1:1) supplemented with 5% FBS, 1X B27, glutamine and

antibiotics. For reprogramming experiments neurons were infected on the following day (day 3) with FUW-tetO-wtYAP and FUdeltaGW-rtTA viral supernatants. Negative controls were provided by neurons transduced with FUdeltaGW-rtTA alone or in combination with FUW-tetO-EGFP or FUW-tetO-MCS (empty vector). For this, for a typical 3.5 cm plate, we mixed 500 μl of FUdeltaGW-rtTA with 250 μl of FUW-tetO-wtYAP (or negative controls) viral supernatants, 250 μl of HEK medium with 1.5 ml of serum-free Neurobasal medium with 2X B27. After 24 hour (day 4), medium was changed and cells were incubated in Neurobasal medium supplemented with 1X B27, glutamine, antibiotics, and 5 μM Ara-C (cytosine β-D-arabinofuranoside; Sigma) for additional 7 days, at the end of which well-differentiated, complex network-forming neurons are visible. To induce yNSCs formation, treated neurons were switched to NSC medium (DMEM/F12 supplemented with 1X N2, 20 ng/ml murine EGF, 20 ng/ml murine bFGF, glutamine, and antibiotics) and 2 μg/ml doxycycline for activating tetracycline-inducible gene expression. After 7 days, fresh doxycycline (final concentration of 2 μg/ml) was added. Sphere formation was evident upon YAP induction after 14 days of doxycycline treatment (see scheme in Figure 10B). These "P0" spheres were gently transferred into a 15 ml-plastic tube and let sediment (typically 10-15 min). After discarding the supernatant, spheres were dissociated with TrypLE Express (Life Technologies) at room temperature for 5 min and mechanical pipetting. TrypLE Express was diluted in NSC medium (in case of clumps of genomic DNA, we recommend to degrade it with DNase I at this stage) and cells were resuspended in NSC medium without doxycycline. For the successive passages, spheres were harvested and dissociated and yNSCs were routinely cultured and passaged without doxycycline in NSC medium, as for normal NSCs.

For the experiment depicted in Figures 11B-D and Figure 12, we obtained cortical neurons from *Syn1-Cre; R26-CAG-LSL-tdTomato/+* embryos (day 1 and 2 as above). When indicated, these cells were transduced as above (day 3). Cells were then treated with AraC/B27 containing medium as before and, after 7 days, switched to doxycycline containing-NSC medium to activate YAP expression and induce yNSC formation from tdTomato-positive neurons. *Syn1-Cre; R26-CAG-LSL-tdTomato/+* neurons transduced with FUdeltaGW-rtTA in combination with FUW-tetO-EGFP or FUW-tetO-YAPS94A never gave rise to any neurospheres. Each embryo genotype

was confirmed on tail biopsies post-brain dissociation; as separate negative controls, neurons derived from *R26-CAG-LSL-tdTomato/+* littermates (*Syn1-Cre* negative) were transduced with FUW-tetO-wtYAP and FUdeltaGW-rtTA viral supernatants as above, and never gave rise to tdTomato-positive yNSCs. These same neurons transduced with FUdeltaGW-rtTA in combination with FUW-tetO-EGFP or FUW-tetO-YAPS94A never gave rise to any neurospheres.
To validate the specificity of the neuronal driver, primary NSCs were derived as below from *Syn1-Cre; R26-CAG-LSL-tdTomato/+* embryos and we verified the negativity for tdTomato (see Figure 12A).

Primary neural stem cells (NSCs) isolation and culture

Neural stem cells (NSCs) were isolated as previously reported (Ray and Gage, 2006) from the telencephalon of C57BL/6J E18 embryos or from mice of the indicated genotype. Telencephalons were minced and digested in trypsin 0.05% for 10 min at 37°C. The cell suspension was treated with DNaseI (Roche) and washed. NSCs were cultured in DMEM/F12 supplemented with N2, 20 ng/ml murine EGF, 20 ng/ml murine bFGF, glutamine and antibiotics. For passages, neurospheres were dissociated into single cells with TrypLE Express (Life Technologies).

NSCs/yNSCs infection and differentiation

For adenoviral infection of wild-type (wt) or double $Yap^{fl/fl}$; $Taz^{fl/fl}$ NSCs (Figure 6C), single cells were plated in NSC medium containing adeno-Cre on ultra-low attachment plates and allowed to form neurospheres for 7 days.
For neuronal differentiation, NSCs or yNSCs were cultured over a thin Matrigel layer. Differentiation medium was Neurobasal supplemented with 1x B27, glutamine.
For astrocyte differentiation, NSCs or yNSCs were plated on fibronectin coated-plate in NSC medium, to allow a 2D culture. The next day, medium was changed to DMEM (Life Technologies) containing 25 ng/ml LIF, 25 ng/ml BMP4, glutamine, and antibiotics for 2 weeks.
For oligodendrocyte differentiation, NSCs or yNSCs were plated on fibronectin coated-plate in NSC medium, to allow a 2D culture. The next day, medium was

changed to Neurobasal (Life Technologies) containing 1x B27, 500 ng/ml IGF, 30 ng/ml T3, glutamine, and antibiotics for 2 weeks.

NSCs transplantation

P0 CD1 mice pups were used for cell transplantations. Pups were anesthetized by hypothermia (3 minutes) and fixed on ice-cold block during cell injection. Cells were resuspended in ice-cold HBSS ($5x10^4$ cells/µl) and injected into both hemispheres of neonatal mice with a 5µl-volume Hamilton syringe (2µl/injection). One month after the procedures, the grafted animals were perfused with PBS and 4%PFA, and the brains were excised and processed for immunofluorescence.

Immunofluorescence, stainings and microscopy

Immunofluorescences on PFA-fixed samples were performed as previously described (Cordenonsi et al., 2011). Briefly, samples were fixed 10 min at room temperature with 4% PFA solution. Slides were permeabilized 10 min at RT with PBS 0.3% Triton X-100, and processed for immunofluorescence using the following conditions: blocking in 10% Goat Serum (GS) in PBS 0.1% Triton X-100 (PBST) for 1 hr followed by incubation with primary antibodies (diluted in 2% GS in PBST) overnight at 4°C, four washes in PBST and incubation with secondary antibodies (1:200 in 2% GS in PBST) for 2 hours at room temperature. Samples were counterstained with ProLong-DAPI (Molecular Probes, Life Technologies) to label cell nuclei.
For immunofluorescence on pancreatic organoids or acini (Figure 5B and Figure 9B), pancreatic acini and organoids were fixed overnight in PBS 4% PFA at 4°C, permeabilized with two washes in PBS 0.5% NP40 for 20 minutes at 4°C, followed by one wash in PBS 0.3% Triton X-100 for 20 minutes at room temperature. After two washes in PBS 0.1% Triton X-100 (PBST) for 15 minutes at room temperature, acini or organoids were blocked with two washes in PBST 10% GS for 1 hour at room temperature, and incubated overnight with primary antibodies. The following day, cells were washed twice in PBST 2% GS for 15 minutes at 4°C, and five more times in PBT 2% GS for 1 hour at 4°C. Secondary antibodies were incubated overnight. The third day, cells were washed five times in PBST for 15 minutes, incubated 20 min with

DAPI solution and mounted in glycerol.

For immunofluorescence on brain tissue, biopsies were fixed with PFA, paraffin-embedded and cut in 10 μm-thick sections. Sections were re-hydrated and antigen retrieval was performed by incubation in citrate buffer 0.01 M pH 6 at 95°C for 20 minutes. Slides were then permeabilized (10 min at RT with PBS 0.3% Triton X-100 for mammary sections and 10 min at RT with PBS 1% Triton X-100 for brain sections) and processed as described above.

Primary antibodies: anti-YAP (4912; 1:25) polyclonal antibody, anti-CNPase (5664S; 1:100) polyclonal antibody, anti-SOX2 (4900; 1:50) monoclonal antibody were from Cell Signaling Technology. anti-TAZ (anti-WWTR1, HPA007415; 1:25) polyclonal antibody, and anti-amylase (A8273: 1:200) rabbit polyclonal antibody was from Sigma. anti-TuJ1 (anti β-III-tubulin; MMS435P-100; 1:500) mouse monoclonal antibody was from Covance. Anti-Synaptophysin (M0776; 1:200) mouse monoclonal antibody and anti-GFAP (Z0334; 1:1000) rabbit polyclonal antibody was from Dako. anti-Nestin (MAB353; 1:300) mouse monoclonal antibody and anti-Sox9 (AB5535; 1:200) and anti-NeuN (ABN78; 1:1000) rabbit polyclonal antibodies were from Millipore. Anti-Mash1 (556604; 1:100) monoclonal antibody was from BD Biosciences. Anti-NeuN (Ab177487; 1:100) rabbit monoclonal antibody and anti-GFP (Ab13970; 1:100) polyclonal antibody were from Abcam. anti-GFP (A6455; 1:100) rabbit serum was from Life Technologies. Anti-YAP (63.7; sc-101199; 1:200) mouse monoclonal antibody, anti-SV2a (E-8; sc-376234; 1:200) mouse monoclonal antibody and anti-Vimentin (Vim C-20, sc-7557-R; 1:100) rabbit polyclonal antibody were from Santa Cruz. anti-Tau (1:100) rabbit polyclonal antibody was from Axell. Anti-Ki67 (M3060; 1:100) rabbit monoclonal antibody was from Spring Bioscience. *K19* was detected using the monoclonal rat anti-*Troma-III* antibody (DSHB; 1:50). Alexa-conjugated secondary antibodies (Life Technologies): Alexa-Fluor-488 donkey anti-mouse IgG (A21202); Alexa Fluor-568 goat anti-mouse IgG (A11031); Alexa-Fluor-647 donkey anti-mouse (A31571); Alexa Fluor-488 goat anti-mouse IgG_{2a} (A21131), Alexa Fluor-647 goat anti-mouse IgG_1 (A21240), Alexa Fluor-488 donkey anti-rabbit IgG (A21206), Alexa-Fluor-568 goat anti-rabbit IgG (A11036), Alexa-Fluor-647 donkey anti-rabbit IgG (A31573); Alexa Fluor-555 goat anti-chicken IgG (A21437). Goat anti-rat Cy3 (112-165-167) was from Jackson Immunoresearch.

Confocal images were obtained with a Leica TCS SP5 equipped with a CCD camera.

Bright field and native-tdTomato images were obtained with a Leica DM IRB inverted microscope equipped with a CCD camera (Leica DFC 450C).

Western blot

Western blots were carried out as described in Cordenonsi et al., 2011. Anti-YAP/TAZ (63.7; sc-101199) was from Santa Cruz. anti-GAPDH (MAB347) monoclonal antibody was from Millipore. Anti-E-cadherin (610181) was from BD Transduction Laboratories

Quantitative Real-Time PCR (qRT-PCR)

Cells or tissues were harvested in TriPure (Roche) for total RNA extraction, and contaminant DNA was removed by DNase treatment. qRT-PCR analyses were carried out on retrotranscribed cDNAs with Rotor-Gene Q (Qiagen) thermal cycler and analyzed with Rotor-Gene Analysis6.1 software. Expression levels are always given relative to *Gapdh,* except for Figure 5C and 9A in which expression levels were normalized to *18-S rRNA*. PCR oligo sequences for mouse samples are listed in Table 2.

Microarray experiments and RNA sequencing

For microarray experiments, Mouse Genome 430 2.0 arrays (Affymetrix, Santa Clara, CA, USA) were used. Total RNA was extracted using TriPure (Roche) from:
1) pancreatic exocrine acini (4 replicates), yDucts (passage 10; 4 replicates), and Ducts (passage 10; 4 replicates).
2) cortical neurons (3 replicates), yNSCs (from YAP wild type-transduced cortical neurons, passage 2; 3 replicates), and native NSCs (3 replicates);
RNA quality and purity were assessed on the Agilent Bioanalyzer 2100 (Agilent Technologies, Waldbronn, Germany); RNA concentration was determined using the NanoDrop ND-1000 Spectrophotometer (NanoDrop Technologies Inc.). RNA was then treated with DNaseI (Ambion). *In vitro* transcription, hybridization and biotin labeling were performed according to Affymetrix 3'IVT protocol (Affymetrix). As

control of effective gene modulation and of the whole procedure, we monitored the expression levels of tissue-specific markers of differentiated cells or stem/progenitors by qRT-PCR prior to microarray hybridization and in the final microarray data.

All data analyses were performed in R (version 3.1.2) using Bioconductor libraries (BioC 3.0) and R statistical packages. Probe level signals were converted to log2 expression values using robust multi-array average procedure RMA (Irizarry et al., 2003) of Bioconductor *affy* package. Raw data are available at Gene Expression Omnibus under accession number GSE70174.

Global unsupervised clustering was performed using the function *hclust* of R *stats* package with Pearson correlation as distance metric and average agglomeration method. Gene expression heatmaps have been generated using the function *heatmap.2* of R *gplots* package after row-wise standardization of the expression values. Before unsupervised clustering, to reduce the effect of noise from non-varying genes, we removed those probe sets with a coefficient of variation smaller than the 90^{th} percentile of the coefficients of variation in the entire dataset. The filter retained 4511 probe sets that are more variable across samples in any of the 2 subsets (i.e., neuron and pancreatic).

Differentially expressed genes were identified using Significance Analysis of Microarray algorithm coded in the *samr* R package as in (Tusher et al., 2001). To identify differentially expressed genes, we selected those probe sets with an FDR $\leq$ 1%.

Genes that were coherently up- or downregulated in yNSC and in NSC in comparison to neurons were functionally annotated to Gene Ontology categories using the DAVID Bioinformatic resources. GO terms were selected with a Benjamini FDR $\leq$ 5%. Upregulated genes are enriched of GO terms related to positive regulation of cell cycle (e.g. GO:0007049~cell cycle, GO:0007067~mitosis, GO:0006260~DNA replication) and to the development of the nervous system and maintenance of the neural progenitor state (e.g.: GO:0051960~regulation of nervous system development, GO:0045165~cell fate commitment, GO:0045665~negative regulation of neuron differentiation). Downregulated genes are enriched of GO terms related to terminal differentiation of neurons (e.g.: GO:0030182~neuron differentiation, GO:0031175~neuron projection development, GO:0007409~axonogenesis), transmission of nerve impulse (e.g.: GO:0007268~synaptic transmission,

GO:0019226~transmission of nerve impulse, GO:0006811~ion transport, GO:0046903~secretion) and nerve cell function (e.g.: GO:0007610~behavior, GO:0007611~learning or memory).
GO terms associated to genes coherently upregulated in Ducts and yDucts in comparison with acinar cells included RNA processing, positive regulation of cell cycle and control of cell death.

Mice

C57BL/6J mice and NOD-SCID mice were purchased from Charles River. Transgenic lines used in the experiments were gently provided by: Duojia Pan (Zhang et al., 2010) (*Yap1*$^{fl/fl}$); Ivan De Curtis and Riccardo Brambilla (*Syn1-Cre*) (Zhu et al., 2001); Giorgio Carmignoto (*R26-CAG-LSL-tdTomato*) (Madisen et al., 2010); Fernando Camargo (*tetO-YAP*^{S127A}) (Camargo et al., 2007). *Taz*$^{fl/fl}$ and double *Yap*$^{fl/fl}$*; Taz*$^{fl/fl}$ conditional knock-out mice were as described in (Azzolin et al., 2014). *Ptf1a-CreERTM* (stock #019378), and *R26-rtTAM2* mice (stock #006965) were purchased from The Jackson Laboratory. Animals were genotyped with standard procedures (Morsut et al., 2010) and with the recommended set of primers. Animal experiments were performed adhering to our institutional guidelines as approved by OPBA.
To obtain *Syn1-Cre* lineage tracing studies, we used *Syn1-Cre* hemizygous females (as transgene expression in male mice results in germline recombination; Rempe et al., 2006) with *R26-CAG-LSL-tdTomato* homozygous males. Littermate embryos derived from these crossings were harvested at E18-19 and kept separate for neurons derivation; genotypes were confirmed on embryonic tail biopsies.
To obtain *R26-rtTAM2/+ ; tetO-YAP*^{S127A} mice, we crossed *R26-rtTAM2/+* mice with *tetO-YAP*^{S127A} mice. *R26-rtTAM2/+* littermates were used as negative control.
To obtain *Ptf1a-CreERTM; R26-LSL-rtTA-IRES-EGFP/+; tetO-YAP*^{S127A} mice, we crossed *Ptf1a-CreERTM; R26-LSL-rtTA-IRES-EGFP/LSL-rtTA-IRES-EGFP* mice with *tetO-YAP*^{S127A} mice. *Ptf1a-CreERTM; R26-LSL-rtTA-IRES-EGFP/+* littermates were used as negative control.

Statistics

The number of biological and technical replicates and the number of animals are indicated in Figure legends and text. All tested animals were included. Animal ages are specified in the text and Experimental procedures. Sample size was not predetermined. For all experiments with error bars the standard deviation (s.d.) was calculated to indicate the variation within each experiment.

REFERENCES

Aragona, M., Panciera, T., Manfrin, A., Giulitti, S., Michielin, F., Elvassore, N., Dupont, S., and Piccolo, S. (2013). A mechanical checkpoint controls multicellular growth through YAP/TAZ regulation by actin-processing factors. Cell *154*, 1047-1059.

Azzolin, L., Panciera, T., Soligo, S., Enzo, E., Bicciato, S., Dupont, S., Bresolin, S., Frasson, C., Basso, G., Guzzardo, V.*, et al.* (2014). YAP/TAZ incorporation in the β-catenin destruction complex orchestrates the Wnt response. Cell 158: 157-170.

Azzolin, L., Zanconato, F., Bresolin, S., Forcato, M., Basso, G., Bicciato, S., Cordenonsi, M., and Piccolo, S. (2012). Role of TAZ as mediator of Wnt signaling. Cell *151*, 1443-1456.

Bailleul, B., Surani, M.A., White, S., Barton, S.C., Brown, K., Blessing, M., Jorcano, J., and Balmain, A. (1990). Skin hyperkeratosis and papilloma formation in transgenic mice expressing a ras oncogene from a suprabasal keratin promoter. Cell *62*, 697-708.

Barry, E.R., Morikawa, T., Butler, B.L., Shrestha, K., de la Rosa, R., Yan, K.S., Fuchs, C.S., Magness, S.T., Smits, R., Ogino, S.*, et al.* (2013). Restriction of intestinal stem cell expansion and the regenerative response by YAP. Nature *493*, 106-110.

Ben-David, U., and Benvenisty, N. (2011). The tumorigenicity of human embryonic and induced pluripotent stem cells. Nature reviews Cancer *11*, 268-277.

Benhamouche, S., Curto, M., Saotome, I., Gladden, A.B., Liu, C.H., Giovannini, M., and McClatchey, A.I. (2010). Nf2/Merlin controls progenitor homeostasis and tumorigenesis in the liver. Genes & development *24*, 1718-1730.

Bhat, K.P., Salazar, K.L., Balasubramaniyan, V., Wani, K., Heathcock, L., Hollingsworth, F., James, J.D., Gumin, J., Diefes, K.L., Kim, S.H.*, et al.* (2011). The transcriptional coactivator TAZ regulates mesenchymal differentiation in malignant glioma. Genes & development *25*, 2594-2609.

Blanpain, C., and Fuchs, E. (2014). Stem cell plasticity. Plasticity of epithelial stem cells in tissue regeneration. Science *344*, 1242281.

Bonaguidi, M.A., McGuire, T., Hu, M., Kan, L., Samanta, J., and Kessler, J.A. (2005). LIF and BMP signaling generate separate and discrete types of GFAP-expressing cells. Development *132*, 5503-5514.

Cai, J., Zhang, N., Zheng, Y., de Wilde, R.F., Maitra, A., and Pan, D. (2010). The Hippo signaling pathway restricts the oncogenic potential of an intestinal regeneration program. Genes & development *24*, 2383-2388.

Camargo, F.D., Gokhale, S., Johnnidis, J.B., Fu, D., Bell, G.W., Jaenisch, R., and Brummelkamp, T.R. (2007). YAP1 increases organ size and expands undifferentiated progenitor cells. Current biology : CB *17*, 2054-2060.

Cao, X., Pfaff, S.L., and Gage, F.H. (2008). YAP regulates neural progenitor cell number via the TEA domain transcription factor. Genes & development *22*, 3320-3334.

Cebola, I., Rodriguez-Segui, S.A., Cho, C.H., Bessa, J., Rovira, M., Luengo, M., Chhatriwala, M., Berry, A., Ponsa-Cobas, J., Maestro, M.A.*, et al.* (2015). TEAD and YAP regulate the enhancer network of human embryonic pancreatic progenitors. Nature cell biology *17*, 615-626.

Chan, S.W., Lim, C.J., Chong, Y.F., Pobbati, A.V., Huang, C., and Hong, W. (2011). Hippo pathway-independent restriction of TAZ and YAP by angiomotin. The Journal of biological chemistry *286*, 7018-7026.

Choi, S.H., Kim, Y.H., Hebisch, M., Sliwinski, C., Lee, S., D'Avanzo, C., Chen, H., Hooli, B., Asselin, C., Muffat, J.*, et al.* (2014). A three-dimensional human neural cell culture model of Alzheimer's disease. Nature *515*, 274-278.

Clevers, H. (2006). Wnt/beta-catenin signaling in development and disease. Cell *127*, 469-480.

Cordenonsi, M., Zanconato, F., Azzolin, L., Forcato, M., Rosato, A., Frasson, C., Inui, M., Montagner, M., Parenti, A.R., Poletti, A.*, et al.* (2011). The Hippo transducer TAZ confers cancer stem cell-related traits on breast cancer cells. Cell *147*, 759-772.

de Lau, W., Barker, N., Low, T.Y., Koo, B.K., Li, V.S., Teunissen, H., Kujala, P., Haegebarth, A., Peters, P.J., van de Wetering, M.*, et al.* (2011). Lgr5 homologues associate with Wnt receptors and mediate R-spondin signalling. Nature *476*, 293-297.

Delacour, A., Nepote, V., Trumpp, A., and Herrera, P.L. (2004). Nestin expression in pancreatic exocrine cell lineages. Mechanisms of development *121*, 3-14.

Dong, J., Feldmann, G., Huang, J., Wu, S., Zhang, N., Comerford, S.A., Gayyed, M.F., Anders, R.A., Maitra, A., and Pan, D. (2007). Elucidation of a universal size-control mechanism in Drosophila and mammals. Cell *130*, 1120-1133.

Dupont, S., Morsut, L., Aragona, M., Enzo, E., Giulitti, S., Cordenonsi, M., Zanconato, F., Le Digabel, J., Forcato, M., Bicciato, S.*, et al.* (2011). Role of YAP/TAZ in mechanotransduction. Nature *474*, 179-183.

Esni, F., Stoffers, D.A., Takeuchi, T., and Leach, S.D. (2004). Origin of exocrine pancreatic cells from nestin-positive precursors in developing mouse pancreas. Mechanisms of development *121*, 15-25.

Favaro, R., Valotta, M., Ferri, A.L., Latorre, E., Mariani, J., Giachino, C., Lancini, C., Tosetti, V., Ottolenghi, S., Taylor, V.*, et al.* (2009). Hippocampal development and neural stem cell maintenance require Sox2-dependent regulation of Shh. Nature neuroscience *12*, 1248-1256.

Fernandez, B.G., Gaspar, P., Bras-Pereira, C., Jezowska, B., Rebelo, S.R., and Janody, F. (2011). Actin-Capping Protein and the Hippo pathway regulate F-actin and tissue growth in Drosophila. Development *138*, 2337-2346.

Fitamant, J., Kottakis, F., Benhamouche, S., Tian, H.S., Chuvin, N., Parachoniak, C.A., Nagle, J.M., Perera, R.M., Lapouge, M., Deshpande, V.*, et al.* (2015). YAP Inhibition Restores Hepatocyte Differentiation in Advanced HCC, Leading to Tumor Regression. Cell reports.

Fuchs, E., and Chen, T. (2013). A matter of life and death: self-renewal in stem cells. EMBO reports *14*, 39-48.

Gao, T., Zhou, D., Yang, C., Singh, T., Penzo-Mendez, A., Maddipati, R., Tzatsos, A., Bardeesy, N., Avruch, J., and Stanger, B.Z. (2013). Hippo signaling regulates differentiation and maintenance in the exocrine pancreas. Gastroenterology *144*, 1543-1553, 1553 e1541.

Gee, S.T., Milgram, S.L., Kramer, K.L., Conlon, F.L., and Moody, S.A. (2011). Yes-associated protein 65 (YAP) expands neural progenitors and regulates Pax3 expression in the neural plate border zone. PloS one *6*, e20309.

George, N.M., Day, C.E., Boerner, B.P., Johnson, R.L., and Sarvetnick, N.E. (2012). Hippo signaling regulates pancreas development through inactivation of Yap. Molecular and cellular biology *32*, 5116-5128.

Halder, G., Dupont, S., and Piccolo, S. (2012). Transduction of mechanical and cytoskeletal cues by YAP and TAZ. Nature reviews Molecular cell biology *13*, 591-600.

Halder, G., and Johnson, R.L. (2011). Hippo signaling: growth control and beyond. Development *138*, 9-22.

Hamaratoglu, F., Willecke, M., Kango-Singh, M., Nolo, R., Hyun, E., Tao, C., Jafar-Nejad, H., and Halder, G. (2006). The tumour-suppressor genes NF2/Merlin and Expanded act through Hippo signalling to regulate cell proliferation and apoptosis. Nature cell biology *8*, 27-36.

Han, X.J., Lu, Y.F., Li, S.A., Kaitsuka, T., Sato, Y., Tomizawa, K., Nairn, A.C., Takei, K., Matsui, H., and Matsushita, M. (2008). CaM kinase I alpha-induced phosphorylation of Drp1 regulates mitochondrial morphology. The Journal of cell biology *182*, 573-585.

Harvey, K., and Tapon, N. (2007). The Salvador-Warts-Hippo pathway - an emerging tumour-suppressor network. Nature reviews Cancer *7*, 182-191.

Heallen, T., Zhang, M., Wang, J., Bonilla-Claudio, M., Klysik, E., Johnson, R.L., and Martin, J.F. (2011). Hippo pathway inhibits Wnt signaling to restrain cardiomyocyte proliferation and heart size. Science *332*, 458-461.

Hockemeyer, D., Soldner, F., Cook, E.G., Gao, Q., Mitalipova, M., and Jaenisch, R. (2008). A drug-inducible system for direct reprogramming of human somatic cells to pluripotency. Cell stem cell *3*, 346-353.

Hossain, Z., Ali, S.M., Ko, H.L., Xu, J., Ng, C.P., Guo, K., Qi, Z., Ponniah, S., Hong, W., and Hunziker, W. (2007). Glomerulocystic kidney disease in mice with a targeted inactivation of Wwtr1. Proceedings of the National Academy of Sciences of the United States of America *104*, 1631-1636.

Hsieh, J., Aimone, J.B., Kaspar, B.K., Kuwabara, T., Nakashima, K., and Gage, F.H. (2004). IGF-I instructs multipotent adult neural progenitor cells to become oligodendrocytes. The Journal of cell biology *164*, 111-122.

Huang, J., Wu, S., Barrera, J., Matthews, K., and Pan, D. (2005). The Hippo signaling pathway coordinately regulates cell proliferation and apoptosis by inactivating Yorkie, the Drosophila Homolog of YAP. Cell *122*, 421-434.

Huch, M., Bonfanti, P., Boj, S.F., Sato, T., Loomans, C.J., van de Wetering, M., Sojoodi, M., Li, V.S., Schuijers, J., Gracanin, A.*, et al.* (2013). Unlimited in vitro expansion of adult bi-potent pancreas progenitors through the Lgr5/R-spondin axis. The EMBO journal *32*, 2708-2721.

Imajo, M., Miyatake, K., Iimura, A., Miyamoto, A., and Nishida, E. (2012). A molecular mechanism that links Hippo signalling to the inhibition of Wnt/beta-catenin signalling. The EMBO journal *31*, 1109-1122.

Irizarry, R.A., Hobbs, B., Collin, F., Beazer-Barclay, Y.D., Antonellis, K.J., Scherf, U., and Speed, T.P. (2003). Exploration, normalization, and summaries of high density oligonucleotide array probe level data. Biostatistics *4*, 249-264.

Justice, R.W., Zilian, O., Woods, D.F., Noll, M., and Bryant, P.J. (1995). The Drosophila tumor suppressor gene warts encodes a homolog of human myotonic dystrophy kinase and is required for the control of cell shape and proliferation. Genes & development *9*, 534-546.

Kim, N.G., Koh, E., Chen, X., and Gumbiner, B.M. (2011). E-cadherin mediates contact inhibition of proliferation through Hippo signaling-pathway components. Proceedings of the National Academy of Sciences of the United States of America *108*, 11930-11935.

Kopp, J.L., von Figura, G., Mayes, E., Liu, F.F., Dubois, C.L., Morris, J.P.t., Pan, F.C., Akiyama, H., Wright, C.V., Jensen, K.*, et al.* (2012). Identification of Sox9-dependent acinar-to-ductal reprogramming as the principal mechanism for initiation of pancreatic ductal adenocarcinoma. Cancer cell *22*, 737-750.

Lavado, A., He, Y., Pare, J., Neale, G., Olson, E.N., Giovannini, M., and Cao, X. (2013). Tumor suppressor Nf2 limits expansion of the neural progenitor pool by inhibiting Yap/Taz transcriptional coactivators. Development *140*, 3323-3334.

Lee, J.H., Kim, T.S., Yang, T.H., Koo, B.K., Oh, S.P., Lee, K.P., Oh, H.J., Lee, S.H., Kong, Y.Y., Kim, J.M.*, et al.* (2008). A crucial role of WW45 in developing epithelial tissues in the mouse. The EMBO journal *27*, 1231-1242.

Lee, K.P., Lee, J.H., Kim, T.S., Kim, T.H., Park, H.D., Byun, J.S., Kim, M.C., Jeong, W.I., Calvisi, D.F., Kim, J.M.*, et al.* (2010). The Hippo-Salvador pathway restrains hepatic oval cell proliferation, liver size, and liver tumorigenesis. Proceedings of the National Academy of Sciences of the United States of America *107*, 8248-8253.

Lim, E., Vaillant, F., Wu, D., Forrest, N.C., Pal, B., Hart, A.H., Asselin-Labat, M.L., Gyorki, D.E., Ward, T., Partanen, A.*, et al.* (2009). Aberrant luminal progenitors as the candidate target population for basal tumor development in BRCA1 mutation carriers. Nature medicine *15*, 907-913.

Liu, C.Y., Zha, Z.Y., Zhou, X., Zhang, H., Huang, W., Zhao, D., Li, T., Chan, S.W., Lim, C.J., Hong, W.*, et al.* (2010). The Hippo tumor pathway promotes TAZ degradation by phosphorylating a phosphodegron and recruiting the SCFbeta-TrCP E3 ligase. The Journal of biological chemistry.

Madisen, L., Zwingman, T.A., Sunkin, S.M., Oh, S.W., Zariwala, H.A., Gu, H., Ng, L.L., Palmiter, R.D., Hawrylycz, M.J., Jones, A.R.*, et al.* (2010). A robust and high-throughput Cre reporting and characterization system for the whole mouse brain. Nature neuroscience *13*, 133-140.

Maitra, S., Kulikauskas, R.M., Gavilan, H., and Fehon, R.G. (2006). The tumor suppressors Merlin and Expanded function cooperatively to modulate receptor endocytosis and signaling. Current biology : CB *16*, 702-709.

Makita, R., Uchijima, Y., Nishiyama, K., Amano, T., Chen, Q., Takeuchi, T., Mitani, A., Nagase, T., Yatomi, Y., Aburatani, H.*, et al.* (2008). Multiple renal cysts, urinary concentration defects, and pulmonary emphysematous changes in mice lacking TAZ. American journal of physiology Renal physiology *294*, F542-553.

Mana-Capelli, S., Paramasivam, M., Dutta, S., and McCollum, D. (2014). Angiomotins link F-actin architecture to Hippo pathway signaling. Molecular biology of the cell *25*, 1676-1685.

Mani, S.A., Guo, W., Liao, M.J., Eaton, E.N., Ayyanan, A., Zhou, A.Y., Brooks, M., Reinhard, F., Zhang, C.C., Shipitsin, M.*, et al.* (2008). The epithelial-mesenchymal transition generates cells with properties of stem cells. Cell *133*, 704-715.

McClatchey, A.I., Saotome, I., Ramesh, V., Gusella, J.F., and Jacks, T. (1997). The Nf2 tumor suppressor gene product is essential for extraembryonic

development immediately prior to gastrulation. Genes & development *11*, 1253-1265.

McPherson, J.P., Tamblyn, L., Elia, A., Migon, E., Shehabeldin, A., Matysiak-Zablocki, E., Lemmers, B., Salmena, L., Hakem, A., Fish, J.*, et al.* (2004). Lats2/Kpm is required for embryonic development, proliferation control and genomic integrity. The EMBO journal *23*, 3677-3688.

Means, A.L., Meszoely, I.M., Suzuki, K., Miyamoto, Y., Rustgi, A.K., Coffey, R.J., Jr., Wright, C.V., Stoffers, D.A., and Leach, S.D. (2005). Pancreatic epithelial plasticity mediated by acinar cell transdifferentiation and generation of nestin-positive intermediates. Development *132*, 3767-3776.

Morin-Kensicki, E.M., Boone, B.N., Howell, M., Stonebraker, J.R., Teed, J., Alb, J.G., Magnuson, T.R., O'Neal, W., and Milgram, S.L. (2006). Defects in yolk sac vasculogenesis, chorioallantoic fusion, and embryonic axis elongation in mice with targeted disruption of Yap65. Molecular and cellular biology *26*, 77-87.

Morsut, L., Yan, K.P., Enzo, E., Aragona, M., Soligo, S.M., Wendling, O., Mark, M., Khetchoumian, K., Bressan, G., Chambon, P.*, et al.* (2010). Negative control of Smad activity by ectodermin/Tif1gamma patterns the mammalian embryo. Development *137*, 2571-2578.

Niehrs, C., and Acebron, S.P. (2012). Mitotic and mitogenic Wnt signalling. The EMBO journal *31*, 2705-2713.

Nishioka, N., Inoue, K., Adachi, K., Kiyonari, H., Ota, M., Ralston, A., Yabuta, N., Hirahara, S., Stephenson, R.O., Ogonuki, N.*, et al.* (2009). The Hippo signaling pathway components Lats and Yap pattern Tead4 activity to distinguish mouse trophectoderm from inner cell mass. Developmental cell *16*, 398-410.

Palmer, T.D., Takahashi, J., and Gage, F.H. (1997). The adult rat hippocampus contains primordial neural stem cells. Molecular and cellular neurosciences *8*, 389-404.

Pan, D. (2010). The hippo signaling pathway in development and cancer. Developmental cell *19*, 491-505.

Pan, F.C., Bankaitis, E.D., Boyer, D., Xu, X., Van de Casteele, M., Magnuson, M.A., Heimberg, H., and Wright, C.V. (2013). Spatiotemporal patterns of multipotentiality in Ptf1a-expressing cells during pancreas organogenesis and injury-induced facultative restoration. Development *140*, 751-764.

Piccolo, S., Dupont, S., and Cordenonsi, M. (2014). The biology of YAP/TAZ: hippo signaling and beyond. Physiological reviews *94*, 1287-1312.

Ramos, A., and Camargo, F.D. (2012). The Hippo signaling pathway and stem cell biology. Trends in cell biology.

Ray, J., and Gage, F.H. (2006). Differential properties of adult rat and mouse brain-derived neural stem/progenitor cells. Molecular and cellular neurosciences *31*, 560-573.

Reginensi, A., Scott, R.P., Gregorieff, A., Bagherie-Lachidan, M., Chung, C., Lim, D.S., Pawson, T., Wrana, J., and McNeill, H. (2013). Yap- and Cdc42-dependent nephrogenesis and morphogenesis during mouse kidney development. PLoS genetics *9*, e1003380.

Robel, S., Berninger, B., and Gotz, M. (2011). The stem cell potential of glia: lessons from reactive gliosis. Nature reviews Neuroscience *12*, 88-104.

Sansores-Garcia, L., Bossuyt, W., Wada, K., Yonemura, S., Tao, C., Sasaki, H., and Halder, G. (2011). Modulating F-actin organization induces organ growth by affecting the Hippo pathway. The EMBO journal *30*, 2325-2335.

Sato, T., Vries, R.G., Snippert, H.J., van de Wetering, M., Barker, N., Stange, D.E., van Es, J.H., Abo, A., Kujala, P., Peters, P.J.*, et al.* (2009). Single Lgr5 stem cells build crypt-villus structures in vitro without a mesenchymal niche. Nature *459*, 262-265.

Sawada, A., Kiyonari, H., Ukita, K., Nishioka, N., Imuta, Y., and Sasaki, H. (2008). Redundant roles of Tead1 and Tead2 in notochord development and the

regulation of cell proliferation and survival. Molecular and cellular biology *28*, 3177-3189.

Schlegelmilch, K., Mohseni, M., Kirak, O., Pruszak, J., Rodriguez, J.R., Zhou, D., Kreger, B.T., Vasioukhin, V., Avruch, J., Brummelkamp, T.R.*, et al.* (2011). Yap1 acts downstream of alpha-catenin to control epidermal proliferation. Cell *144*, 782-795.

Seymour, P.A., Freude, K.K., Tran, M.N., Mayes, E.E., Jensen, J., Kist, R., Scherer, G., and Sander, M. (2007). SOX9 is required for maintenance of the pancreatic progenitor cell pool. Proceedings of the National Academy of Sciences of the United States of America *104*, 1865-1870.

Silvis, M.R., Kreger, B.T., Lien, W.H., Klezovitch, O., Rudakova, G.M., Camargo, F.D., Lantz, D.M., Seykora, J.T., and Vasioukhin, V. (2011). alpha-catenin is a tumor suppressor that controls cell accumulation by regulating the localization and activity of the transcriptional coactivator Yap1. Science signaling *4*, ra33.

Skibinski, A., Breindel, J.L., Prat, A., Galvan, P., Smith, E., Rolfs, A., Gupta, P.B., Labaer, J., and Kuperwasser, C. (2014). The Hippo transducer TAZ interacts with the SWI/SNF complex to regulate breast epithelial lineage commitment. Cell reports *6*, 1059-1072.

Song, H., Ramus, S.J., Tyrer, J., Bolton, K.L., Gentry-Maharaj, A., Wozniak, E., Anton-Culver, H., Chang-Claude, J., Cramer, D.W., DiCioccio, R.*, et al.* (2009). A genome-wide association study identifies a new ovarian cancer susceptibility locus on 9p22.2. Nat Genet *41*, 996-1000.

Sorrentino, G., Ruggeri, N., Specchia, V., Cordenonsi, M., Mano, M., Dupont, S., Manfrin, A., Ingallina, E., Sommaggio, R., Piazza, S.*, et al.* (2014). Metabolic control of YAP and TAZ by the mevalonate pathway. Nature cell biology *16*, 357-366.

Tapon, N., Harvey, K.F., Bell, D.W., Wahrer, D.C., Schiripo, T.A., Haber, D., and Hariharan, I.K. (2002). salvador Promotes both cell cycle exit and apoptosis in Drosophila and is mutated in human cancer cell lines. Cell *110*, 467-478.

Tetteh, P.W., Farin, H.F., and Clevers, H. (2015). Plasticity within stem cell hierarchies in mammalian epithelia. Trends in cell biology *25*, 100-108.

Tusher, V.G., Tibshirani, R., and Chu, G. (2001). Significance analysis of microarrays applied to the ionizing radiation response. Proceedings of the National Academy of Sciences of the United States of America *98*, 5116-5121.

Varelas, X., Sakuma, R., Samavarchi-Tehrani, P., Peerani, R., Rao, B.M., Dembowy, J., Yaffe, M.B., Zandstra, P.W., and Wrana, J.L. (2008). TAZ controls Smad nucleocytoplasmic shuttling and regulates human embryonic stem-cell self-renewal. Nature cell biology *10*, 837-848.

Wang, J., Wang, H., Zhang, Y., Zhen, N., Zhang, L., Qiao, Y., Weng, W., Liu, X., Ma, L., Xiao, W.*, et al.* (2014). Mutual inhibition between YAP and SRSF1 maintains long non-coding RNA, Malat1-induced tumourigenesis in liver cancer. Cellular signalling *26*, 1048-1059.

Xin, M., Kim, Y., Sutherland, L.B., Murakami, M., Qi, X., McAnally, J., Porrello, E.R., Mahmoud, A.I., Tan, W., Shelton, J.M.*, et al.* (2013). Hippo pathway effector Yap promotes cardiac regeneration. Proceedings of the National Academy of Sciences of the United States of America *110*, 13839-13844.

Yi, C., Shen, Z., Stemmer-Rachamimov, A., Dawany, N., Troutman, S., Showe, L.C., Liu, Q., Shimono, A., Sudol, M., Holmgren, L.*, et al.* (2013). The p130 isoform of angiomotin is required for Yap-mediated hepatic epithelial cell proliferation and tumorigenesis. Science signaling *6*, ra77.

Yimlamai, D., Christodoulou, C., Galli, G.G., Yanger, K., Pepe-Mooney, B., Gurung, B., Shrestha, K., Cahan, P., Stanger, B.Z., and Camargo, F.D. (2014). Hippo pathway activity influences liver cell fate. Cell *157*, 1324-1338.

Yin, F., Yu, J., Zheng, Y., Chen, Q., Zhang, N., and Pan, D. (2013). Spatial organization of Hippo signaling at the plasma membrane mediated by the tumor suppressor Merlin/NF2. Cell *154*, 1342-1355.

Yu, F.X., Zhao, B., Panupinthu, N., Jewell, J.L., Lian, I., Wang, L.H., Zhao, J., Yuan, H., Tumaneng, K., Li, H.*, et al.* (2012). Regulation of the Hippo-YAP pathway by G-protein-coupled receptor signaling. Cell *150*, 780-791.

Yu, J., Zheng, Y., Dong, J., Klusza, S., Deng, W.M., and Pan, D. (2010). Kibra functions as a tumor suppressor protein that regulates Hippo signaling in conjunction with Merlin and Expanded. Developmental cell *18*, 288-299.

Zanconato, F., Forcato, M., Battilana, G., Azzolin, L., Quaranta, E., Bodega, B., Rosato, A., Bicciato, S., Cordenonsi, M., and Piccolo, S. (2015). Genome-wide association between YAP/TAZ/TEAD and AP-1 at enhancers drives oncogenic growth. Nature cell biology *17*, 1218-1227.

Zhang, H., Liu, C.Y., Zha, Z.Y., Zhao, B., Yao, J., Zhao, S., Xiong, Y., Lei, Q.Y., and Guan, K.L. (2009). TEAD transcription factors mediate the function of TAZ in cell growth and epithelial-mesenchymal transition. The Journal of biological chemistry *284*, 13355-13362.

Zhang, H., Pasolli, H.A., and Fuchs, E. (2011). Yes-associated protein (YAP) transcriptional coactivator functions in balancing growth and differentiation in skin. Proceedings of the National Academy of Sciences of the United States of America *108*, 2270-2275.

Zhang, N., Bai, H., David, K.K., Dong, J., Zheng, Y., Cai, J., Giovannini, M., Liu, P., Anders, R.A., and Pan, D. (2010). The Merlin/NF2 tumor suppressor functions through the YAP oncoprotein to regulate tissue homeostasis in mammals. Developmental cell *19*, 27-38.

Zhang, W., Nandakumar, N., Shi, Y., Manzano, M., Smith, A., Graham, G., Gupta, S., Vietsch, E.E., Laughlin, S.Z., Wadhwa, M.*, et al.* (2014). Downstream of mutant KRAS, the transcription regulator YAP is essential for neoplastic progression to pancreatic ductal adenocarcinoma. Science signaling *7*, ra42.

Zhao, B., Li, L., Lei, Q., and Guan, K.L. (2010). The Hippo-YAP pathway in organ size control and tumorigenesis: an updated version. Genes & development *24*, 862-874.

Zhao, B., Wei, X., Li, W., Udan, R.S., Yang, Q., Kim, J., Xie, J., Ikenoue, T., Yu, J., Li, L.*, et al.* (2007). Inactivation of YAP oncoprotein by the Hippo pathway is involved in cell contact inhibition and tissue growth control. Genes & development *21*, 2747-2761.

Zhao, B., Ye, X., Yu, J., Li, L., Li, W., Li, S., Lin, J.D., Wang, C.Y., Chinnaiyan, A.M., Lai, Z.C.*, et al.* (2008). TEAD mediates YAP-dependent gene induction and growth control. Genes & development *22*, 1962-1971.

Zhou, D., Conrad, C., Xia, F., Park, J.S., Payer, B., Yin, Y., Lauwers, G.Y., Thasler, W., Lee, J.T., Avruch, J.*, et al.* (2009). Mst1 and Mst2 maintain hepatocyte quiescence and suppress hepatocellular carcinoma development through inactivation of the Yap1 oncogene. Cancer cell *16*, 425-438.

Zhou, D., Zhang, Y., Wu, H., Barry, E., Yin, Y., Lawrence, E., Dawson, D., Willis, J.E., Markowitz, S.D., Camargo, F.D.*, et al.* (2011). Mst1 and Mst2 protein kinases restrain intestinal stem cell proliferation and colonic tumorigenesis by inhibition of Yes-associated protein (Yap) overabundance. Proceedings of the National Academy of Sciences of the United States of America *108*, E1312-1320.

Zhu, Y., Romero, M.I., Ghosh, P., Ye, Z., Charnay, P., Rushing, E.J., Marth, J.D., and Parada, L.F. (2001). Ablation of NF1 function in neurons induces abnormal development of cerebral cortex and reactive gliosis in the brain. Genes & development *15*, 859-876.

TABLES

Table1. Full list of neuronal markers expressed by primary neurons, compared to native neural stem cells (NSCs) by microarray analysis. Related to Figure 13B.

Symbol	***Description***	*Fold expression over NSC*	*q-value (%)*
Calb1	calbindin 1	287,26	0
Snap25	synaptosomal-associated protein 25	245,49	0
Neurod6	neurogenic differentiation 6	236,53	0
Syt4	synaptotagmin IV	229,84	0
Tubb3	TuJ1, tubulin, beta 3 class III	205,60	0
Gabrb2	gamma-aminobutyric acid (GABA) A receptor, subunit beta 2	189,16	0
Gabra1	gamma-aminobutyric acid (GABA) A receptor, subunit alpha 1	175,44	0
Scn2a1	sodium channel, voltage-gated, type II, alpha 1	166,39	0
Sv2b	synaptic vesicle glycoprotein 2 b	156,71	0
Chgb	chromogranin B	140,16	0
Dlg2	discs, large homolog 2 (Drosophila)	132,72	0
Reln	reelin	110,51	0
Caln1	calneuron 1	105,63	0
Scg2	secretogranin II	57,92	0
Sst	somatostatin	57,54	0
Cacnb4	calcium channel, voltage-dependent, beta 4 subunit	57,02	0
Nrxn3	neurexin III	52,71	0
Gria1	glutamate receptor, ionotropic, AMPA1 (alpha 1)	51,75	0
Scn3b	sodium channel, voltage-gated, type III, beta	51,10	0
Scn3a	sodium channel, voltage-gated, type III, alpha	50,63	0
Kcnq2	potassium voltage-gated channel, subfamily Q, member 2	49,92	0
Scn2b	sodium channel, voltage-gated, type II, beta	47,45	0
Gad1	glutamate decarboxylase 1	43,65	0
Nsg2	neuron specific gene family member 2	43,48	0
Clstn2	calsyntenin 2	42,07	0
Rims1	regulating synaptic membrane exocytosis 1	42,04	0
Mapt	microtubule-associated protein tau	41,97	0
Kcnj3	potassium inwardly-rectifying channel, subfamily J, member 3	40,73	0
Ina	internexin neuronal intermediate filament protein, alpha	40,06	0
Npy	neuropeptide Y	39,21	0
Mturn	maturin, neural progenitor differentiation regulator homolog (Xenopus)	38,25	0
Cacna2d3	calcium channel, voltage-dependent, alpha2/delta subunit 3	34,25	0
Gabra4	gamma-aminobutyric acid (GABA) A receptor, subunit alpha 4	33,32	0
Caly	calcyon neuron-specific vesicular protein	32,83	0

Symbol	***Description***	*Fold expression over NSC*	*q-value (%)*
Syt1	synaptotagmin I	32,59	0
Scn1a	sodium channel, voltage-gated, type I, alpha	31,56	0
Syn3	synapsin III	31,15	0
Rbfox3	NeuN, RNA binding protein, fox-1 homolog (C. elegans) 3	27,34	0
Cend1	cell cycle exit and neuronal differentiation 1	26,58	0
Cnr1	cannabinoid receptor 1 (brain)	26,35	0
Nrsn1	neurensin 1	26,07	0
Chga	chromogranin A	26,07	0
Nxph2	neurexophilin 2	23,44	0
Kcnc2	potassium voltage gated channel, Shaw-related subfamily, member 2	23,39	0
Syp	synaptophysin	23,22	0
Syngr1	synaptogyrin 1	22,62	0
Grin2b	glutamate receptor, ionotropic, NMDA2B (epsilon 2)	21,67	0
Syngr3	synaptogyrin 3	21,61	0
Nefl	neurofilament, light polypeptide	20,18	0
Stx1a	syntaxin 1A (brain)	20,03	0
Cacna1b	calcium channel, voltage-dependent, N type, alpha 1B subunit	19,85	0
Penk	preproenkephalin	19,78	0
Snap91	synaptosomal-associated protein 91	19,19	0
Neurod1	neurogenic differentiation 1	18,91	0
Calb2	calbindin 2	16,47	0
Camk2a	calcium/calmodulin-dependent protein kinase II alpha	16,07	0
Synpr	synaptoporin	15,80	0
Nalcn	sodium leak channel, non-selective	13,80	0
Slc6a17	solute carrier family 6 (neurotransmitter transporter), member 17	12,90	0
Nrcam	neuronal cell adhesion molecule	12,82	0
Kcnab1	potassium voltage-gated channel, shaker-related subfamily, beta member 1	12,42	0
Nrgn	neurogranin	12,10	0
Syt16	synaptotagmin XVI	11,94	0
Cadps2	Ca2+-dependent activator protein for secretion 2	11,79	0
Atcay	ataxia, cerebellar, Cayman type homolog (human)	11,66	0
Atxn1	ataxin 1	11,36	0
Cacna1d	calcium channel, voltage-dependent, L type, alpha 1D subunit	11,29	0
Negr1	neuronal growth regulator 1	11,18	0
Gabrb3	gamma-aminobutyric acid (GABA) A receptor, subunit beta 3	11,13	0
Npas2	neuronal PAS domain protein 2	10,59	0
Pclo	piccolo (presynaptic cytomatrix protein)	10,33	0
Cadps	Ca2+-dependent secretion activator	9,94	0
Ncdn	neurochondrin	9,55	0

Symbol	***Description***	*Fold expression over NSC*	*q-value (%)*
Mdk	midkine	9,15	0
Scg3	secretogranin III	8,89	0
Elavl3	ELAV (embryonic lethal, abnormal vision, Drosophila)-like 3 (Hu antigen C)	8,87	0
Ntrk2	neurotrophic tyrosine kinase, receptor, type 2	8,77	0
Kcna1	potassium voltage-gated channel, shaker-related subfamily, member 1	8,77	0
Elavl2	ELAV (embryonic lethal, abnormal vision, Drosophila)-like 2 (Hu antigen B)	8,69	0
Kcnf1	potassium voltage-gated channel, subfamily F, member 1	8,46	0
Cacng2	calcium channel, voltage-dependent, gamma subunit 2	7,99	0

Table 2. PCR oligo sequences. Related to Experimental Procedures.

MOUSE GENE	For	Rev
18S rRNA	TGTCTCAAAGATTAAGCCATGC	GCGACCAAAGGAACCATAAC
AmotL2	GCAAGGGCTCGTATCCAGTG	CGTCTCTGCTGCCATGTTTG
Amy (Amy2A)	GGTTGCCTTCAGGAATGTGG	GTGAGCTTTGCCATCACTGC
AnkrD1	CTGTGAGGCTGAACCGCTAT	TCTCCTTGAGGCTGTCGAAT
Axin2	GAGATGACGCCTGTGGAACC	CCTGCTCAGACCCCTCCTTT
Axl	CGAGGCCAAACTCCCTATCC	GGGCAGAGCCTTCAGTGTGT
c-Myc	AGGCGGACACACAACGTCTT	TGCTCGTCTGCTTGAATGGA
Camk2a	CCCTGGAATGACAGCCTTTG	GAGGGTTCAGGATGGTGGTG
CD44	GCTTGGGGACTTTGCCTCTT	TGCTCAGGGCCAACTTCATT
CD133	TGCGGACCCTCTGAATTTGT	TGGGCACAGTCTCAACATCG
Cpa1	TGACATCTCTACACGGGACCAA	GCAGGCAGCAGGAAACCTCT
Ctgf	CTGCCTACCGACTGGAAGAC	CATTGGTAACTCGGGTGGAG
CyclinD1	GACCTTTGTGGCCCTCTGTG	AAAGTGCGTTGTGCGGTAGC
Cyr61	GCTCAGTCAGAAGGCAGACC	GTTCTTGGGGACACAGAGGA
Ela (CEla1)	CTGGGGCTCCTCTGTGAAGA	GGCTTCCTGGCGACATTACA
Gapdh	ATCCTGCACCACCAACTGCT	GGGCCATCCACAGTCTTCTG
Hes1	CCCGGCATTCCAAGCTAGAG	CGTTGATCTGGGTCATGCAG
Hey2	TGAGAAGACTAGTGCCAACAGC	TGGGCATCAAAGTAGCCTTTA
K19	AGGAGCTGAACACCCAGGTC	GGGCTTCAAAACCGCTGAT
Msi1	GTTCCAAGCCACGACCTACG	AAGCCGTGAGAGGGATAGCTG
Msi2	CAGCCGAAAGAAGTCATGTTCC	TCTGCCATAGGTTGCCACAA
Nestin	CCCTGAAGTCGAGGAGCTG	CTGCTGCACCTCTAAGCGA
NeuN	GCGTTCCCACCACTCTCTTG	GGATCAGCAGCGGCATAGAC
Ptf1a	TCCACACTTTAGCTGTACGGATG	CCAGGCCCAGAAGGTTATCA
SNAP25	CAACTGGAACGCATTGAGGAA	GGCCACTACTCCATCCTGATTAT
Snca	TGTGGCTGCTGCTGAGAAAA	TCACCACTGCTCCTCCAACA
Sox2	GCGGAGTGGAAACTTTTGTCC	CGGGAAGCGTGTACTTATCCTT
Sox9	AGGCCACGGAACAGACTCAC	CCCCTCTCGCTTCAGATCAA
Syn1	CCCACAGCCAGTCTTCATCC	CGGTCCAAGGCCAGAAAGAT
Syp	GGTGGTGTTTGGCTTCCTGA	AGGAGCTGGTTGCTTTTCTGG
Syt1	CTGTCACCACTGTTGCGAC	GGCAATGGGATTTTATGCAGTTC
Thy1	GCCAACTTCACCACCAAGGA	GAGGAGGGAGAGGGAAAGCA
TuJ1	TAGACCCCAGCGGCAACTAT	GTTCCAGGTTCCAAGTCCACC
Vim	CGTCCACACGCACCTACAG	GGGGGATGAGGAATAGAGGCT

FIGURES

Figure 1. Hippo-YAP/TAZ pathway in organ size control

(A) Schematic representation of the mammalian Hippo pathway. Adapted from (Piccolo et al., 2014).
(B-C) Overexpression of the YAP/TAZ orthologue Yorkie leads to organ overgrowth in *Drosophila*. (B) Flies expressing a Hippo-insensitive form of Yorkie in the eye primordium develop enlarged, folded eyes and excess head cuticle (*Right*) compared to control (*Left*). Adapted from (Dong et al., 2007).
(C) *Drosophila* wing imaginal discs containing multiple *yorkie*-overexpressing clones (*Right*) reach up to eight times the area of control wing discs (*Left*). Adapted from (Huang et al., 2005).
(D-E) Hyper-activation of YAP/TAZ results in organ overgrowth in transgenic mice. (D) Salvador knockout murine neonate hearts display cardiomegaly (*Right*) compared to wild-type controls (*Left*); ra, right atrium; la, left atrium; rv, right ventricle; lv, left ventricle. Adapted from (Heallen et al., 2011).
(E) Overexpression of YAP in transgenic mice leads to a massive increase in liver size (*Right*) compared to control mice (*Left*). Adapted from (Dong et al., 2007).

A

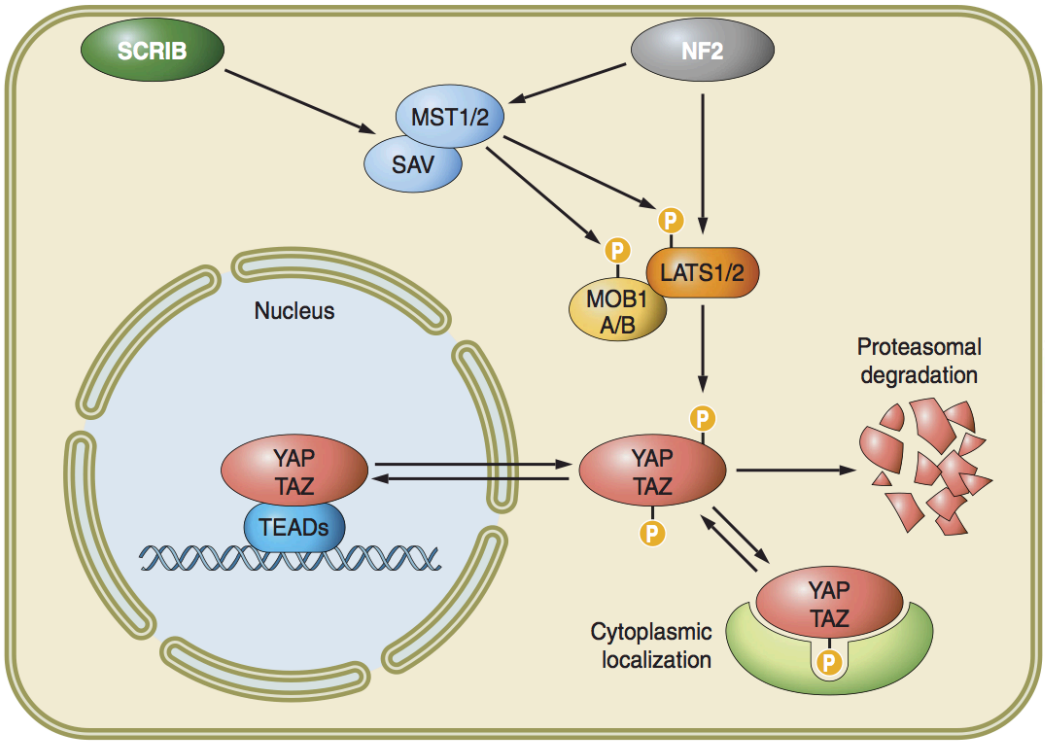

B

D

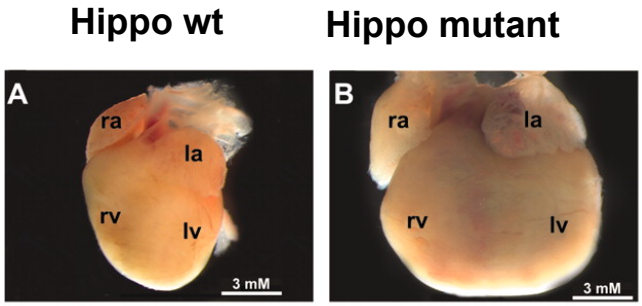

C

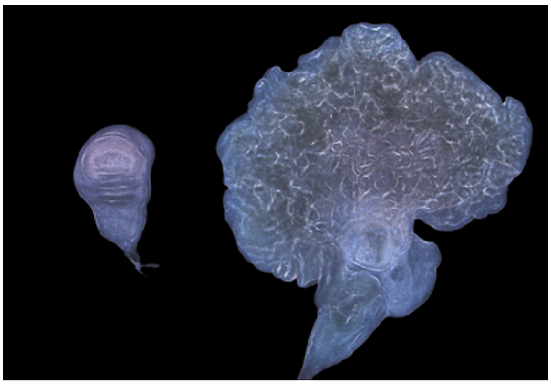

E

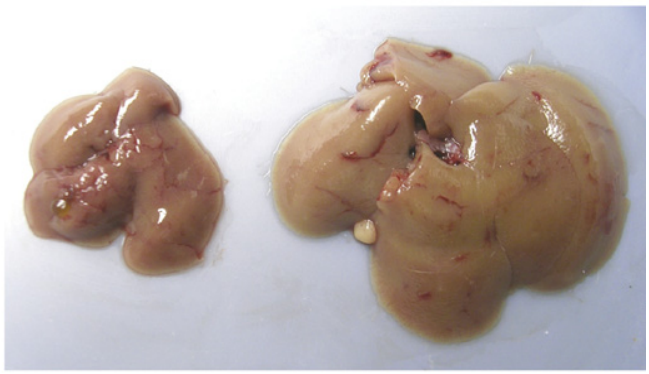

Figure 1

Figure 2. YAP/TAZ regulation by cell density and tissue architecture.

As published in Mariaceleste Aragona, **Tito Panciera**, Andrea Manfrin, Stefano Giulitti, Federica Michielin, Nicola Elvassore, Sirio Dupont, Stefano Piccolo. *A mechanical checkpoint controls multicellular growth through YAP/TAZ regulation by actin-processing factors*. Cell 154: 1047–1059, 2013.

(A-C) High cell density leads to restriction of cell area, YAP/TAZ relocalization, and growth arrest.

(A) Immortalized human mammry epithelial cells (MECs) were plated at different densities (3,000 cells/cm^2 : "Sparse"; 15,000 cells/cm^2: "Confluent"; and 75,000 cells/cm^2: "Dense"); after 2 days, cells were incubated for 1 hour with a pulse of BrdU to label cells undergoing DNA duplication. *Top panels:* Cells were fixed and processed for anti-BrdU immunofluorescence (αBRDU), nuceli are counterstained with DAPI. *Right:* Quantitation of proliferation measured as the percentage of BrdU-positive cells. Data are presented as mean + SD. Overt growth arrest occurs only when cells are plated as dense cultures. Treatment with YAP/TAZ siRNAs (siY/T) shows that proliferation in these cells is YAP/TAZ dependent. (B) MECs were plated as in A and stained for immunofluorescence with anti-YAP/TAZ antibody (αYAP/TAZ). TOTO3 is a nuclear counterstain. Scale bar, 20 μm. *Right:* Quantification of the proportion of cells displaying preferentially nuclear YAP/TAZ localization (N, black), even distribution of YAP/TAZ in nucleus and cytoplasm (N/C, gray), or cytoplasmic YAP/TAZ (C, white). YAP/TAZ are strongly excluded from the nucleus in the majority of cells only when MECs are plated as a densely packed monolayer. (C) Cells in a dense monolayer display less YAP/TAZ transcriptional activity than cells in a confluent monolayer. MECs were plated as in A. Real-time PCR analysis of the YAP/TAZ target genes *CTGF* (purple), *CYR61* (yellow) and *ANKRD1* (violet) is a read-out of YAP/TAZ activity. Target gene levels are relative to *GAPDH* expression.

(D-E) Restricting cell-substrate adhesion area to levels comparable to those of dense cells is sufficient to cause YAP/TAZ nuclear exclusion and inhibition of proliferation. MECs were seeded as individual cells plated on fibronectin-coated glass (Large) or on square microprinted fibronectin islands of 300 μm^2 (Small). In D, cells were fixed after 1 day for immunofluorescence with anti-YAP/TAZ antibody (αYAP/TAZ). DAPI is a nuclear counterstain. Scale bar, 20 μm. *Bottom panel:* YAP/TAZ

nucleo/cytoplasmic localization was scored as in B. In E, cells were processed for BrdU incorporation to quantify cell proliferation as in A. Data are presented as mean + SD.

(F-G) Stretching of an epithelial monolayer overcomes YAP/TAZ inhibition and growth arrest in contact-inhibited cells.

(F) A monolayer stretching device was employed to reproduce some of the mechanical challenges experienced by tissues. MECs were seeded on the upper surface of a PDMS substrate to obtain a dense monolayer (see also A). Underneath the PDMS is a chamber filled with fluid (white space between the PDMS and glass). At atmospheric pressure (Dense, $p = 0$), the cell monolayer remains flat; when pressure is applied to the fluid inside the chamber (Stretched, $p > 0$), the increase of the chamber volume causes a corresponding increase of the surface to which the monolayer is attached. *Left:* After 2 days, cells were subjected to 6 hours of static stretching, fixed with the device still under pressure, and then processed for immunofluorescence with anti-YAP/TAZ antibody (αYAP/TAZ). DAPI is a nuclear counterstain. Scale bar, 20 μm. *Right:* Proportion of cells displaying preferentially nuclear YAP/TAZ localization (N, black), even distribution of YAP/TAZ between the nucleus and the cytoplasm (N/C, gray), or prevalently cytoplasmic YAP/TAZ (C, white). Stretching of the epithelial monolayer is sufficient to partially rescue YAP/TAZ nuclear localization. Similar results were obtained after 3 hr of stretching (not shown). (G) MECs were plated on the stretching device as described in F. *Left:* After 2 days, cells were subjected to 6 hours of static stretching in the presence of BrdU to label cells undergoing DNA duplication. Scale bar, 20 μm. *Right*: Quantitation of proliferation measured as the percentage of BrdU-positive cells. Data are presented as mean + SD. Stretching of the epithelial monolayer is sufficient to partially rescue cell proliferation.

(H-I) F-actin-capping and -severing proteins are YAP/TAZ inhibitors.

(H) A loss-of function screening identifies Capz, Cofilin and Gelsolin as YAP/TAZ inhibitors. An siRNA screen for 62 known negative regulators of the F-actin cytoskeleton was set up. MECs were transfected with two independent couples of siRNAs against each gene. The day after transfection, cells were replated as single cells on a soft ECM hydrogel (0.7 kPa) and harvested after 2 more days for qRT-PCR analysis of the endogenous target *CTGF,* to assess YAP/TAZ transcriptional activity. Results of the screening are presented as points of the purple line, where each point

corresponds to a single siRNA/gene. The orange diamonds indicate the effects of controls and of selected siRNAs that were further validated. Cfl, Cofilin; Gsn, Gelsolin. The dotted line represents *CTGF* levels in cells transfected with siControl (siCo.) but plated on a stiff ECM substrate. *CTGF* levels are relative to *GAPDH* expression. (I) Loss of Capzb, Cfl1 and Gsn induces formation of thicker actin bundles, supporting the notion that F-actin-capping and -severing proteins work through F-actin modification to regulate YAP/TAZ. Panels are close-up confocal immunofluorescence of MECs transfected with the indicated siRNAs and stained for F-actin with phalloidin (green) and nuclei (TOTO3, red). Scale bar, 20 μm.

(J) Panels show representative colorimetric stacked images of BrdU incorporation, used to visualize spatial variations of proliferation in cell monolayers of defined shape and dimensions as developed by (Nelson et al., 2005). MECs were transfected with the indicated siRNA and were replated after 1 day as monolayers on large microprinted fibronectin islands (side, 500 μm). After 2 days, cells were incubated for 1 hr with a pulse of BrdU to label cells undergoing DNA duplication. Cells were fixed and processed for anti-BrdU immunofluorescence. Pictures of BrdU stainings of 50 individual multicellular islands were turned into binary signals, superimposed to obtain the relative pixel frequency, and color-coded using ImageJ. A pixel value of 70 indicates that cells at that location proliferate in 70% of the individual pictures. The color scale indicates the extent of cell proliferation in a given position of the monolayers. In control conditions the proliferation rate decreases to nearly undetectable levels at the center of the circle due to CIP (black/blue color), while cells continue proliferating along the border of the cellular sheet (green/red color). Depletion of CapZ rescues cell proliferation at the center of the island in a YAP/TAZ dependent manner. Of note, depletion of the Hippo pathway component LATS1/2 alone cannot rescue CIP and leaves proliferation of cells at the border still sensitive to inhibitors of cytoskeletal tension, whereas combined depletion of LATS1/2 and Capzb completely rescues contact inhibition of proliferation.

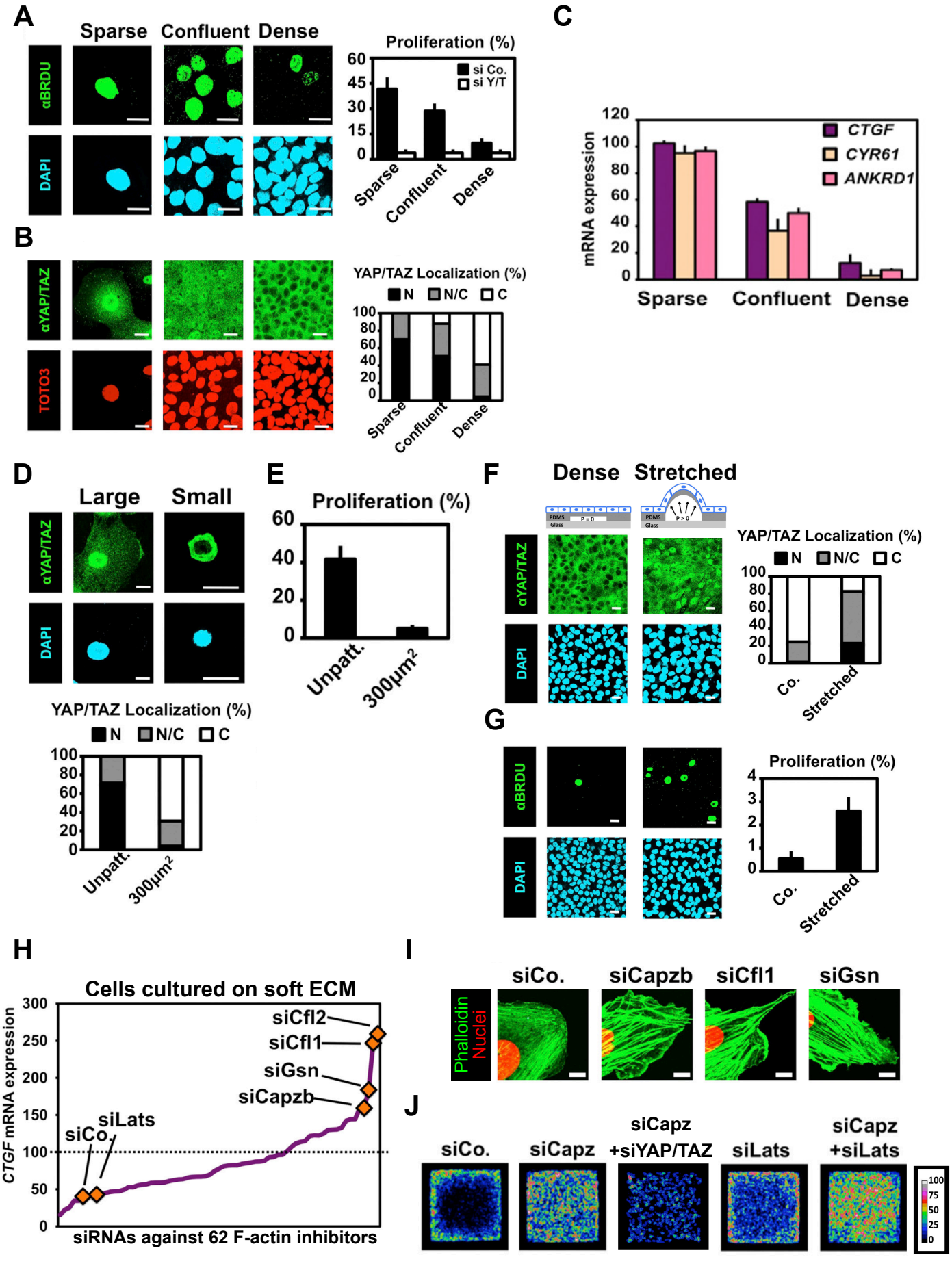
A
Sparse
Confluent
Dense
αBRDU
DAPI
Proliferation (%)
si Co.
si Y/T
Sparse
Confluent
Dense
B
αYAP/TAZ
TOTO3
YAP/TAZ Localization (%)
N
N/C
C
Sparse
Confluent
Dense
C
mRNA expression
CTGF
CYR61
ANKRD1
Sparse
Confluent
Dense
D
Large
Small
αYAP/TAZ
DAPI
YAP/TAZ Localization (%)
N
N/C
C
Unpatt.
300μm²
E
Proliferation (%)
Unpatt.
300μm²
F
Dense
Stretched
PDMS
Glass
P = 0
P > 0
αYAP/TAZ
DAPI
YAP/TAZ Localization (%)
N
N/C
C
Co.
Stretched
G
αBRDU
DAPI
Proliferation (%)
Co.
Stretched
H
Cells cultured on soft ECM
CTGF mRNA expression
siCfl2
siCfl1
siGsn
siCapzb
siLats
siCo.
siRNAs against 62 F-actin inhibitors
I
siCo.
siCapzb
siCfl1
siGsn
Phalloidin
Nuclei
J
siCo.
siCapz
siCapz
+siYAP/TAZ
siLats
siCapz
+siLats

Figure 2

Figure 3. YAP/TAZ orchestrate the Wnt response.

As published in Luca Azzolin, **Tito Panciera**, Sandra Soligo, Elena Enzo, Silvio Bicciato, Sirio Dupont, Silvia Bresolin, Chiara Frasson, Giuseppe Basso, Vincenza Guzzardo, Ambrogio Fassina, Michelangelo Cordenonsi, Stefano Piccolo. *YAP/TAZ incorporation in the beta-catenin destruction complex orchestrates the Wnt response*. Cell 158: 157– 170, 2014.

(A-C) YAP/TAZ are activated by Wnt ligand stimulation.

(A) Confluent HEK293 cells were treated with the canonical Wnt ligand Wnt3A or left untreated. After 8 hours, cells were fixed for immunofluorescence with anti-YAP-specific antibody. Wnt treatment results in nuclear accumulation of YAP protein. Nuclei are counterstained with DAPI. Scale bars, 20 μm. (B) HEK293 cells were transfected with control (lanes 1 and 2) or two independent YAP/TAZ (lanes 3 and 4) siRNAs and either left untreated (lane 1) or treated with Wnt3A (lanes 2–4). The panel represents the results of luciferase assays with the 8xGTIIC-Lux reporter, recording YAP/TAZ-dependent transcriptional activity. Wnt treatment leads to activation of the reporter in a YAP/TAZ dependent manner. (C) ST-2 cells were transfected with control (lanes 1 and 2) or two independent YAP/TAZ (lanes 3 and 4) siRNAs and either left untreated (lane 1) or exposed to Wnt3A (lanes 2–4). The panel represents qRT-PCR for the YAP/TAZ endogenous target gene *Cyr61*, relative to *Gapdh* expression. Wnt treatment triggers YAP/TAZ transcriptional activity. In B and C Data are normalized to lane 1 and presented as mean + SD.

(D) Wnt releases YAP/TAZ from the β-catenin destruction complex. HEK293 cells were treated with Wnt3A and harvested at different time points as indicated. Lysates were subjected to IP using an antibody directed against the central scaffold component of the β-catenin destruction complex Axin1, or rabbit IgG as control. Co-precipitating proteins were visualized by western blot. YAP and TAZ proteins are integral components of the destruction complex in Wnt-off state; Wnt stimulation leads to recruitment of the destruction complex to the LRP6 transmembrane co-receptor with ensuing release of YAP/TAZ.

(E-G) Depletion of destruction complex components releases YAP/TAZ from inhibition.

(E-F) Representative confocal images of YAP (E) or TAZ (F) in MII cells transfected

with the indicated siRNAs against the destruction complex components APC or Axin1/2. Scale bar, 20 μm. Depletion of destruction complex components results in YAP/TAZ nuclear accumulation. G) qRT-PCR for the YAP/TAZ endogenous target gene *CTGF*, normalized to *GAPDH* expression, in MII cells transfected as in (E), in combination with control or YAP/TAZ siRNAs as indicated. Data are normalized to control siRNA-treated cells and presented as mean + SD. Depletion of destruction complex components triggers YAP/TAZ transcriptional activity.

(H-I) YAP/TAZ are required for β-catenin inhibition in Wnt-off state.

(H) Depletion of YAP/TAZ decreases the amount of the ubiquitin ligase β-TrCP associated with the Axin1 complex. HEK293 cells were transfected with two independent control (lanes 2 and 3) or two independent YAP/TAZ (lanes 4 and 5) siRNAs. Lysates were then subjected to IP using an anti-Axin1 antibody, and co-precipitating endogenous proteins were detected by western blot. Lysates from Axin1-depleted cells (lane 1) were used as specificity control. (I) YAP/TAZ depletion in Wnt-off state triggers β-catenin transcriptional activity. Luciferase assay using the TOP-FLASH reporter, recording β-catenin-dependent transcriptional activity in HEK293 cells transfected with control or two independent YAP/TAZ siRNAs, compared to the effect of Axin1/2 siRNA or Wnt3A stimulation. Bars are mean + SD. Treatment with β-catenin siRNAs shows that inductions are β-catenin dependent.

(J) Model depicting the roles of YAP/TAZ as components of the destruction complex and β-catenin inhibitors in the WNT OFF state (left) and as Wnt transducers in the WNT ON state (right).

(K) YAP and TAZ are required for Wnt-driven biological effects in the mouse small intestine. Mice of the genotypes *Villin-CreERT2 Villin-CreERT2; Apc*$^{fl/fl}$, *Villin-CreERT2; Apc*$^{fl/fl}$*; Yap*$^{fl/fl}$*; Taz*$^{fl/fl}$ and *Villin-CreERT2; Yap*$^{fl/fl}$*; Taz*$^{fl/fl}$ were injected with tamoxifen. Panels are representative immunohistochemical stainings of the small intestine for the proliferation marker Ki-67 of mice with the indicated genotypes at day 3 or 21 after tamoxifen injection. Loss of APC induces crypt expansion associated with rapid demise of the animals, and these phenotypes are rescued by concomitant deletion of YAP/ TAZ. Note that YAP/TAZ knockout *per se* is inconsequential for normal intestinal homeostasis.

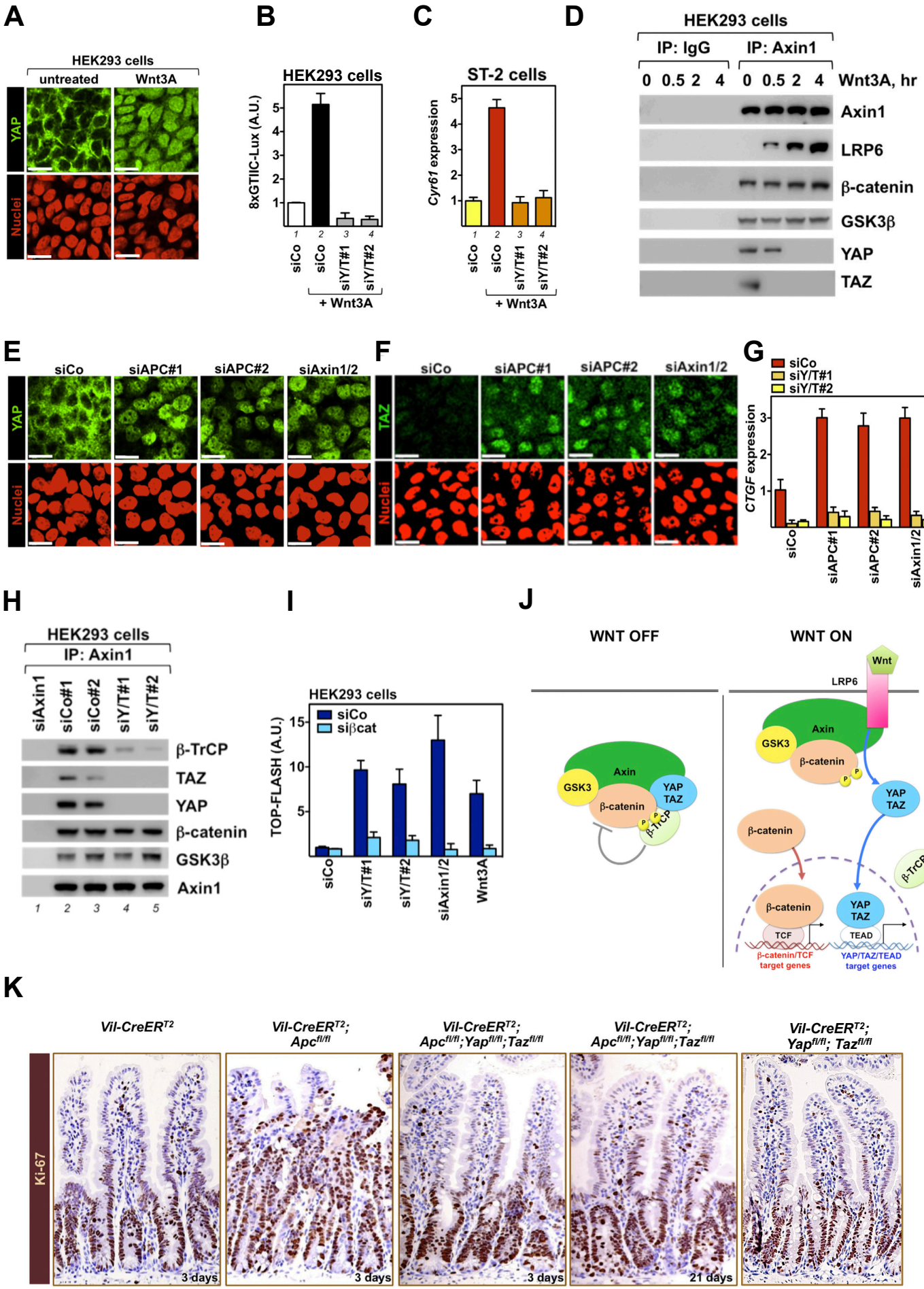
A
HEK293 cells
untreated
Wnt3A
YAP
Nuclei
B
HEK293 cells
8xGTIIC-Lux (A.U.)
siCo
siCo
siY/T#1
siY/T#2
+ Wnt3A
C
ST-2 cells
Cyr61 expression
siCo
siCo
siY/T#1
siY/T#2
+ Wnt3A
D
HEK293 cells
IP: IgG
IP: Axin1
0 0.5 2 4
0 0.5 2 4
Wnt3A, hr
Axin1
LRP6
β-catenin
GSK3β
YAP
TAZ
E
siCo
siAPC#1
siAPC#2
siAxin1/2
YAP
Nuclei
F
siCo
siAPC#1
siAPC#2
siAxin1/2
TAZ
Nuclei
G
siCo
siY/T#1
siY/T#2
CTGF expression
siCo
siAPC#1
siAPC#2
siAxin1/2
H
HEK293 cells
IP: Axin1
siAxin1
siCo#1
siCo#2
siY/T#1
siY/T#2
β-TrCP
TAZ
YAP
β-catenin
GSK3β
Axin1
1 2 3 4 5
I
HEK293 cells
siCo
siβcat
TOP-FLASH (A.U.)
siCo
siY/T#1
siY/T#2
siAxin1/2
Wnt3A
J
WNT OFF
WNT ON
Wnt
LRP6
Axin
GSK3
β-catenin
YAP
TAZ
β-TrCP
TCF
TEAD
β-catenin/TCF target genes
YAP/TAZ/TEAD target genes
K
Vil-CreER^T2
Vil-CreER^T2; Apc^fl/fl
Vil-CreER^T2; Apc^fl/fl;Yap^fl/fl;Taz^fl/fl
Vil-CreER^T2; Apc^fl/fl;Yap^fl/fl;Taz^fl/fl
Vil-CreER^T2; Yap^fl/fl; Taz^fl/fl
Ki-67
3 days
3 days
3 days
21 days

Figure 3

Figure 4. YAP/TAZ are required for the expansion of intestinal crypt organoids.

(A) Mice of the genotype *Villin-CreERT2* were injected with tamoxifen. After 3 days, intestinal crypts and villi were explanted, and lysates were subjected to western blot analysis for YAP, TAZ, and E-cadherin. GAPDH serves as loading control.
(B and C) YAP and TAZ are required for survival of explanted intestinal crypts. (B) Representative images of organoids formed by crypts explanted from *Villin-CreERT2* or *Villin-CreERT2; Yap$^{fl/fl}$; Taz$^{fl/fl}$* and cultured *ex vivo* for 3 days. Where indicated, tamoxifen was added to the culture medium at seeding.
(C) Quantification of the number of organoids formed by each of the samples depicted in (B).
(D) Genotyping of organoids as shown in Figure 4B, confirming correct recombination induced by tamoxifen.

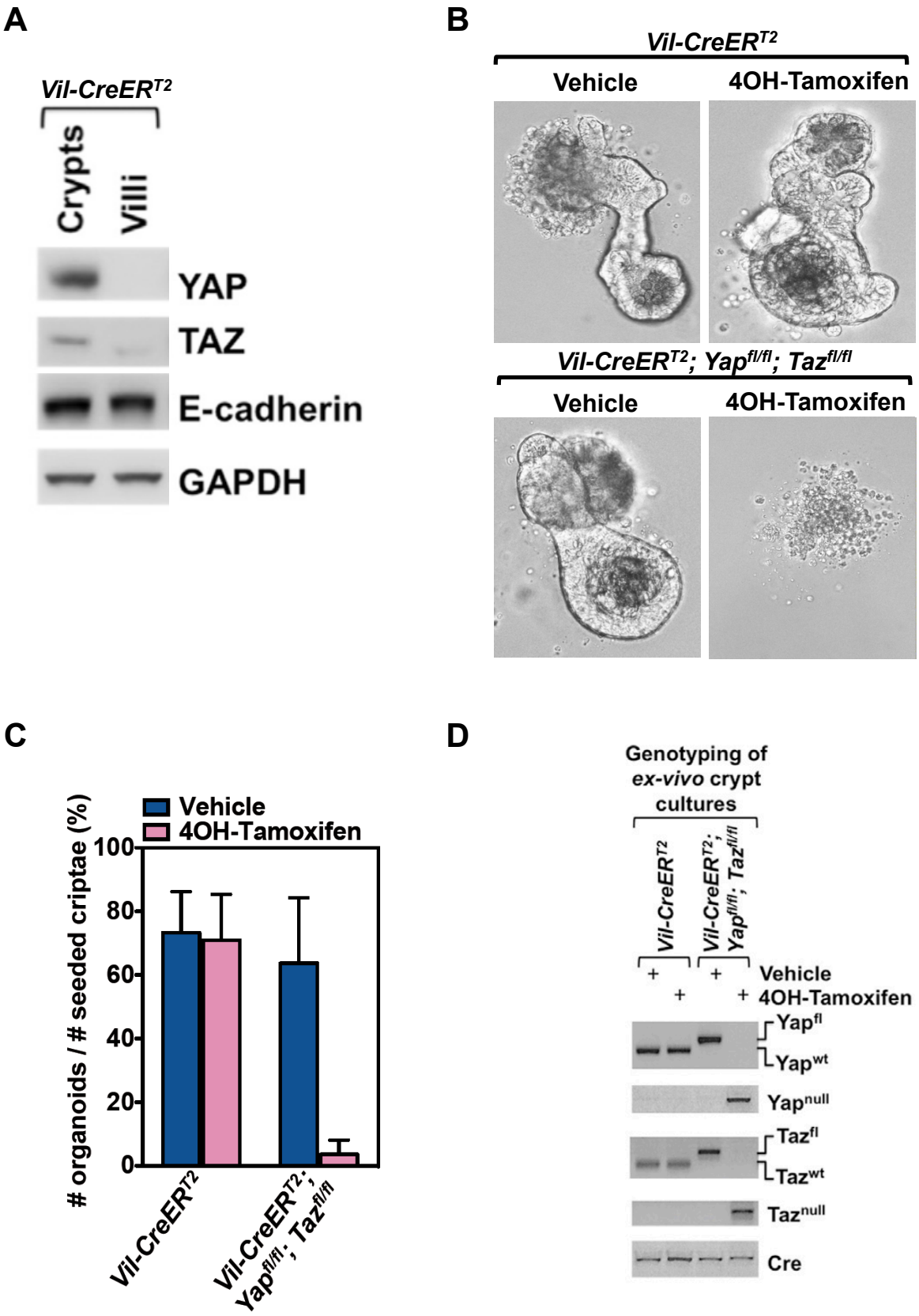
A
Vil-CreER^{T2}
Crypts
Villi
YAP
TAZ
E-cadherin
GAPDH
B
Vil-CreER^{T2}
Vehicle
4OH-Tamoxifen
Vil-CreER^{T2}; Yap$^{fl/fl}$; Taz$^{fl/fl}$
Vehicle
4OH-Tamoxifen
C
Vehicle
4OH-Tamoxifen
organoids / # seeded criptae (%)
100
80
60
40
20
0
Vil-CreER^{T2}
Vil-CreER^{T2}; Yap$^{fl/fl}$; Taz$^{fl/fl}$
D
Genotyping of ex-vivo crypt cultures
Vil-CreER^{T2}
Vil-CreER^{T2}; Yap$^{fl/fl}$; Taz$^{fl/fl}$
+
+
Vehicle
+
+
4OH-Tamoxifen
Yap^{fl}
Yap^{wt}
Yap^{null}
Taz^{fl}
Taz^{wt}
Taz^{null}
Cre

Figure 4

Figure 5. YAP/TAZ are required for the expansion of pancreatic progenitors as organoids.

(A) Representative images of a pancreatic duct fragment growing in pancreatic organoid medium at the indicated times and after four passages in fresh Matrigel (rightmost panel). Pictures are representative of three independent experiments performed with four technical replicates. Scale bars, 290 μm.
(B) Pancreatic ductal organoids ("Ducts", bottom panels) display nuclear YAP/TAZ by immunofluorescence. YAP/TAZ are not detected in pancreatic acini (top panels). Scale bar, 80μm.
(C) qRT-PCRs for the known YAP/TAZ targets genes *Axl, Ctgf, AmotL2 and AnkrD1* in primary pancreatic acini and pancreatic ductal organoids (mean + s.d). Results are representative of three independent experiments performed in triplicate. Data were normalized to *18S rRNA* expression.
(D) Ducts were derived from wild-type (*wt*) or $Yap^{fl/fl}$; $Taz^{fl/fl}$ mice and, during passaging at the single cell level, transduced with Ad-Cre or Ad-GFP as control. Panels are representative images of resulting outgrowths. Scale bars, 70 μm.
(E) Quantifications of the number of outgrowths formed by the indicated cells, treated as in D.

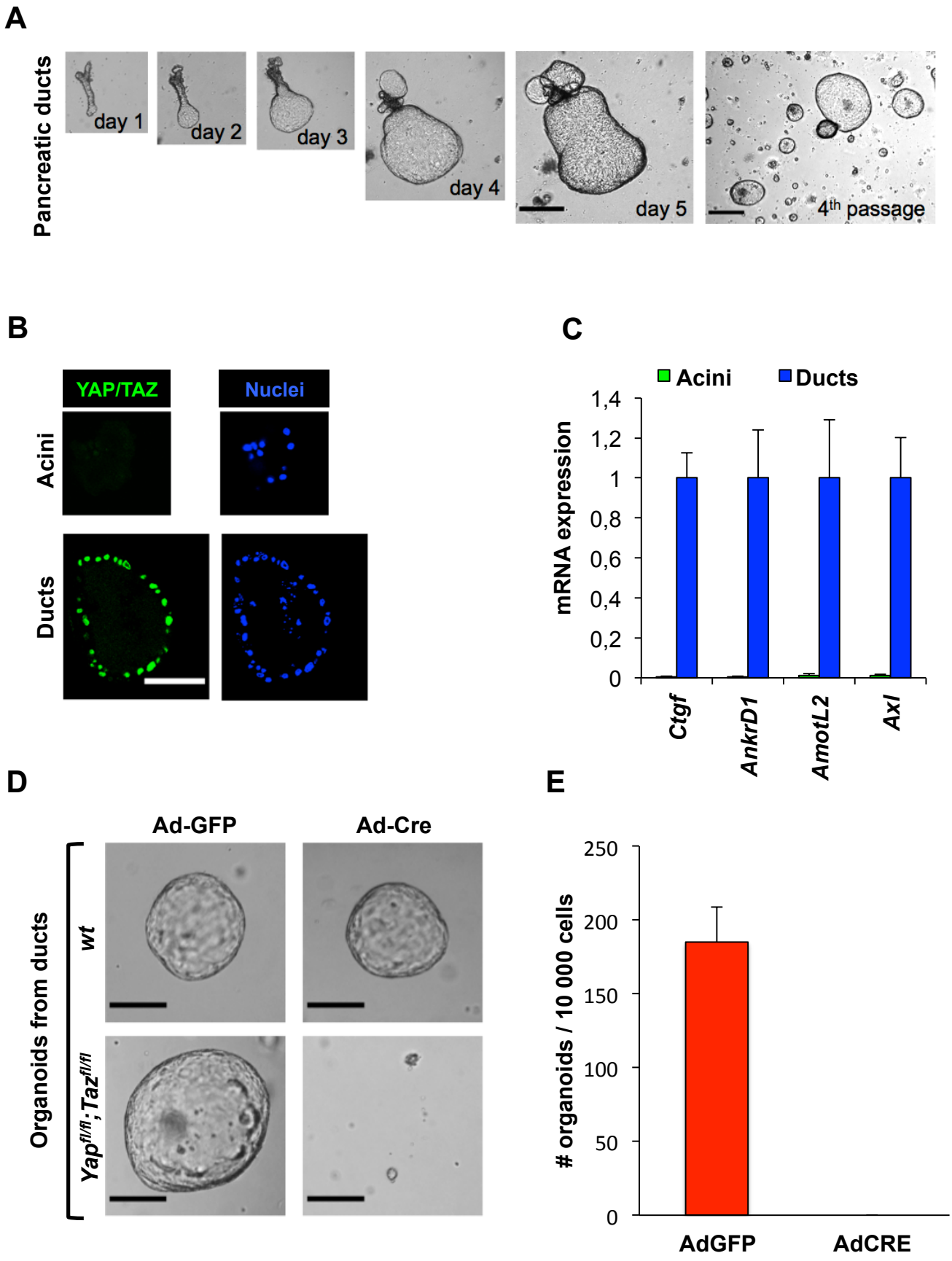
A
Pancreatic ducts
day 1
day 2
day 3
day 4
day 5
4th passage
B
YAP/TAZ
Nuclei
Acini
Ducts
C
Acini
Ducts
mRNA expression
1,4
1,2
1
0,8
0,6
0,4
0,2
0
Ctgf
AnkrD1
AmotL2
Axl
D
Ad-GFP
Ad-Cre
Organoids from ducts
wt
Yap^fl/fl;Taz^fl/fl
E
organoids / 10 000 cells
250
200
150
100
50
0
AdGFP
AdCRE

Figure 5

Figure 6. YAP/TAZ are genetically required for the expansion NSCs *ex vivo*.

(A) Representative confocal images of NSCs (plated as monolayer) and neurons, co-stained for YAP/Nestin or TAZ/Nestin and YAP/TuJ1 or TAZ/TuJ1, respectively. Nuclei were stained with DAPI. Scale bar: 23 μm.
(B) qRT-PCRs for the known YAP/TAZ targets genes *Axl, Cyr61 and AmotL2* in neurons and NSCs (mean + s.d). Results are representative of three independent experiments performed in triplicate. Data were normalized to *Gapdh* expression.
(C) Representative images of neurospheres from wild-type (wt) or $Yap^{fl/fl}$; $Taz^{fl/fl}$ NSCs transduced with Ad-Cre. Scale bar, 250 μm.

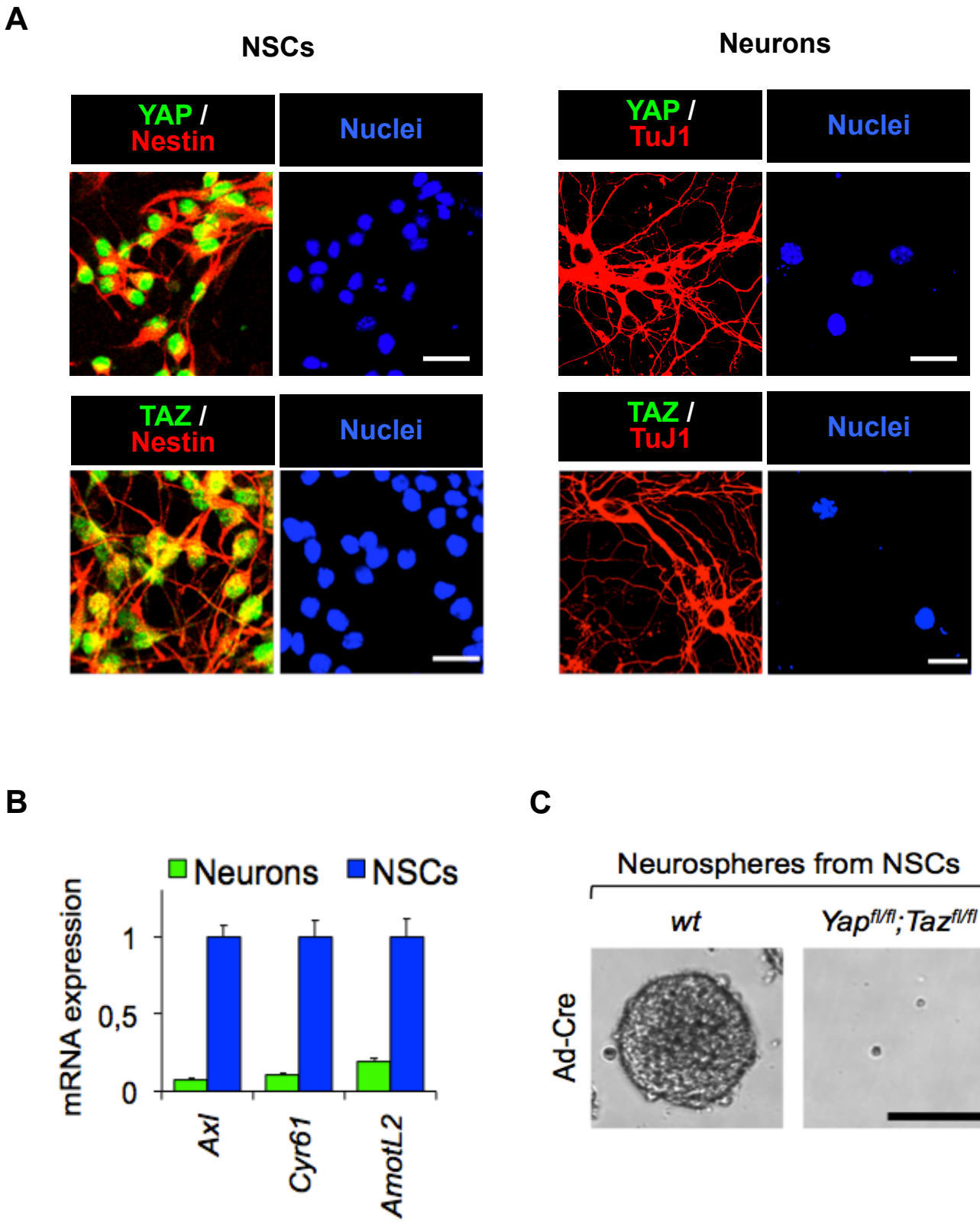
A
NSCs
Neurons
YAP / Nestin
Nuclei
YAP / TuJ1
Nuclei
TAZ / Nestin
Nuclei
TAZ / TuJ1
Nuclei
B
Neurons
NSCs
mRNA expression
1
0,5
0
Axl
Cyr61
AmotL2
C
Neurospheres from NSCs
wt
Yap^fl/fl;Taz^fl/fl
Ad-Cre

Figure 6

Figure 7. YAP converts pancreatic acinar cells to duct-like organoids.

(A) Schematic representation of the experiments performed with pancreatic acinar explants. Pancreatic acini were isolated from *R26-rtTA; tetO-YAP* ^{S127A} mice and seeded as whole acini in collagen (see Experimental procedures). Acinar cells were cultured in the presence of doxycycline until primary organoids appeared. Organoids obtained from these culture conditions were then passaged in fresh Matrigel in the absence of doxycycline every 10 days.

(B-C) Serial images of a whole acinus derived from *R26-rtTA; tetO-YAP*^{S127A} growing as cyst-like organoid at the indicated time points (B) after doxycycline addition and after one or four passages in fresh Matrigel (C) in the absence of doxycycline. Scale bars, 70 μm in B; 290 μm in C.

(D) Quantification of the ability of whole acini to form ductal organoids upon transgenic YAP overexpression as in B. Data are presented as mean + s.d. and are representative of five independent experiments, performed with four technical replicates.

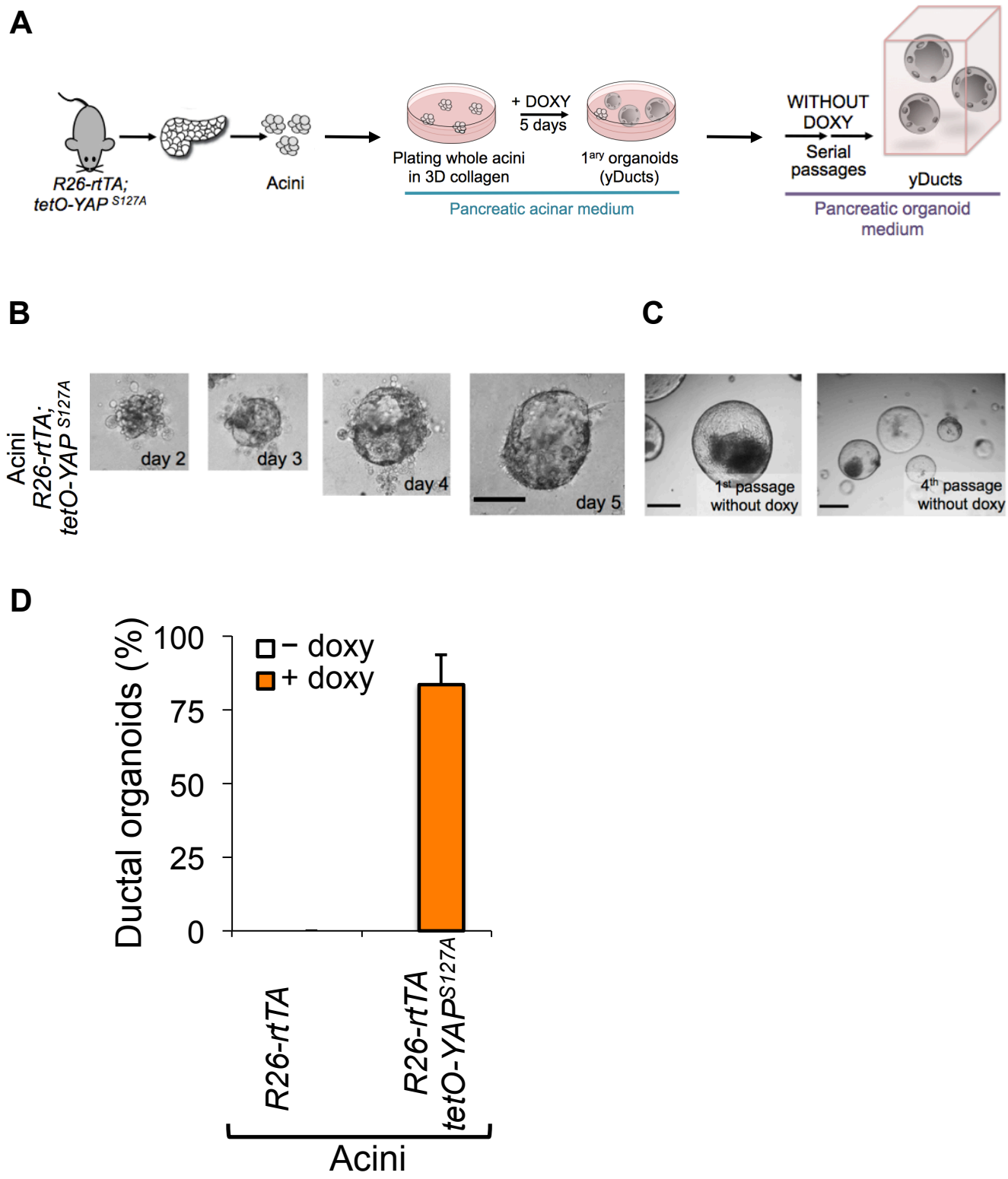
A
R26-rtTA;
tetO-YAP S127A
Acini
Plating whole acini
in 3D collagen
+ DOXY
5 days
1ary organoids
(yDucts)
Pancreatic acinar medium
WITHOUT
DOXY
Serial
passages
yDucts
Pancreatic organoid
medium
B
Acini
R26-rtTA;
tetO-YAP S127A
day 2
day 3
day 4
day 5
C
1st passage
without doxy
4th passage
without doxy
D
Ductal organoids (%)
100
75
50
25
0
− doxy
+ doxy
R26-rtTA
R26-rtTA
tetO-YAPS127A
Acini

Figure 7

Figure 8. Lineage tracing and single cell gene expression profiling of acinar cell cultures.

(A) Schematic representation of the experiments performed with lineage-traced pancreatic acinar explants. Pancreatic acini were isolated from *Ptf1a-CreERTM; R26-LSL-rtTA-IRES-EGFP; tetO-YAP*^{S127A} mice and seeded as whole acini in collagen (see Experimental procedures). Acinar cells were cultured in the presence of doxycycline until primary organoids appeared. Organoids obtained from these culture conditions were then passaged in fresh Matrigel in the absence of doxycycline every 10 days.

(B) Panels are bright field and GFP-fluorescence pictures of *Ptf1a-CreERTM; R26-LSL-rtTA-IRES-EGFP; tetO-YAP*^{S127A} ductal progenitors, at the indicated passage of organoid culture, showing that no endogenous pancreatic progenitor is labeled by the genetic lineage tracing strategy employed. Scale bar, 290 μm.

(C) Negative control of the experiment shown in D-E . Panels are bright field and GFP-fluorescence pictures of *Ptf1a-CreERTM; R26-LSL-rtTA-IRES-EGFP; tetO-YAP*^{S127A} exocrine acini, at the indicated time points in absence of doxycycline treatment (Negative controls). Scale bar, 33μm.

(D,E) Lineage-tracing experiments using the *Ptf1a-CreERTM* driver. Panels are bright field and GFP-fluorescence pictures of transgenic YAP-expressing exocrine acini derived from *Ptf1a-CreERTM; R26-LSL-rtTA-IRES-EGFP; tetO-YAP*^{S127A} mice, at the indicated time points of doxycycline treatment (D) and after passaging in absence of doxycycline in fresh Matrigel (E). Scale bars, 33 μm in D; 70 μm in E.

(F) Single cell gene expression profile of pancreatic cultures of the *R26-rtTA; tetO-YAP*^{S127A} genotype during the YAP-induced conversion of acinar cells to yDucts. day 0 = starting acini (without doxycycline); day 2 = cultures that have experienced 48 hours of doxycycline; day 4 = cultures that have experienced 96 hours of doxycycline. Heatmap represents expression levels as log2ratio normalized to *18S-rRNA*. Rows are evaluated genes and columns are individual cells.

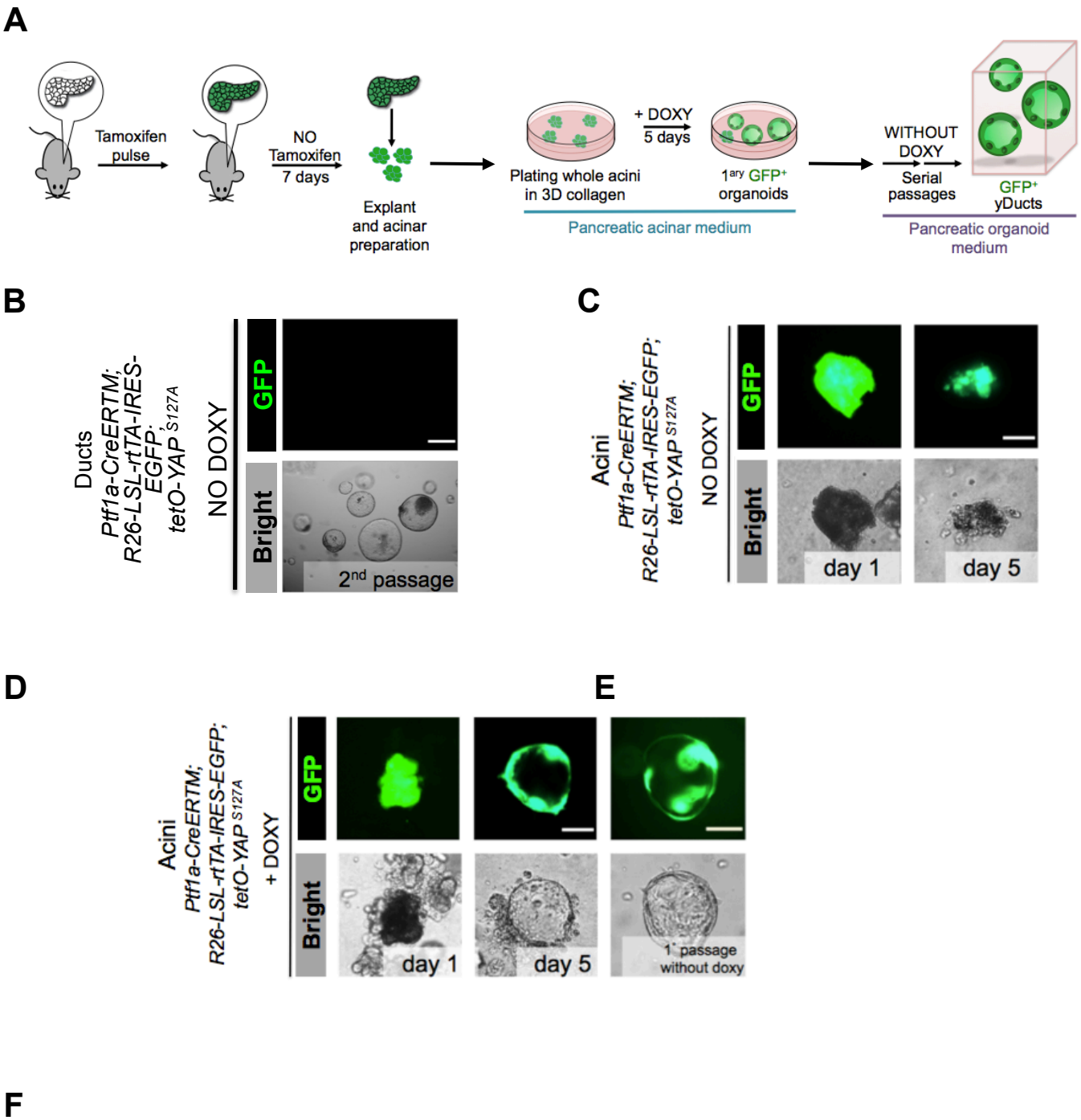
A
Tamoxifen pulse
NO Tamoxifen 7 days
Explant and acinar preparation
Plating whole acini in 3D collagen
+ DOXY 5 days
1ary GFP+ organoids
Pancreatic acinar medium
WITHOUT DOXY
Serial passages
GFP+ yDucts
Pancreatic organoid medium
B
Ducts
Ptf1a-CreERTM; R26-LSL-rtTA-IRES-EGFP; tetO-YAP S127A
NO DOXY
GFP
Bright
2nd passage
C
Acini
Ptf1a-CreERTM; R26-LSL-rtTA-IRES-EGFP; tetO-YAP S127A
NO DOXY
GFP
Bright
day 1
day 5
D
Acini
Ptf1a-CreERTM; R26-LSL-rtTA-IRES-EGFP; tetO-YAP S127A
+ DOXY
GFP
Bright
day 1
day 5
E
1° passage without doxy
F
day 0
day 2
day 4
yDucts
Amy
Ptf1a
Nestin
Pdx1
Sox9
K19
Car2
Ctgf
Myc
CyclinD1
-3.0
-0.5
3.0
Log2 ratio

Figure 8

Figure 9. Characterization of yDucts

(A) qRT-PCRs for the indicated exocrine and Ductal/progenitor markers in fresh pancreatic acini, yDucts and Ducts. Data are normalized to *18S* rRNA expression and are referred to Acini for exocrine differentiation markers, and to Ducts for Ductal/progenitor genes (each set to 1). Results are representative of four independent experiments performed in triplicate. Data are presented as mean + s.d.

(B) Organoids from duct fragments (Ducts, bottom panels) and YAP-induced organoids (yDucts, middle panels) expressed the ductal marker SOX9 and were negative for the exocrine marker Amylase (data not shown), by immunofluorescence. Acinar cells (top panel) are shown as control. Scale bar, 80 μm.

(C) Unsupervised hierarchical clustering of gene expression profiles in acini, yDucts and Ducts. Each column represents one separated biological sample. Genes are ordered according to the decreasing average expression level in acini. Representative genes upregulated in acinar cells (red) or in Ducts and yDucts (green) are on the left.

(D) Representative immunofluorescences for the ductal marker K19 and the exocrine marker CPA1 before (day 0) and after yDuct differentiation (day 8). Similar results were obtained with organoids from normal ducts (not shown). Scale bars:19 μm (day 0), 16 μm (day8).

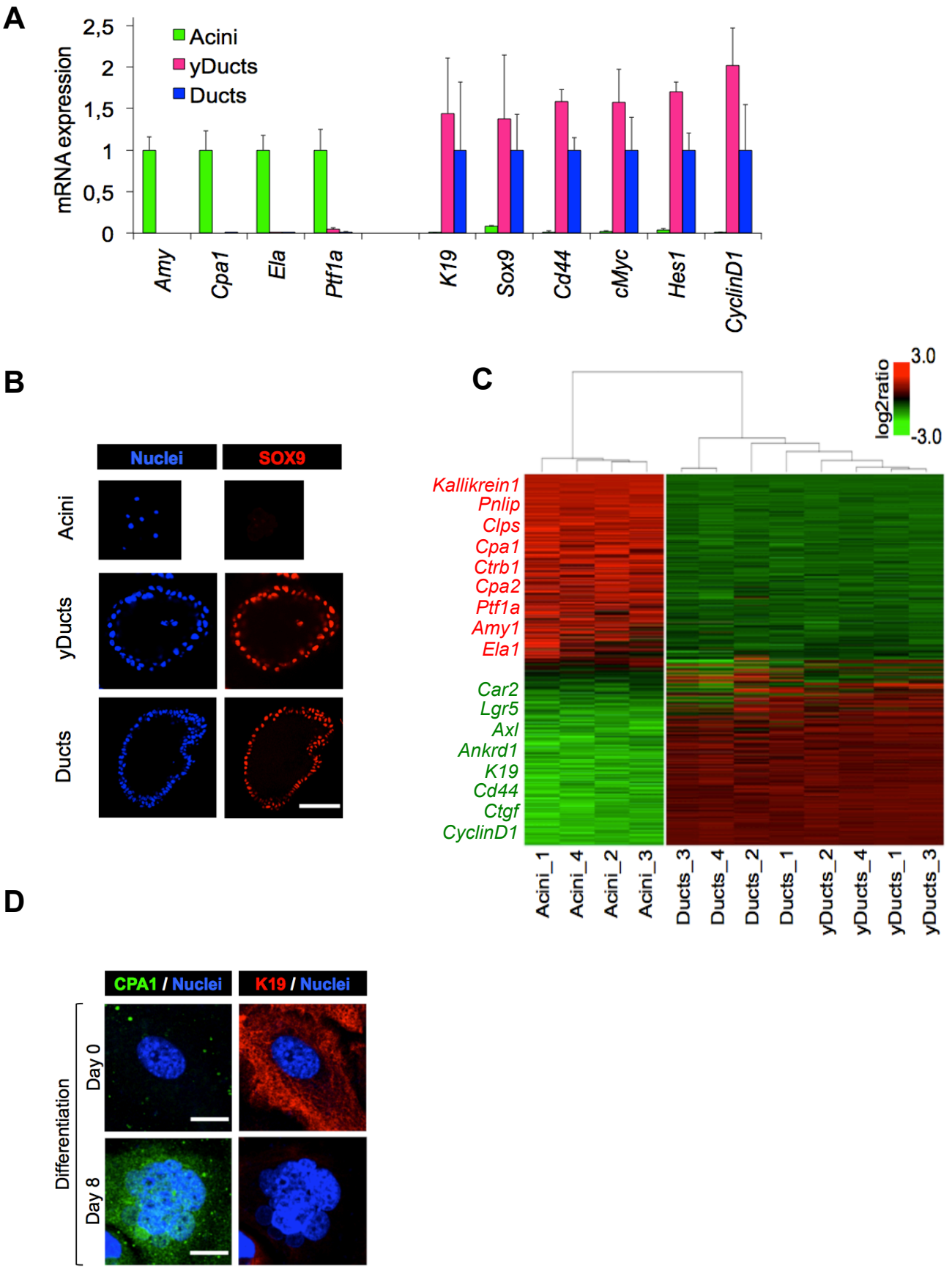
A
mRNA expression
2,5
2
1,5
1
0,5
0
Acini
yDucts
Ducts
Amy
Cpa1
Ela
Ptf1a
K19
Sox9
Cd44
cMyc
Hes1
CyclinD1
B
Nuclei
SOX9
Acini
yDucts
Ducts
C
log2ratio
3.0
-3.0
Kallikrein1
Pnlip
Clps
Cpa1
Ctrb1
Cpa2
Ptf1a
Amy1
Ela1
Car2
Lgr5
Axl
Ankrd1
K19
Cd44
Ctgf
CyclinD1
Acini_1
Acini_4
Acini_2
Acini_3
Ducts_3
Ducts_4
Ducts_2
Ducts_1
yDucts_2
yDucts_4
yDucts_1
yDucts_3
D
CPA1 / Nuclei
K19 / Nuclei
Differentiation
Day 0
Day 8

Figure 9

Figure 10. YAP converts neurons in neural stem cell-like cells.

(A) Representative confocal images of cortical neurons, co-stained for Synaptophysin/Tau, showing that primary neurons were extensively decorated by synaptic structures. Scale bars, 15 μm - top panels, 5.8 μm - bottom panels.
(B) Schematic representation of the experiments performed with hippocampal or cortical neurons. Primary mouse neurons were infected with lentiviral vectors and subsequently subjected to AraC selection for post-mitotic cells for 1 week (See Experimental procedures). After 15 days of doxycycline treatment in NSC medium, YAP-expressing neurons formed floating spheres that could be passaged multiple times in absence of doxycycline.
(C) Representative images of yNSCs neurospheres (second passage, P2) derived from hippocampal (top panels) or cortical neurons (bottom panels). Images from negative control transduced neurons (rtTA/EGFP and rtTA/YAPS94A for hippocampal or rtTA/EGFP for cortical neurons, respectively) are shown as negative controls. Neurospheres from native NSCs are presented as comparison. Scale bars, 210 μm.
(D) P1 yNSCs were dissociated to single cells and replated at clonal density for neurosphere formation in the absence of doxycycline for further passages (P2, P3, P4). Graphs are quantifications of neurospheres formed by the indicated cells. Native NSCs are presented as comparison. Results are representative of at least 8 (P2), 6 (P3) and 3 (P4) independent experiments performed in six replicates. Data are presented as mean + s.d.

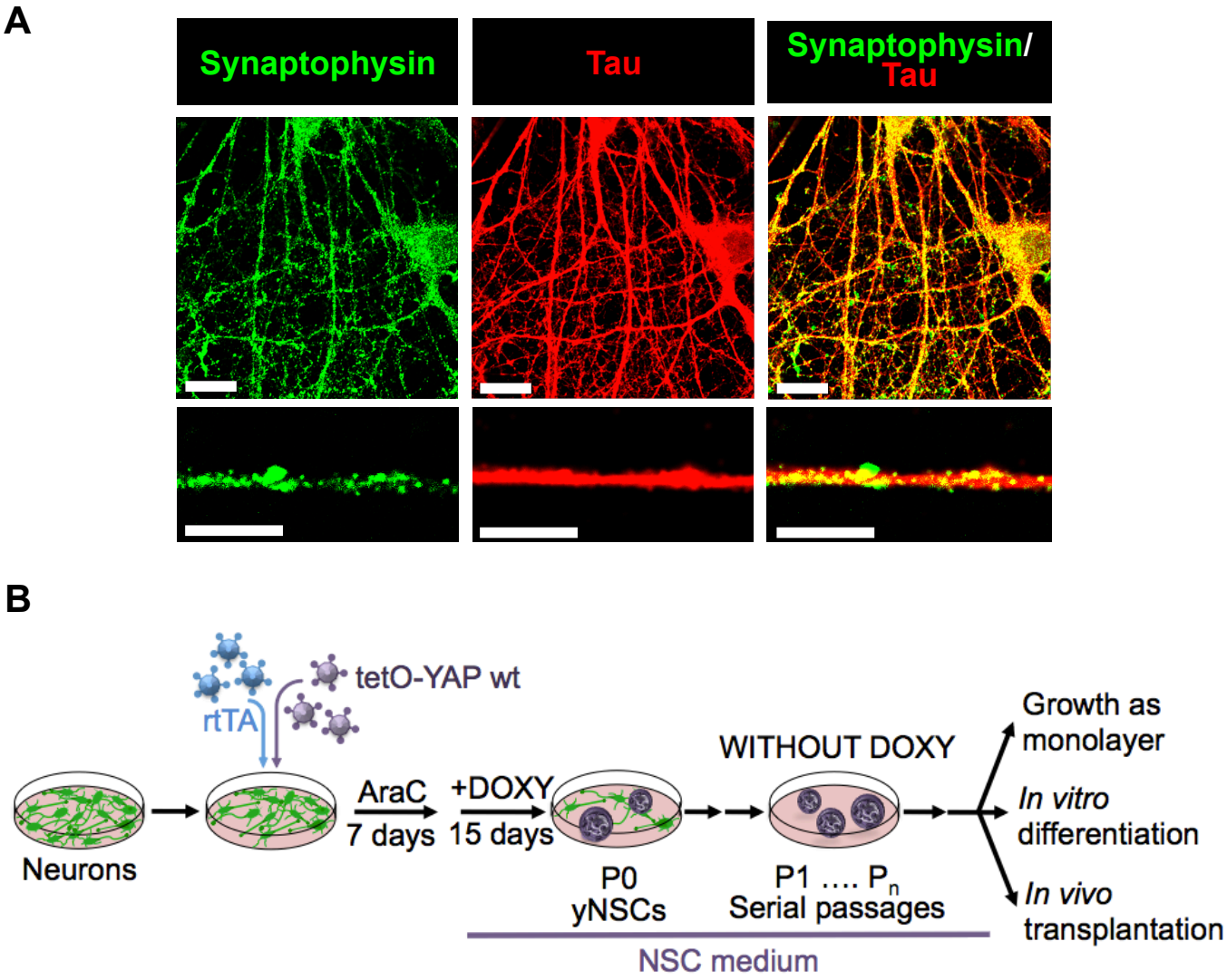
A
Synaptophysin
Tau
Synaptophysin/
Tau
B
tetO-YAP wt
rtTA
Neurons
AraC
7 days
+DOXY
15 days
P0
yNSCs
WITHOUT DOXY
P1 …. Pn
Serial passages
Growth as
monolayer
In vitro
differentiation
In vivo
transplantation
NSC medium
C
Hippocampal
neurons:
rtTA/EGFP
Hippocampal
neurons:
rtTA/YAPS94A
yNSCs
P2
Cortical neurons:
rtTA/EGFP
yNSCs
P2
Native NSCs
P2
D
NSCs
yNSCs
# of neuroshperes /
2,000 cells
35
30
25
20
15
10
5
0
P2
P3
P4
without DOXY

Figure 10

Figure 11. Lineage tracing experiments showing that yNSCs originate from terminally differentiated neurons.

(A) Schematic representation of the genetic lineage tracing strategy used to trace neurons ex-vivo.
(B) Quantifications of the percentage of Syn1-Cre traced neurons positive for the indicated markers (as quantified by counting the number of cells positive for each marker by immunofluorescence analyses).
(C) tdTomato fluorescence and immunostaining for the indicated markers in cortical neurons obtained from *Syn1-Cre; R26-CAG-LSL-tdTomato* mice. tdTomato-positive neurons were also positive for the neuronal markers TuJ1, NeuN and Tau, but negative for the progenitor markers Nestin, Vimentin and Mash1 and for the proliferation markers EdU and Ki67 (see also quantifications in B). Scale bar, 19 μm.
(D) Immunofluorescence for the synaptic markers Synaptophysin and SV2a in neurons derived from *Syn1-Cre; R26-CAG-LSL-tdTomato* mice. Scale bars, 11 μm (upper panels) and 5.7 μm in magnifications (lower panels).

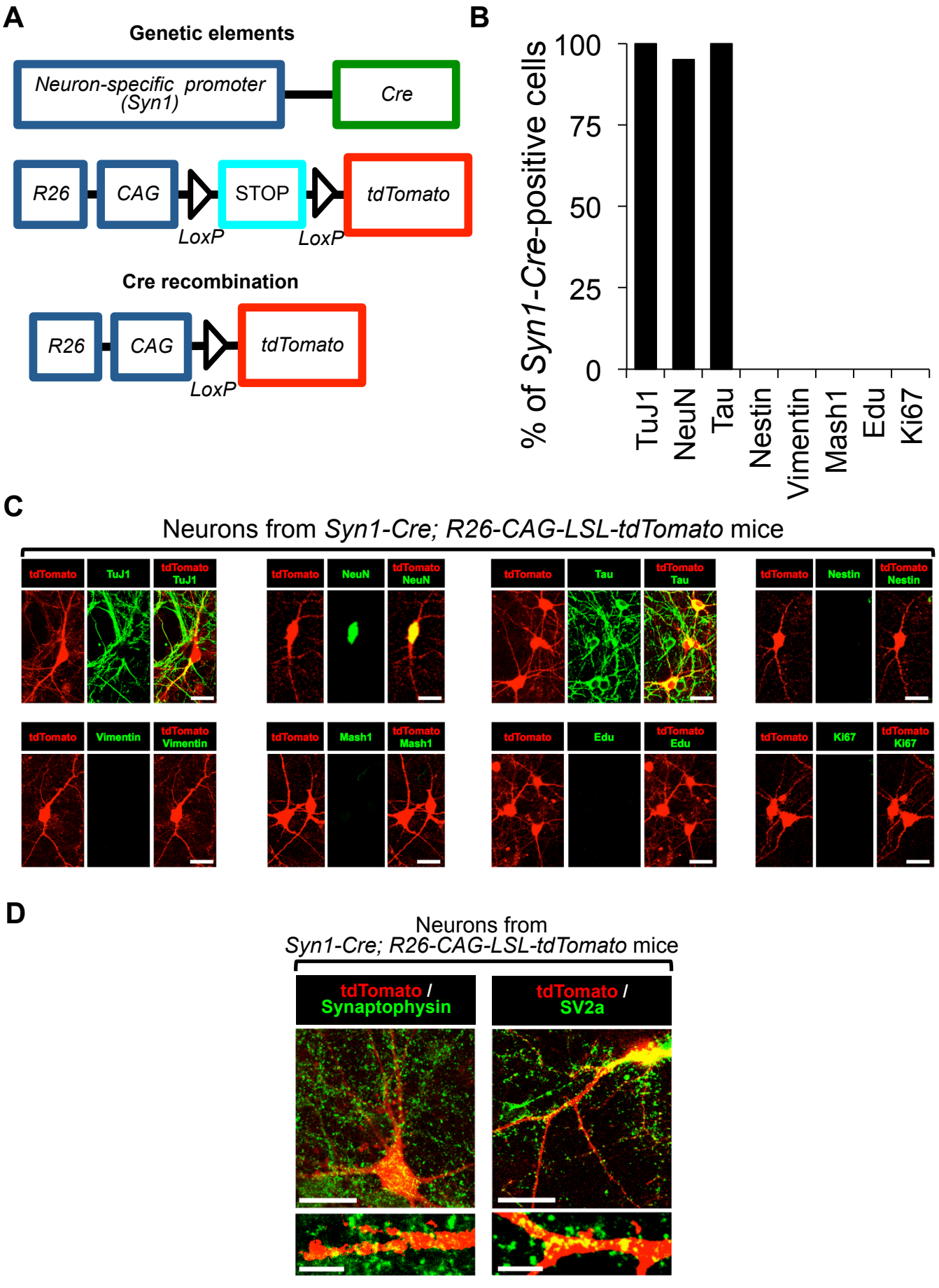
A
Genetic elements
Neuron-specific promoter (Syn1)
Cre
R26
CAG
STOP
tdTomato
LoxP
LoxP
Cre recombination
R26
CAG
tdTomato
LoxP
B
% of Syn1-Cre-positive cells
100
75
50
25
0
TuJ1
NeuN
Tau
Nestin
Vimentin
Mash1
Edu
Ki67
C
Neurons from Syn1-Cre; R26-CAG-LSL-tdTomato mice
tdTomato
TuJ1
tdTomato TuJ1
tdTomato
NeuN
tdTomato NeuN
tdTomato
Tau
tdTomato Tau
tdTomato
Nestin
tdTomato Nestin
tdTomato
Vimentin
tdTomato Vimentin
tdTomato
Mash1
tdTomato Mash1
tdTomato
Edu
tdTomato Edu
tdTomato
Ki67
tdTomato Ki67
D
Neurons from
Syn1-Cre; R26-CAG-LSL-tdTomato mice
tdTomato / Synaptophysin
tdTomato / SV2a

Figure 11

Figure 12. Lineage tracing and characterization of the early stages of neuronal reprograming.

(A) Time-course experiment with cortical neurons from *Syn1-Cre; R26-CAG-LSL-tdTomato* mice, showing pictures of the same field of genetically-traced neurons taken at the indicated time points during YAP-induced reprogramming (top panels). Bottom panels are bright field (insets) and tdTomato-fluorescence pictures of yNSCs derived from genetically lineage-traced neurons (at the indicated passages). Neurospheres from *Syn1-Cre; R26-CAG-LSL-tdTomato* NSCs are presented as negative control.
(B) Immunofluorescence for the indicated markers during the conversion of Syn1-Cre/tdTomato-traced YAP-expressing neurons (day 0) to yNSCs (day 2*; * means that the experiment was done in the presence of the anti-mitotic drug AraC).
(C) Quantifications of the percentage of td-Tomato-positive/YAP-expressing cells stained positive for the indicated markers, as in B.

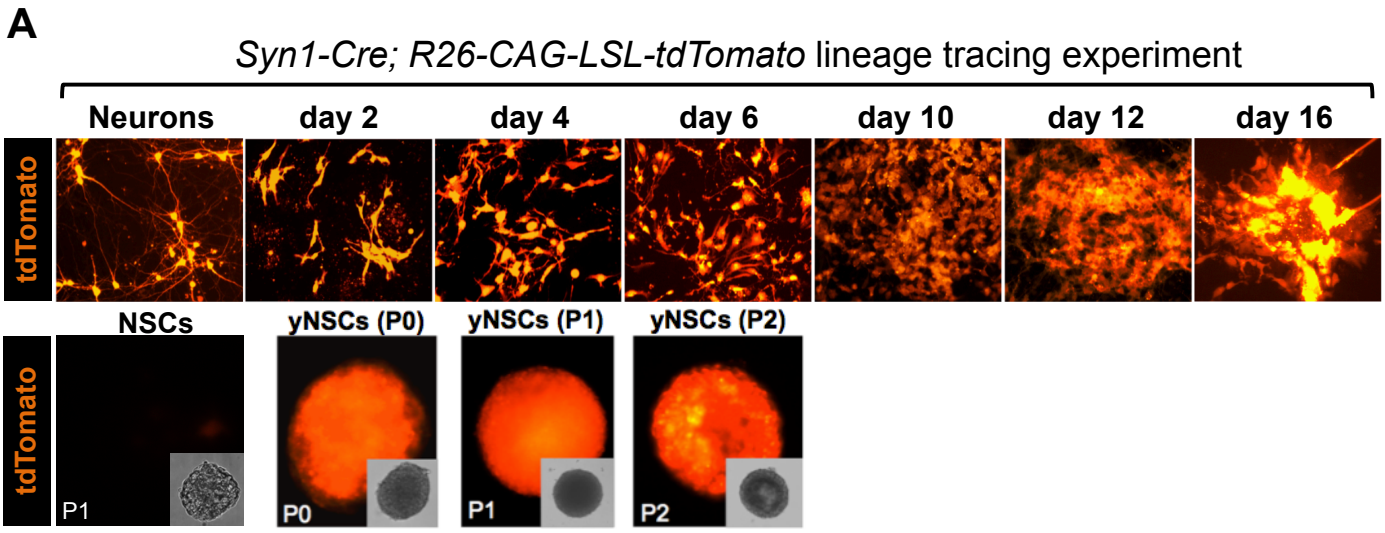
A
Syn1-Cre; R26-CAG-LSL-tdTomato lineage tracing experiment
Neurons
day 2
day 4
day 6
day 10
day 12
day 16
tdTomato
NSCs
yNSCs (P0)
yNSCs (P1)
yNSCs (P2)
tdTomato
P1
P0
P1
P2

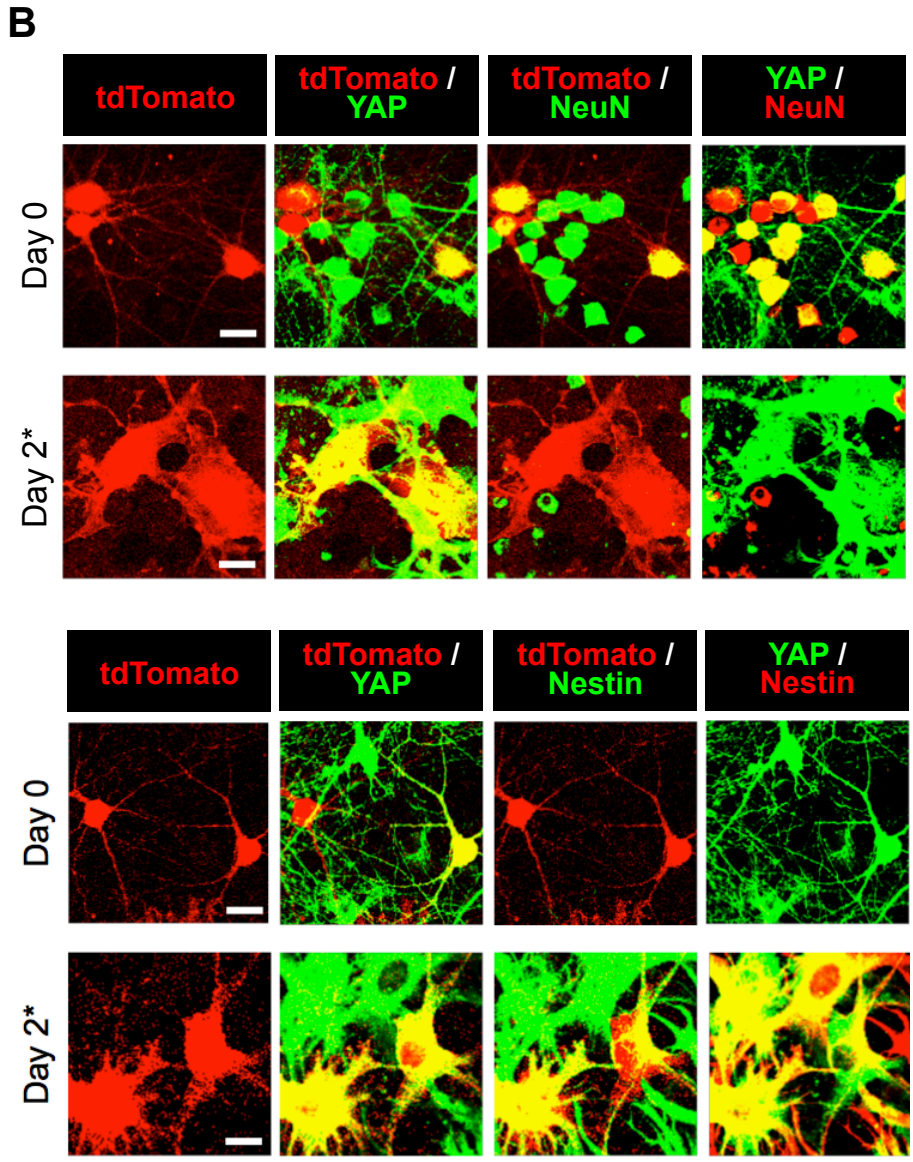
B
tdTomato
tdTomato / YAP
tdTomato / NeuN
YAP / NeuN
Day 0
Day 2*
tdTomato
tdTomato / YAP
tdTomato / Nestin
YAP / Nestin
Day 0
Day 2*

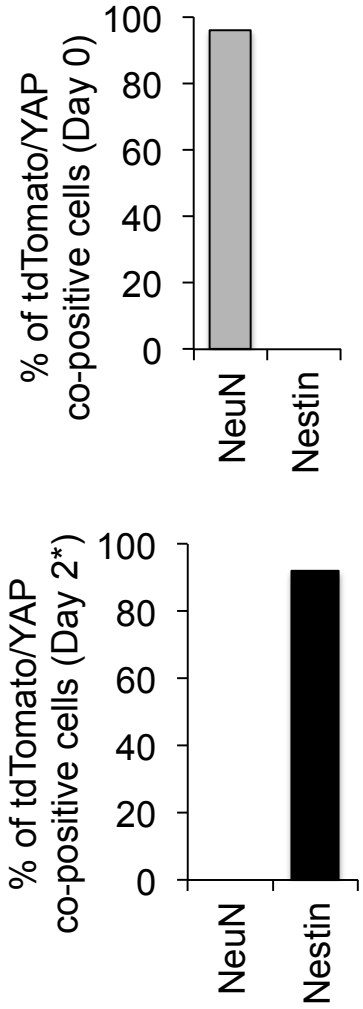
C
% of tdTomato/YAP co-positive cells (Day 0)
100
80
60
40
20
0
NeuN
Nestin
% of tdTomato/YAP co-positive cells (Day 2*)
100
80
60
40
20
0
NeuN
Nestin

Figure 12

Figure 13. Characterization of yNSCs.

(A) Immunofluorescence for the indicated markers in neurons and established yNSCs plated as monolayer. Endogenous NSCs serve as positive control. yNSCs lost the expression of the neuronal markes TuJ1, Tau and NeuN and acquired the expression of NSC markers Vimentin, Nestin and SOX2. Scale bar, 23 μm.
(B) Unsupervised hierarchical clustering of gene expression profiles in cortical neurons, yNSCs and NSCs. Each column represents one separated biological sample. Genes are ordered according to the decreasing average expression level in neurons. Representative genes upregulated in neurons (red) or in NSCs and yNSCs (green) are on the left. See also Table 1 for a full list of genes upregulated in neurons.
(C) qRT-PCRs for the indicated neuronal and neural stem cell markers in neurons, yNSCs and NSCs. Data are normalized to *Gapdh* expression and are referred to neurons for neuronal genes, and to NSCs for neural stem cell markers (each set to 1). Results are representative of at least three independent experiments performed in triplicate.

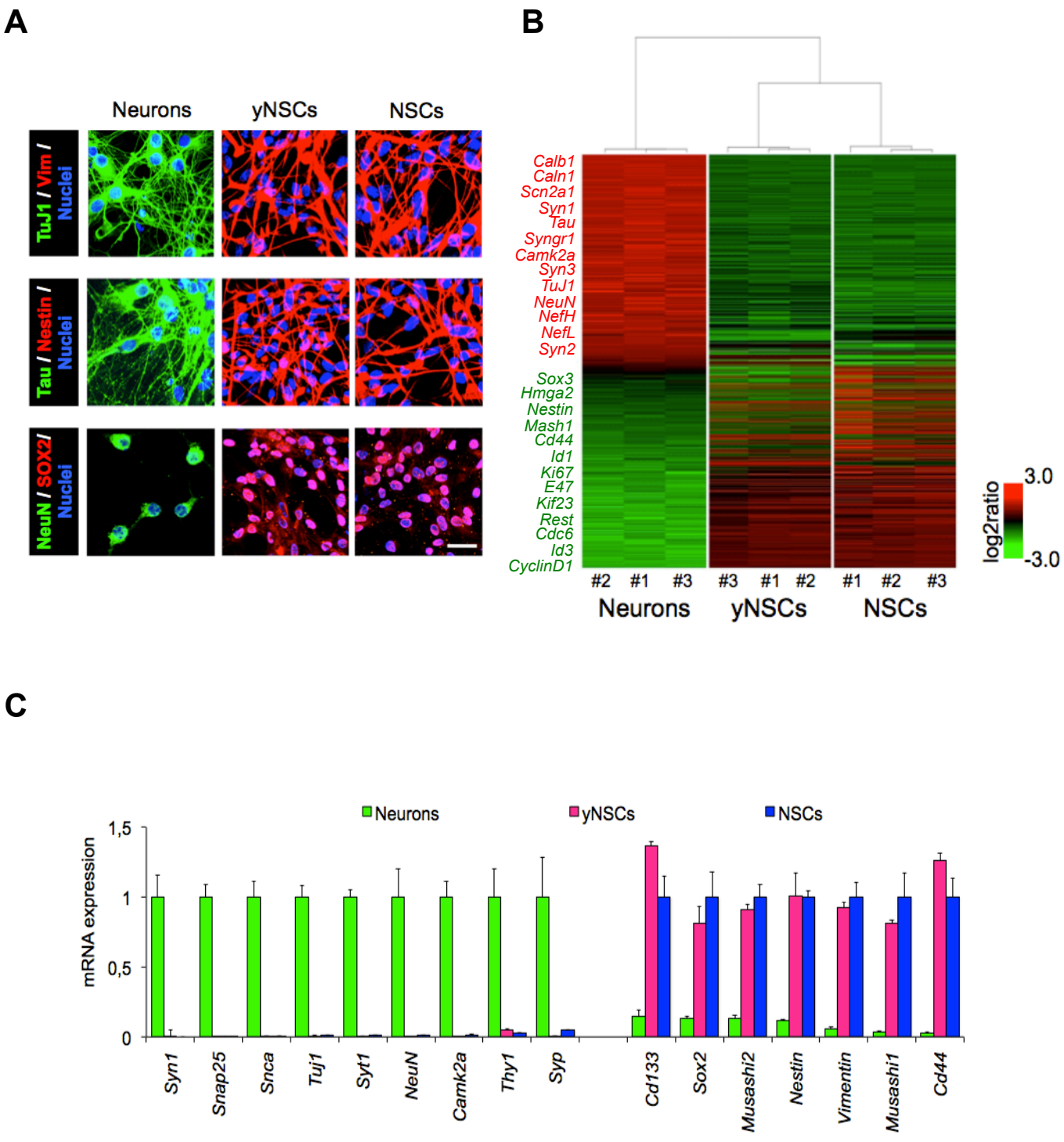
A
Neurons
yNSCs
NSCs
TuJ1 / Vim / Nuclei
Tau / Nestin / Nuclei
NeuN / SOX2/ Nuclei
B
Calb1
Caln1
Scn2a1
Syn1
Tau
Syngr1
Camk2a
Syn3
TuJ1
NeuN
NefH
NefL
Syn2
Sox3
Hmga2
Nestin
Mash1
Cd44
Id1
Ki67
E47
Kif23
Rest
Cdc6
Id3
CyclinD1
#2 #1 #3 #3 #1 #2 #1 #2 #3
Neurons
yNSCs
NSCs
log2ratio
3.0
-3.0
C
Neurons
yNSCs
NSCs
mRNA expression
1,5
1
0,5
0
Syn1
Snap25
Snca
Tuj1
Syt1
NeuN
Camk2a
Thy1
Syp
Cd133
Sox2
Musashi2
Nestin
Vimentin
Musashi1
Cd44

Figure 13

Figure 14. yNSCs display tripotent differentiation potential.

(A) YAP-induced yNSCs, and endogenous NSCs as positive control, were plated and differentiated toward an astrocytic, a neuronal or an oligodendrocytic fate (see Experimental procedures). Panels represent confocal images for the astrocytic marker GFAP (left panels), neuronal differentiation markers TuJ1 and Tau (middle panels) and the oligodendrocytic marker CNPase (right panels). Results are representative of three independent experiments performed in triplicate. Scale bars, 50 μm.

(B) These refer to Figure 14A. By immunofluorescence, neurons differentiated from yNSCs werre TuJ1-positive or Tau-positive but were negative for Nestin. Scale bars, 9μm.

(C-G) yNSCs were transduced with a constitutive EGFP-expressing vector and injected in the brains of recipient mice. Four weeks later, brains were fixed and processed for immunofluorescence analyses. C) Panels are representative confocal images showing that injected cells (GFP-positive) lost expression of the NSC marker Nestin. A field of the subventricular zone (SVZ) of the same brain sections is shown as positive control of the anti-Nestin antibody staining. D-E) Panels are representative confocal images showing that injected yNSCs (GFP-positive) integrate in the brain parenchyma and massively differentiate into an astrocytic fate, as indicated by GFAP expression (arrows). V3 = third ventricle; TH= thalamus. F) Panels are a representative image showing that injected yNSCs (GFP-positive) migrated away from the graft and partly colonized the neuronal hippocampal area CA1; HPF= hippocampal formation. G) Panels are representative confocal images showing that injected yNSCs (GFP-positive) differentiated in NeuN- and TuJ1-positive neurons (arrows) or CNPase-positive oligodendrocytes. Scale bars in C,E,G, 19 μm.

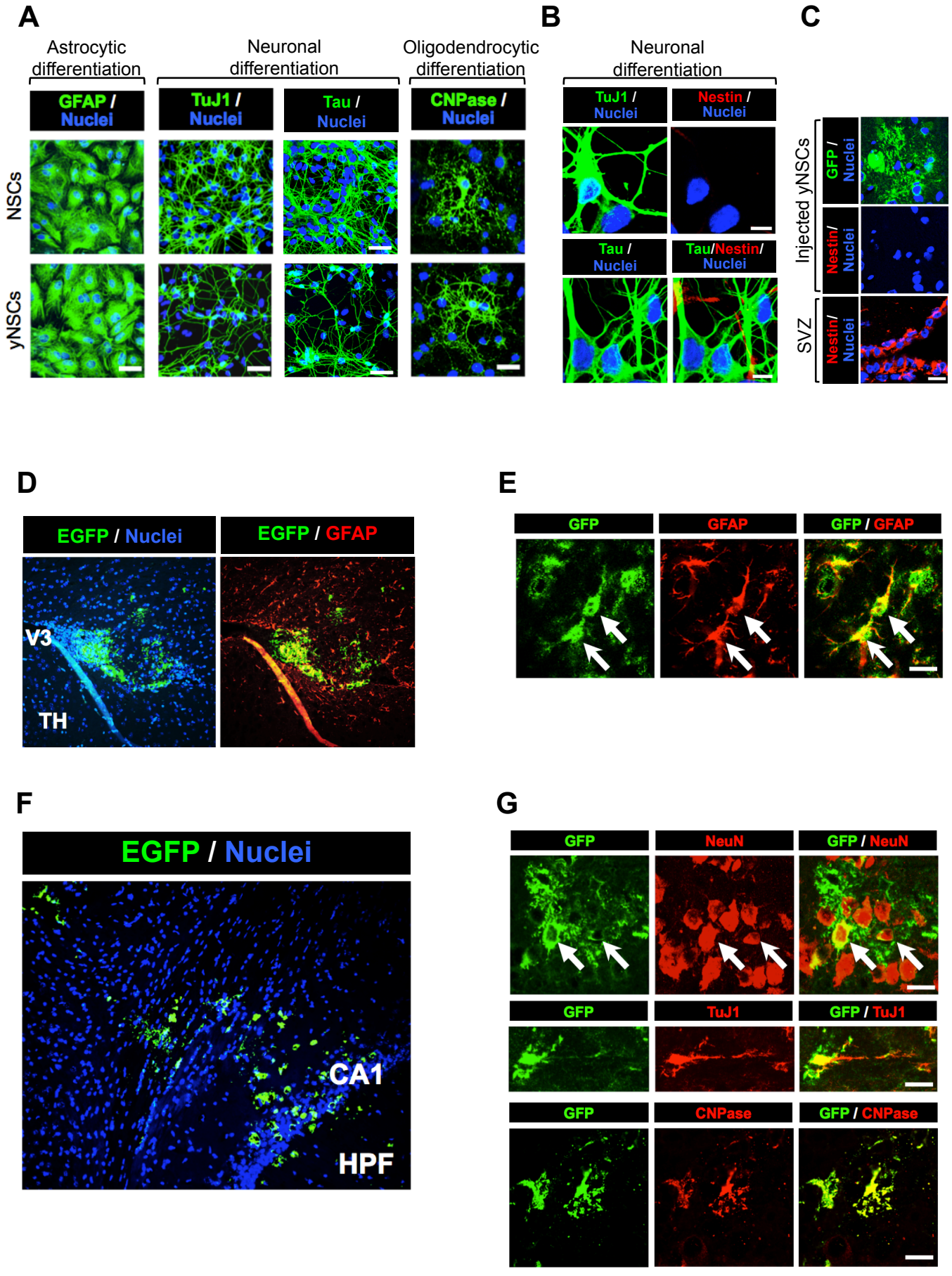
A
Astrocytic differentiation
Neuronal differentiation
Oligodendrocytic differentiation
GFAP / Nuclei
TuJ1 / Nuclei
Tau / Nuclei
CNPase / Nuclei
NSCs
yNSCs
B
Neuronal differentiation
TuJ1 / Nuclei
Nestin / Nuclei
Tau / Nuclei
Tau/Nestin/ Nuclei
C
Injected yNSCs
GFP / Nuclei
Nestin/ Nuclei
SVZ
Nestin/ Nuclei
D
EGFP / Nuclei
EGFP / GFAP
V3
TH
E
GFP
GFAP
GFP / GFAP
F
EGFP / Nuclei
CA1
HPF
G
GFP
NeuN
GFP / NeuN
GFP
TuJ1
GFP / TuJ1
GFP
CNPase
GFP / CNPase

Figure 14